

Summation of Harmonics in Offshore Wind Farm Based on Probability Theory

Thesis Report

Mohammad Alhayek



Summation of Harmonics in Offshore Wind Farm Based on Probability Theory

Thesis Report

by

Mohammad Alhayek

to obtain the degree of Master of Science in Electrical Engineering
at The Delft University of Technology,
to be defended publicly on Wednesday August 25, 2021 at 09:00.

Student number:	5059917
Project duration:	November 9, 2020 – August 25, 2021
Daily Supervisor:	L. Beloqui Larumbe TU Delft
Thesis committee:	Prof. dr. ir. P. Bauer, TU Delft, Responsible Professor Dr. Z. Qin, TU Delft, Supervisor Dr. S. Tindemans, TU Delft

An electronic version of this thesis is available at <http://repository.tudelft.nl/>.

to Maryam, Abdulaziz and Salman

Acknowledgements

I would like to acknowledge and express my sincere appreciation to my daily supervisor Lucia Beloqui Larumbe for her guidance, mentorship and support during the thesis project. Her supportive leadership style, encouragement and constructive feedback during the 9 months of the thesis had been immense and influential in supporting me to finish this thesis project. I would also like to thank Dr. Zian Qin and Professor Pavol Bauer for their supervision, valuable feedback and guidance on the thesis.

The entire master program opportunity would not have been possible if it were not for Saudi Aramco sponsorship. Thus, I would like to take this opportunity to appreciate and thank Saudi Aramco management back in Dhahran, Saudi Arabia for availing this valuable and enriching experience to advance my career. I would also like to thank my academic supervisor Marc Mason for his guidance and support during the last two years.

I'm eternally grateful to my family and friends who have been encouraging and supporting during my master program. Especial thanks to my parents and my in-laws' for their utmost support and care to my wife and sons during my stay in the Netherlands. I would like to thank my dearest friends Yaqoub and Reda, and my new friends at Delft Belkasssem, Serge, Avinash, Jan Vit, Ramon, Waleed, and Habib for motivating me during this journey.

*Mohammad Alhayek
Rotterdam, August 16, 2021*

Abstract

The global energy transition that is shifting the industry to renewable energy sources is at the center of many countries' strategic plans as demonstrated by the increasing number of offshore wind farms connected to the grid. However, modern-day wind turbine with full-scale back-to-back converter is considered as a main source of harmonics, which can be amplified through the network due to low frequency resonance points created by the combination of long capacitive HVAC submarine cables and the many inductive transformers. The amplification of harmonics could lead to a grid non-compliance, and hence the developers of Offshore Wind Power Plants (OWPPs) might be obligated to install inflexible and expensive filters.

Prior to the construction of a wind farm and during the design stage, it is necessary to perform harmonic studies to estimate the harmonic emission from the wind farm and to predict whether there would be a harmonic non-compliance problem and the necessity or not to plan for remedial measures. The industry currently utilizes the IEC second summation rule to estimate harmonic distortion at the PCC of OWPPs. However, there is many proof in the literature that conclude the ineffectiveness of the summation rule as it leads to inaccurate estimation of harmonics compared to actual measurements. Therefore, there is a rising necessity to develop new accurate methods to estimate the harmonic distortion at the PCC of OWPPs.

It has been shown in the literature that harmonics injected by wind turbine converters are statistically random, and both of their magnitudes and phase angles can be represented by probability distribution functions. In contrast, the IEC summation rule utilizes a deterministic 95th percentile magnitude and indirectly compensates for the phase angle by an exponent. These two assumptions could be the main sources of its inaccuracy. Therefore, the objective of this thesis is to develop a new method to estimate harmonic distortion at the PCC of an OWPP using probability theory considering the probability distribution functions of harmonics.

First, a literature review is performed to acquire probability distribution functions of different harmonics based on actual measurements of a full-scale back-to-back converter, and on the modelling of the converter and other elements of the wind farm for harmonic studies. Then, an offshore wind power plant is modelled in DIgSilent PowerFactory software to perform both phase-correct (proposed method) and IEC harmonic load flows. The harmonic load flow for the proposed method is automated using Monte Carlo programmed in Python codes to calculate the harmonic distortions at the PCC, from which histograms can be computed to represent the statistical nature of the results. As the 95th percentile of the harmonic distortion at the PCC is the value used in harmonic studies to prove compliance, it is computed and used for comparison to the IEC summation rule results for four case studies.

In case A, the IEC second summation rule underestimates low order harmonics such as the 5th and 7th harmonics and overestimates the 8th harmonic compared to the Monte Carlo method. It is demonstrated that the probability distribution functions of the magnitude and phase angle of the harmonics significantly impact the distribution of the harmonic distortion at the PCC. It is shown in the thesis that the probabilistic phase-correct (Monte Carlo) method provides closer results to the expected results, as seen from measurements, than IEC does, hence with the Monte Carlo method the uncertainty in grid-compliance studies is lower.

In case B, it is studied whether the variation of the grid impedance could lead to grid code violation that could not have been predicted using a fixed grid impedance. The variation of the grid impedance reveals a big difference between the lowest and highest harmonic distortion that could be as high as 5 times, while the error between the probabilistic and IEC summation rule methods could be as twice high. This case concludes that the variation of the grid impedance is an important factor that should not be neglected in harmonic studies.

In case C, the nonlinear behavior of the converter is included in the model and the impact of the frequency coupling phenomenon on the harmonic distortion at the PCC is studied. The phenomenon results in low errors when compared to the probabilistic method, however the error is quite high when compared to IEC summation rule. In case D, the frequency coupling phenomenon is analyzed while varying the grid impedance, which results in higher errors when compared to IEC summation rule. The results of the last two cases support the argument to include the frequency coupling phenomenon in harmonic studies. Therefore, it is concluded that the accuracy of harmonic studies could be improved by including the statistical nature of the wind turbine harmonics, the variation of the grid impedance and the frequency coupling phenomenon of the wind turbine converters.

Contents

Acknowledgements	iii
Abstract	v
List of Figures	ix
List of Tables	1
1 Introduction	1
1.1 Background	1
1.2 Research Objectives	4
1.3 Research Questions	5
1.4 Thesis Outline	6
2 Theoretical Background	7
2.1 Harmonics in OWPPs	7
2.1.1 Harmonic Emissions	7
2.1.2 Harmonic Resonance	8
2.1.3 Harmonic Indices	9
2.1.4 Harmonic Emission Limits	9
2.1.5 Current Industry Practice for Harmonic Emission Studies	10
2.1.6 Harmonic Emission from a Wind Turbine Converter and its Random Behavior	10
2.1.7 IEC Summation Rule Criticism	15
2.2 Statistics Fundamentals	16
2.2.1 Probability Distribution Functions (PDFs)	16
2.2.2 Law of Large Numbers	17
2.2.3 Central Limit Theorem	17
2.2.4 Monte Carlo Simulation	17
3 Modelling of the OWPP for Harmonic Studies	19
3.1 Wind Turbine Harmonic Sources Literature Review	19
3.1.1 WTs Harmonic Currents PDFs	19
3.1.2 Chosen WTs and their harmonic PDFs	21
3.2 Offshore Wind Power Plant Design Basis and Modelling	23
3.2.1 Wind Turbines	26
3.2.2 Pulse Width Modulation (PWM) Filters	29
3.2.3 Wind Turbine Transformer	29
3.2.4 Array Cables	30
3.2.5 Three-Winding Transformer	34
3.2.6 Export Cable Systems	35
3.2.7 Shunt Reactors	38
3.2.8 External Grid	39
3.3 Simplified Model	39
3.4 PowerFactory Harmonic Analysis and Simulation	40
3.4.1 Power Load Flow	40
3.4.2 Harmonic Load Flow	41
3.4.3 Frequency Sweep	41
3.4.4 Python Scripting	42

4	Results and Discussions	45
4.1	Simulation and Network Analysis	45
4.1.1	Monte Carlo Simulation	45
4.1.2	OWPP Amplification Analysis	46
4.1.3	OWPP Network Analysis	49
4.2	Case A (linear and fixed grid impedance)	54
4.2.1	Background	54
4.2.2	Simulation Results	54
4.2.3	Case A Conclusion	58
4.3	Case B (linear and variable grid impedance)	60
4.3.1	Background	60
4.3.2	Simulation Results	60
4.3.3	Case B Conclusion	70
4.4	Case C (non-linear and fixed grid impedance)	72
4.4.1	Background	72
4.4.2	Modelling in PowerFactory and Coding in Python	73
4.4.3	Simulation Results	75
4.4.4	Case C Conclusion	77
4.5	Case D (non-linear and variable grid impedance)	79
4.5.1	Background	79
4.5.2	Simulation Results	79
5	Conclusion and Future Work	87
5.1	Conclusion	87
5.2	Future Work	88
A	Appendix	91
A.1	Amplification Factor and Network Impedance Verification	91

List of Figures

1.1	Wind Power Capacity in Europe	1
1.2	Forecast of Wind Power Installation in Europe	2
1.3	Typical Offshore Wind Power Plant	3
1.4	Harmonic Propagation in Offshore Wind Power Plant	4
2.1	a) Parallel and b) Series Resonance Circuits	8
2.2	Harmonics Categories	11
2.3	a) WT Thévenin Equivalent b) WT Norton Equivalent	12
2.4	Wind Turbine Generator Back-to-Back Converter	13
2.5	Normal Distribution	16
3.1	Wind Turbine Generator Types	22
3.2	The PDFs of the Harmonic Current Magnitude	23
3.3	The PDFs of the Harmonic Current Phase Angles	23
3.4	Offshore Wind Power Plant Schematic	24
3.5	Single Line Diagram of Group 1 WTs	25
3.6	Single Line Diagram of Offshore System	25
3.7	Single Line Diagram of Onshore System	26
3.8	WT Positive Sequence	27
3.9	WT Negative Sequence	27
3.10	WT Zero Sequence	27
3.11	Wind Turbine Impedance	28
3.12	Power Transformer Model in Frequency Domain	29
3.13	WT Transformer Frequency-Dependent Resistance (Example)	30
3.14	<i>TypCabmult</i> Array Cable-General	32
3.15	<i>TypCabmult</i> Array Cable-Pipe Definitions	33
3.16	<i>TypCabmult</i> Array Cable-Conductor Coordinates	33
3.17	Three-Winding Transformer HV-LV Frequency-Dependent Resistance (Example)	35
3.18	Three-Winding Transformer HV-LV Frequency-Dependent Reactance (Example)	35
3.19	Three-Winding Transformer LV-LV Frequency-Dependent Resistance (Example)	35
3.20	Three-Winding Transformer LV-LV Frequency-Dependent Reactance (Example)	36
3.21	Example of a Major Section of a Cross-Bonded Cable	37
3.22	An Example of an External Grid Frequency-Dependent Impedance (similar to the impedance used in the thesis)	39
3.23	Simplified Model	40
3.24	Python Script Flow Chart	43
4.1	The Iteration Graph	46
4.2	Amplification Factor- Deterministic Magnitude Scenario	47
4.3	Amplification Factor- Random Magnitude Scenario	48
4.4	Amplification Factor- Random Phase Angle Scenario	48
4.5	External Grid Background Distortion	49
4.6	Amplification Factor- Background Distortion Impact Scenario	49
4.7	OWPP Impedance Matrix- Magnitudes	50
4.8	OWPP Impedance Matrix- Phase Angles	51
4.9	PCC Impedance Matrix- Magnitudes	52
4.10	PCC Impedance Matrix- Phase Angles	52
4.11	Simple Wind Farm Model	53
4.12	Aggregated Simple Wind Farm Model	53

4.13 OWPP Amplification Analysis	53
4.14 The 95 th Percentile of the 5 th Harmonic Order	55
4.15 The 5 th Harmonic Order Histogram	56
4.16 The 95 th Percentile of the 7 th Harmonic Order Scenarios	57
4.17 The 7 th Harmonic Order Histogram	57
4.18 The 95 th Percentile of the 8 th Harmonic Order Scenarios	58
4.19 The 8 th Harmonic Order Histogram	59
4.20 Background Impedance Loci- Case B	60
4.21 95 th Harmonic Distortion of the 5 th Harmonic Order on Impedance Loci- Monte Carlo	61
4.22 Comparison of the 95 th Harmonic Distortion of the 5 th Harmonic Order between Monte Carlo and IEC methods	62
4.23 95 th Harmonic Distortion of the 5 th Harmonic Order on Impedance Loci- IEC Method	63
4.24 The Harmonic Gain Impedance Matrix for the 5 th Harmonic Order	63
4.25 The PCC Impedance Matrix for the 5 th Harmonic Order	64
4.26 The PCC Resistance and Reactance for the 5 th Harmonic Order	64
4.27 95 th Harmonic Distortion of the 7 th Harmonic Order on Impedance Loci-Monte Carlo	65
4.28 Comparison of the 95 th Harmonic Distortion of the 7 th Harmonic Order between Monte Carlo and IEC methods	66
4.29 95 th Harmonic Distortion of the 7 th Harmonic Order on Impedance Loci- IEC Method	66
4.30 The Harmonic Gain Impedance Matrix for the 7 th Harmonic Order	67
4.31 The PCC Impedance Matrix for the 7 th Harmonic Order	67
4.32 The PCC Resistance and Reactance for the 7 th Harmonic Order	68
4.33 95 th Harmonic Distortion of the 8 th Harmonic Order on Impedance Loci-Monte Carlo	69
4.34 Comparison of the 95 th Harmonic Distortion of the 8 th Harmonic Order between Monte Carlo and IEC methods	70
4.35 95 th Harmonic Distortion of the 8 th Harmonic Order on Impedance Loci- IEC Method	70
4.36 The Harmonic Gain Impedance Matrix for the 8 th Harmonic Order	71
4.37 The PCC Impedance Matrix for the 8 th Harmonic Order	71
4.38 The PCC Resistance and Reactance for the 8 th Harmonic Order	72
4.39 The Non-Linear Model of the Converter	73
4.40 Coupling Admittance $Y_{c1}(\omega)$ for the Negative-Sequence Harmonics	75
4.41 Coupling Admittance $Y_{c1}(\omega)$ for the Positive-Sequence Harmonics	75
4.42 Flow Chart of Case C Python Code	76
4.43 5 th Order Harmonic Distortion Histogram	77
4.44 7 th Order Harmonic Distortion Histogram	77
4.45 95 th Percentile of Harmonic Distortion for Case A versus Case C	77
4.46 95 th Percentile of Harmonic Distortion for IEC versus Case C	78
4.47 95 th Harmonic Distortion of the 5 th Harmonic Order on Impedance Loci-Monte Carlo Case D	79
4.48 Comparison of the 95 th Harmonic Distortion of the 5 th Harmonic Order between Cases D and B (Monte Carlo VS. Monte Carlo)	81
4.49 Comparison of the 95 th Harmonic Distortion of the 5 th Harmonic Order between Cases D and B (Monte Carlo VS. IEC)	81
4.50 The Error in the 95 th Harmonic Distortion of the 5 th Harmonic Order between Cases B and D (Monte Carlo VS. Monte Carlo)	82
4.51 The Error in the 95 th Harmonic Distortion of the 5 th Harmonic Order between Cases B and D (IEC VS. Monte Carlo)	82
4.52 95 th Harmonic Distortion of the 7 th Harmonic Order on Impedance Loci-Monte Carlo Case D	83
4.53 Comparison of the 95 th Harmonic Distortion of the 7 th Harmonic Order between Cases D and B (Monte Carlo VS. Monte Carlo)	84
4.54 Comparison of the 95 th Harmonic Distortion of the 7 th Harmonic Order between Cases D and B (Monte Carlo VS. IEC)	84
4.55 The Error in the 95 th Harmonic Distortion of the 7 th Harmonic Order between Cases B and D (Monte Carlo VS. Monte Carlo)	85
4.56 The Error in the 95 th Harmonic Distortion of the 7 th Harmonic Order between Cases B and D (IEC VS. Monte Carlo)	85

A.1 Simple 7 WTs Network	93
------------------------------------	----

List of Tables

2.1	IEC Harmonic Emission Limits	9
2.2	The IEC α Exponent Values	10
2.3	Harmonic Sequence	11
2.4	Confidence Level for Normal Distribution Random Variables	18
3.1	Avedøre Holme Wind Farm	20
3.2	Burbo Bank Wind Farm	20
3.3	Gunfleet Wind Farm	20
3.4	The Harmonic Current PDFs Parameters	22
3.5	The 95 th Percentile of the Magnitude the Harmonics	23
3.6	WTG Parameter	26
3.7	Wind Turbine Transformer Specification	29
3.8	3 Core Array Cables' Specifications	34
3.9	Three-Winding Transformer Specification	34
3.10	Offshore and Onshore Cables Specifications	38
3.11	Shunt Reactors Specifications	38
4.1	5 th Harmonic Order Simulation Results	45
4.2	Amplification Factors-Random Magnitude	47
4.3	Amplification Factors-Random Phase	48
4.4	5 th Harmonic Order Scenarios' Results	54
4.5	7 th Harmonic Order Scenarios' Results	56
4.6	8 th Harmonic Order Scenarios' Results	58
4.7	5 th Harmonic Order Monte Carlo Results-Case B	61
4.8	5 th Harmonic Order Results Comparison - Case B	62
4.9	7 th Harmonic Order Monte Carlo Results - Case B	64
4.10	7 th Harmonic Order Results Comparison -Case B	65
4.11	8 th Harmonic Order Monte Carlo Results - Case B	68
4.12	8 th Harmonic Order Monte Carlo Accuracy Results-Case B	68
4.13	8 th Harmonic Order Accuracy Results Comparison - Case B	69
4.14	95 th Percentile of the 5 th and 7 th Harmonic Distortion at PCC-IEC VS. Monte Carlo	76
4.15	5 th Harmonic Order Monte Carlo Results- Case D	79
4.16	5 th Harmonic Order Results Comparison - Case D	80
4.17	7th Harmonic Order Monte Carlo Results- Case D	82
4.18	7th Harmonic Order Results Comparison - Case D	83

Introduction

1.1. Background

The European Union (EU) is targeting to achieve climate-neutrality by 2050 with net-zero greenhouse gas emissions under its commitment to the Paris Agreement [1]. Many critical sectors such as energy, transportation, industry and agriculture are being transformed to assist in meeting the goal. The energy sector in particular has to be decarbonized by increasing the share of the renewable energy sources to replace conventional energy sources in the energy production. Moreover, while the energy consumption is increasing, the future's energy demand is planned to be met by renewable energy [1]. Therefore, large-scale deployment of renewable energy sources such as Wind Power (WP) is at the center of this strategy. Onshore and offshore wind are two of the cheapest energy sources, making future investment advantageous [2].

In 2020, WP supplied 16% of Europe's electricity demand and this figure is expected to increase as the International Energy Agency (IEA) is forecasting WP to be on top of the energy sources supply in Europe by 2027 [2]. Figure 1.1 demonstrates the growth of the WP capacity in Europe over the last 10 years. The capacity increased from 98 Gigawatts (GW) in 2011 to 220 GW in 2020. Currently, 89% of the installation is onshore while the remaining 11% is offshore [3].

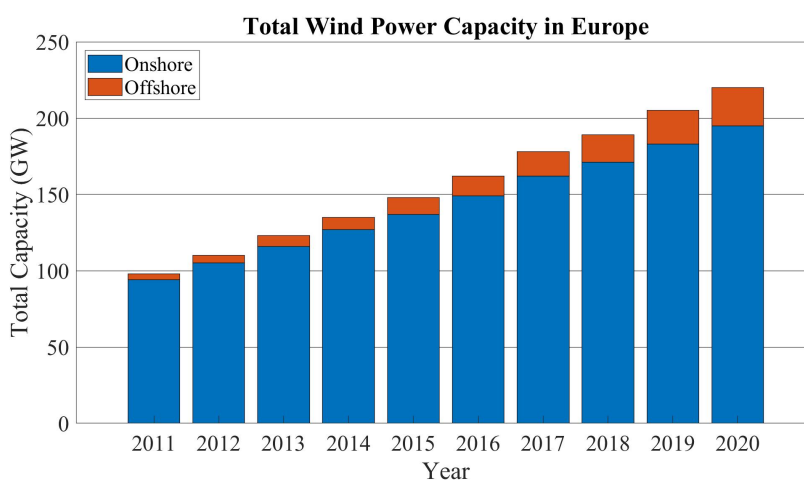


Figure 1.1: Wind Power Capacity in Europe
[3]

The WP capacity is expected to increase to 318 GW by year 2025 [3]. However, the onshore's share of WP is anticipated to drop from the current 89% to 72% in these five years indicating an increase in the offshore installation. Figure 1.2 shows the breakdown of these additional WP installation in the coming five years. The share of Offshore Wind Power (OWP) in the energy mix will continue to increase as it is supported by the available regulatory policies, fiscal incentives and public funding [4]. Moreover, The Offshore Renewable Energy Strategy, which is part of the EU Green Deal, proposed favorable legislation to offshore wind with a target of 400 GW by year 2050 [5].

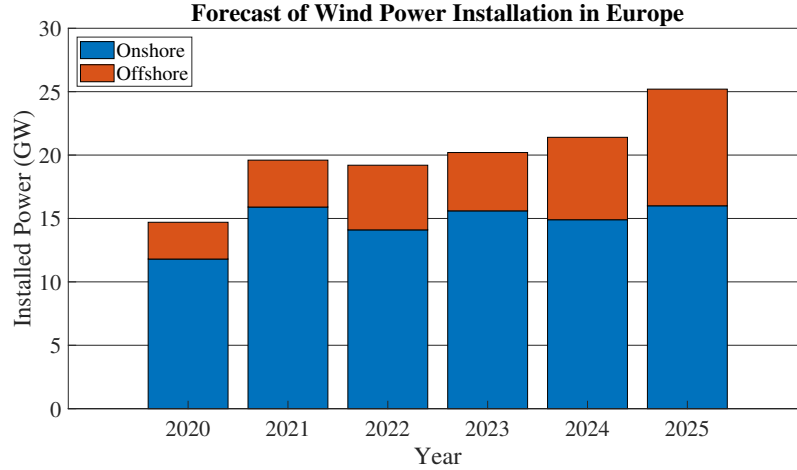


Figure 1.2: Forecast of Wind Power Installation in Europe [3]

There are some advantages and disadvantages for Offshore Wind Farms (OWF) over onshore wind farms that are evaluated when a decision is made with regard to the location of the wind power plant. Some of the advantages include larger areas in the sea, higher average wind speed and less turbulence, all of which allow for higher power capacity installation [4]. Moreover, there is less visual pollution, as the OWF are usually situated far away from the coast. On the other hand, capital expenditure of OWF is usually higher than onshore wind farms since the former requires expensive submarine cables and/or converter stations and sub-sea foundations [4]. In addition, the accessibility to the sea to perform maintenance becomes more difficult and adds to the operational expenditure [4]. Nonetheless, the higher capital is sometimes offset by the higher installed capacity that keeps the Offshore Wind Farms favorable in many cases [4].

A typical Offshore Wind Power Plant (OWPP) as shown in figure 1.3 consists of clusters of many Wind Turbines (WTs) connected by array cables in a radial formation, or other formations, to an offshore substation or connection point. High voltage export submarine cables are laid from the offshore substation to an onshore substation. From there, high voltage onshore cables are used to export the generated electricity to the Point of Common Coupling (PCC) where the OWPP is formally connected to the grid.

The OWPP can be connected to the onshore grid by either High Voltage Alternating Current (HVAC) or High Voltage Direct Current (HVDC) transmission cables with converter stations. The decision for each OWPP will be made based on many variables such as the available technologies, economic evaluation, voltage level and the transmitting distance. The main features of HVDC transmission system are [6]:

- The HVDC cables have lower power losses and voltage drop, hence higher efficiency.
- There is no resonance points between the transmission system and the AC transformers/ cables.
- They require converter stations which increase the capital cost of OWPP.
- Although, the converters have high switching losses, the total losses could be lower than the losses of HVAC transmission system as seen in [7].

On the other hand, HVAC transmission systems have the following features [6]:

- Lower substation costs leading to a lower capital expenditure.

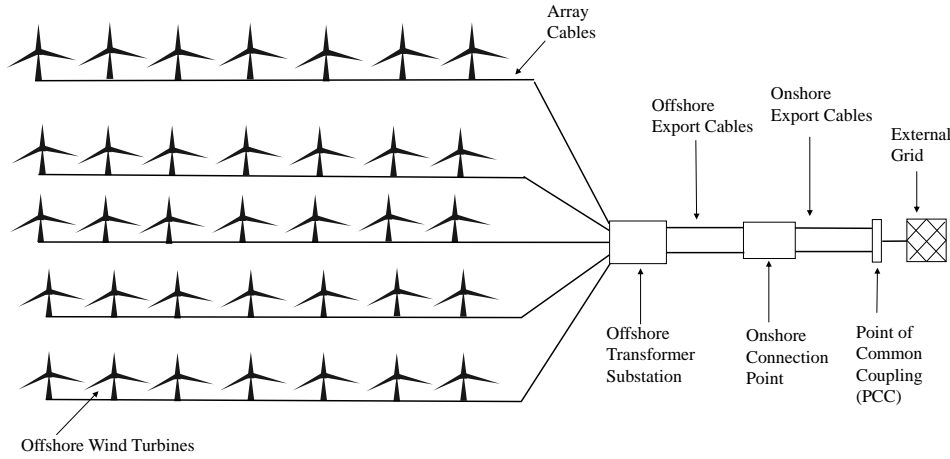


Figure 1.3: Typical Offshore Wind Power Plant

- There could be resonance points between the transmission system and other AC component in OWPP due to the cable's high capacitance that could amplify the harmonic distortion.
- HVAC cables' high capacitance generates considerable reactive current in the network mandating compensation devices to be installed within the OWPP.

In [4], HVAC transmission system is recommended for OWPP with distances between 15 and 50 km, after which the limitations of the system become more apparent and HVDC transmission system becomes a viable solution. However, the sensitivity analysis performed in [6] revealed a break-even point of about 90 km to the onshore substation. Regardless of the limitations of HVAC transmission systems, many OWPP are HVAC-connected for similar or longer distances. For example, Hornsea Two Offshore Wind Farm in the United Kingdom is located approximately 89 km from the shore [8] and Gemini Offshore Wind Farm in the Netherlands is connected via approximately 100 km HVAC ring cabling system [9].

Electrical power systems are expected to supply perfect sinusoidal voltage and current signals to customers to protect and properly operate their electrical equipment and appliances. However, the sinusoidal waveforms could sometimes have deviations that are expressed as harmonic distortion [10]. The excessive harmonic distortion could have devastating impact on electrical systems that could lead to failure of equipment or instabilities [11]. The harmonic current and voltage could cause overheating of transformers and power cables, malfunction of protection equipment, and incorrect reading of meters [10].

Active equipment such Power Electronic Converters (PECs) used in modern-days WTs are considered as a source of harmonic emission. Their nonlinear operation and high-frequency switching, amongst other factors, cause the injected currents to have non-fundamental components that can propagate within the OWPP [10]. Moreover, the OWPP has long submarine cables with high capacitance and other inductive electrical equipment such as transformers that could create resonance peaks at low frequencies leading to unexpected harmonic distortion amplification [12]. Furthermore, the OWPP could be connected to weak grids in remote areas that have time-varying impedance, which when connected with the impedance of the OWPP can create other unforeseen resonance points [13]. Moreover, there is background distortion coming from the external grid that should be considered when performing harmonic analysis. These conditions could lead to unacceptable harmonic distortion levels at the PCC as shown in figure 1.4, and hence violate grid's limits set by the Transmission System Operators (TSOs). Therefore, if not prevented or mitigated, harmonic distortion could present negative impact on the OWPP and the external grid, some of these are [10]:

- Lowering the generation and transmission efficiency of the OWPP.
- Thermal stress of electrical equipment that reduces their life-cycle.
- Failures of OWPP components and protection devices, and hence reducing the reliability of the OWPP.

- Possible amplification of harmonics due to series and parallel resonances.

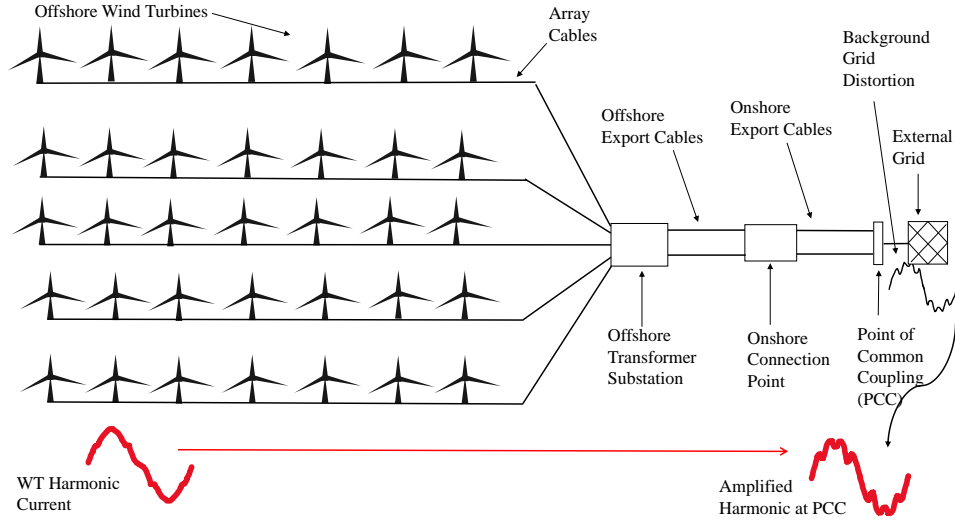


Figure 1.4: Harmonic Propagation in Offshore Wind Power Plant

OWPP designers could be required to install passive filters to mitigate the impact of harmonic distortion on the grid. For example, in [14] a high-pass filter was required to be installed and tuned to the 5th harmonic order to mitigate the excessive harmonic emission and meet the permissible limits. In [15], passive and active filters are discussed and compared for their implementation in OWPP. Although the passive filter have low cost compared to the active filters, but they have many disadvantages such as the big size, additional losses and difficulties in re-tuning. On the other hand, active filters have still a high cost and is a developing technology. Thus, it is important that the need for filters is avoided by design of the OWPP by avoiding critical resonance points that amplify WTs harmonic emissions or background distortion in the grid.

In light of the above, harmonic emission estimation at the PCC in HVAC-connected Offshore Wind Power Plant will be studied in this thesis as harmonic distortion problems in similar wind farms have provided a great opportunity for further research [16–18].

1.2. Research Objectives

The industry mandates the measurement and assessment of harmonics generated from WTs by following applicable standards such as IEC 61400-21 and to include the results in the power quality certificates prior to grid-connection approval [10]. However, the required information might not be fully available for OWPP designers to perform comprehensive harmonic studies at OWPP scale during the design stage due to confidentiality of data or lack of measurements [13]. Moreover, carrying out a detailed harmonic analysis is a complex problem as it requires detailed modelling of the different components in OWPP [10]. Measuring and processing harmonic data of OWPP is difficult and can only be performed after the start-up of the plant. Thus, these measurements cannot be utilized in proving compliance to the grid's code. However, harmonic studies are required to be performed as prerequisite to the grid-connection to demonstrate the compliance to the harmonic limits set by the TSOs [10].

The current practice in the industry is to utilize the second summation rule outlined in IEC 61000-3-6. The summation rule requires the OWPP developers to only use the 95th percentile of the magnitude of the WT harmonic current while the effect of the phase angle variation and the possible harmonic cancellation in the wind farm is approximated by elevating the current magnitude to a certain exponent. This procedure was designed for classical power systems in which PECs were not widely deployed. However, there is enough evidence in the literature today that the summation rule does not provide accurate results when used with the high penetration of PECs, which has been shown in [16–19]. For example, in [16] the IEC summation rule underestimates the low frequency harmonic orders such as the 5th, 7th and 13th while it overestimates the higher order switching harmonics, i.e. 45th and 47th.

Therefore, it is imperative that other methods to determine the harmonic distortion in OWPP are developed in the industry and the scientific community by capitalizing on the understanding of the behavior of

the harmonic emissions of WT in OWPP and how they react to the resonant points in the harmonic emission studies. The following important points are highlighted:

- The harmonic currents have complex values with magnitude and phase angle for each harmonic order. Thus, the harmonic emission studies should consider both values.
- Each WT could have different magnitude and phase angle based on its PECs characteristics and operating points. Hence, the harmonic currents could add up, subtract, diminish or amplify, which would impact the harmonic distortion at the PCC. Thus, assigning one value to represent the harmonic emission from all WTs would not represent their actual behavior.
- The harmonic currents and their fundamental components are continuously changing in time due to the variations in the OWPP configurations, WTs operating points [19, 20], and PECs nonlinear behavior [21]. Thus, the magnitudes and the phase angles of the harmonic currents are not deterministic values, but statistically random variables [22] and should be represented as such.
- There is much evidence from OWPP measurements that the magnitude and phase angles of the harmonic currents are random variables and have Probability Distribution Functions (PDFs) [10, 18, 19, 22]. Therefore, harmonic emission studies should be performed based on probability theory [18, 21].

The main research objective of this thesis is to determine if the summation of harmonics based on probability theory when considering both the magnitude and phase angle (phase-correct studies) of the harmonic current would provide more accurate results than the IEC summation rule. The following main steps will be taken to achieve the thesis objective:

- An OWPP will be modelled using DIgSilent PowerFactory software for harmonic studies.
- Probability Distribution Functions of WT harmonic current magnitude and phase angle will be used from the literature to represent the possible variations of the values in the model.
- Various harmonic orders will be studied under different conditions using Monte Carlo simulation.
- Recommendations will be made in light of the obtained simulation results.

1.3. Research Questions

The outlined research objective can be accomplished by answering three main questions:

1. How does the harmonic grid compliance results compare when studies are performed based on probability distribution function of magnitude and phase angle versus studies performed with the summation rule.
2. How does the variation of the grid impedance impact the harmonic distortion level at the PCC.
3. How does the presence of frequency coupling between harmonics impact the distortion level at the PCC compared to the frequency decoupled harmonic cases.

As mentioned previously, IEC summation rule does not consider the phase angle directly in the harmonic studies, but compensates for it through the use of an exponent. It also does not consider the statistical variation of harmonics, however considers the 95th percentile of the magnitude only. Thus, the first research question is to determine the differences between the IEC and phase-correct studies. The answer of the question will provide insights on how the statistical variation of the magnitude and phase angle of harmonic current yield different results to the IEC summation rule. The results of this case would demonstrate whether probability theory can be considered as an accurate method to measure the harmonic distortion.

The harmonic emission in OWPP can come from the WT and the background grid. The latter's impedance can change based on the connected loads, emergencies and other conditions and an impedance loci is used to represent this behavior by TSOs. Therefore, the answers from the second question will provide insights on how the grid's impedance variations impact the harmonic distortion in the IEC and phase-correct studies.

The first two questions are answered with the assumption that each harmonic is independent from each other, hence decoupled. While in reality different harmonic orders are coupled [13, 23] and can impact each

other, which would lead to a different harmonic distortion level at the PCC. Thus, the answer to the third question will provide knowledge on how the frequency coupling impacts the harmonic distortion level at the PCC, and whether this phenomenon should be included in harmonic studies of OWPP.

The research questions will be answered by implementing four case studies in DIgSilent PowerFactory software. The case studies are:

1. **Case A:** linear (frequencies are independent) and fixed grid impedance.

A fixed grid impedance will be used in the PowerFactory model to determine the harmonic distortion at PCC for each harmonic order separately. The harmonic spectrum will be randomly taken from the probability distribution functions of each harmonic order in an automated Monte Carlo simulation.

2. **Case B:** linear (frequencies are independent) and variable grid impedance.

Case A will be repeated with variable grid impedance implemented using a grid impedance loci. Each harmonic order will be simulated separately to determine the harmonic distortion at the PCC with the variable grid impedance.

3. **Case C:** non-linear (frequencies are coupled) and fixed grid impedance.

This case will examine the coupling relationship between the different harmonics with a fixed grid impedance. As each harmonic order can impact the distortion of another one, it is important to examine and understand how it can be defined in an OWPP. Thus, the real contribution of harmonic distortion from a specific harmonic can be known precisely.

4. **Case D:** non-linear (frequencies are coupled) and variable grid impedance.

This case is similar to case C but will be examined with variable grid impedance implemented by an impedance Loci in the model.

1.4. Thesis Outline

1. **Chapter 1: Introduction**

This chapter covers the background, research objectives and questions and the case studies for the thesis.

2. **Chapter 2: Theoretical Background**

The second chapter explains the theoretical background of harmonics in OWPP, their propagation in OWPP, the standard distortion limits, the current industry practice for harmonic emission studies, and the harmonic emission from WT converter and its statistical behavior. A review of some concepts in probability theory, statistics and Monte Carlo simulation are also included to describe the methods used in the thesis.

3. **Chapter 3: Modelling of the OWPP for Harmonic Studies**

The third chapter starts with the literature review of the probability distribution functions of the harmonics utilized in the OWPP model. Then, it explains the modelling of the OWPP in DIgSilent PowerFactory software for harmonic studies. Then, it provides an overview of various PowerFactory simulations and Python scripting interface.

4. **Chapter 4: Results and Discussions**

The fourth chapter presents the results of the four cases outlined in the research questions and explains the findings from the simulations.

5. **Chapter 5: Conclusion and Future Work**

The last chapter presents the main recommendations from the thesis and its limitations as well the future work that could be accomplished based on the thesis's findings.

2

Theoretical Background

2.1. Harmonics in OWPPs

Two main harmonic analyses are performed during the design stage of OWPP: harmonic emission and harmonic resonance [13]. Harmonic emission studies address the injections of periodic distorted current waveforms by the wind turbines into the OWPP and analyze their amplifications at the PCC to determine if harmonic limits are met. In contrast, harmonic resonance studies analyzes the OWPP impedance against the frequency spectrum to detect peaks and dips that could interact with harmonic currents and lead to higher harmonic amplification at the PCC [13]. Nevertheless, in this thesis, it is shown how, actually, looking at the equivalent impedance of the OWPP, of the grid, or the combination of both is not enough to determine the amplification that the harmonics will have in the network. This is further explained in Chapter 4.

2.1.1. Harmonic Emissions

Alternating Current (AC) waveforms are ideally pure sinusoidal with a constant magnitude [24]. The deviation from these perfect sinusoidal current waveforms for one cycle from the grid frequency is regarded as harmonic distortion that could be emitted into the power network [24]. Nonlinear devices draw or inject non-sinusoidal currents that have both fundamental and non-fundamental current components. They are considered as one of the main causes for harmonic distortion in power systems [10]. Moreover, power electronic converters used in modern-day wind turbines are active components that can operate at frequencies other than the fundamental frequency creating harmonic distortion [10].

The high-frequency switching of PECs, saturation of inductors and non-linear behavior are among the main reasons of harmonic emissions in OWPP [13]. The power electronic converters have switches that go ON and OFF at the switching frequency, which make the harmonic currents injections by WTs inevitable [25]. In addition, there are harmonic emissions from the external grid into the Point of Common Coupling that shall be considered when performing harmonic studies. The OWPP is considered as a low-impedance path to low frequency harmonics from the grid where low-frequency harmonics tend to propagate from the grid to the OWPP [26], which is known as sink effect [13]. On the other hand, the high-frequency harmonics tend to propagate from the OWPP to the grid [26]. Therefore, analyzing the grid's harmonic distortion contribution at the PCC is very important to accurately determine the Total Harmonic Distortion.

Harmonics are periodic and they can be decomposed using Fourier series into their fundamental and higher order harmonic components at integer and non-integer harmonic [20]. Mathematically, the Fourier series provide the relationship between the time and frequency domains, and it can be represented for a periodic function $f(t)$ with period T and harmonic order h as in equation 2.1 [20]:

$$f(t) = C_0 + \sum_{h=1}^{\infty} C_h \sin(h\omega t + \theta_h) \quad (2.1)$$

where the angular frequency is:

$$\omega = \frac{2\pi}{T} \quad (2.2)$$

The magnitude of the DC component and peak value of the harmonic component C_h are, respectively:

$$C_0 = \frac{a_0}{2} \quad (2.3)$$

$$C_h = \sqrt{a_h^2 + b_h^2} \quad (2.4)$$

The phase angle of the harmonic current is:

$$\theta_h = \tan^{-1} \frac{a_h}{b_h} \quad (2.5)$$

and the Fourier coefficients a_0 , a_h and b_h are:

$$a_0 = \frac{2}{T} \int_{-T/2}^{T/2} f(t) dt \quad (2.6)$$

$$a_h = \frac{2}{T} \int_{-T/2}^{T/2} f(t) \cos(h) dt \quad (2.7)$$

$$b_h = \frac{2}{T} \int_{-T/2}^{T/2} f(t) \sin(h) dt \quad (2.8)$$

2.1.2. Harmonic Resonance

The harmonic distortion level at the PCC of an Offshore Power Plant is largely dependent on the harmonic resonance. Resonance occurs when inductive reactance and capacitive reactance are equal in absolute value [10]. The fact that a typical OWPP consists of many HVAC submarine cables that have high capacitance and many inductive transformers makes resonance analysis an important objective. Resonance can be parallel or series where the former is a high impedance and the latter is a low impedance to the flow of harmonic current [10].

Parallel resonance points happen when the capacitance and inductance of the network at a specific frequency are equal in magnitude and they have high impedance categorized by peaks [10]. Therefore, harmonic voltage distortions at these peaks could be very high regardless of how small or big the harmonic currents are. On the other hand, when the reactance of the inductor and the capacitor are equal at a particular frequency, but with opposite sign then a series resonance will be created that is categorized as a dip in the impedance [10]. Therefore, series resonance can be serious in creating high harmonic currents even for small harmonic voltage distortion such as power grid into the OWPP [13]. Figure 2.1 shows the simplified circuits of both parallel and series resonance circuits. The resonance frequency is calculated as in equation 2.9 [25].

$$f_r = \frac{1}{2\pi\sqrt{LC}} \quad (2.9)$$

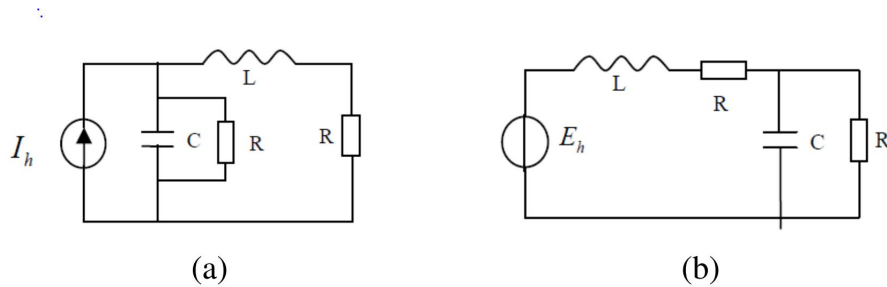


Figure 2.1: a) Parallel and b) Series Resonance Circuits

[13]

2.1.3. Harmonic Indices

Harmonic emission is measured and represented by the Total Harmonic Distortion (THD) that includes harmonic distortion from all the harmonic orders under assessment [25]:

$$THD = \frac{\sqrt{\sum_n^h V_n^2}}{V_1} \times 100 \quad (2.10)$$

where h is the highest harmonic order under assessment, V_1 is the fundamental frequency voltage at the measurement point and V_n is the harmonic voltage at the n^{th} harmonic order [25].

The Harmonic Distortion (HD) of a waveform describes the individual harmonic contribution at a particular harmonic order [27]:

$$HD_h = \frac{V_h}{V_1} \times 100 \quad (2.11)$$

The voltage can be replaced with current in equations 2.10 and 2.11 to measure the harmonic current distortion in lieu of the voltage harmonic distortion.

2.1.4. Harmonic Emission Limits

IEC 1000-3-6:1996 has three levels to regulate the harmonic emission limits [13].

- Compatibility levels: These are the reference values for the emissions from the consumer and the grid. They are usually based on the 95% percentile of the whole systems.
- Planning levels (L_{hHV}) : These are utilized to assess the impact from all consumers including the background grid distortion on the supply system and could be equal or smaller than the compatibility levels to ensure proper functioning of the system.
- Individual emission limits (E_{Uhi}) : This is the allowed contribution of harmonic emission from each power system installation as part of the planning level.

The planning levels are specified by IEC 61000-3-6:2008 while the individual emission limits are calculated using the below equation from IEC 1000-3-6:1996 [13]:

$$E_{Uhi} = L_{hHV} \sqrt[\alpha]{\frac{S_i}{S_t}} \quad (2.12)$$

where α is the summation factor coefficient presented in table 2.2, S_i is the installed power of the OWPP and S_t is the total power at the PCC. Table 2.1 shows the planning levels and individual emission limits in percentage that will be compared against the results. These levels can be converted to voltage by multiplying them by the rated voltage of the measured terminal, i.e. PCC in this thesis.

Harmonic Order	Planning levels (L_{hHV}) %	Individual emission limits (E_{Uhi}) %
5 th Harmonic	2.00	0.65
7 th Harmonic	2.00	0.65
8 th Harmonic	0.40	0.13

Table 2.1: IEC Harmonic Emission Limits

The harmonic emissions at the PCC could be a result of harmonic emission from the OWPP and the external grid, therefore the planning levels are used to assess the harmonic distortion and whether the system is in compliance. Moreover, it is required to assess the harmonic distortion coming from the power system installation only, i.e. the OWPP, by comparing it to the individual emission limits. The planning levels are used in the thesis for the scenarios where the background harmonic distortions are included while the individual emission limits are used when they are excluded.

2.1.5. Current Industry Practice for Harmonic Emission Studies

OWPPs are required to be modelled accurately in a software package that can perform harmonic calculations to estimate the Total Harmonic Distortion and individual Harmonic Distortion prior to grid-connection to prove compliance to the grid code. The infrastructure of the OWPP such as the WTs, transformers, array cables, and export cables are all required to be modelled in the frequency domain, or time domain, in order to perform the harmonic emission study [16].

The current practice in the industry is to perform the pre-compliance harmonic assessment according to the second summation rule in IEC 61000-3-6 given in equation 2.13 [16, 17] to estimate the harmonic current distortion at the PCC. The results of the study are essential in order to propose and implement mitigation measures such as active or passive filters, or to modify some of the OWPP design parameters to meet the grid code set by the Transmission System Operators. However, active and passive filters could be expensive, require large installation area, increase power losses or even still be a developing technology [14, 15], and modification of the OWPP design could be a lengthy-process and expensive. Therefore, it is crucial that the results from the harmonic study are as accurate as possible to eliminate the possibility of using an over-sized/undersized filters or OWPP modification, and to operate the OWPP within the harmonics allowable limits [17].

$$I_h = \sqrt[\alpha]{\sum_{n=1}^N I_{h_n}^\alpha} \quad (2.13)$$

The same equation is also used for harmonic voltage by replacing the current with voltage values. The parameters of the equation are [16]:

- I_h is the resulting harmonic current for the h^{th} harmonic order. This value is the 95% percentile.
- I_{h_n} is the 95th percentile of the harmonic current magnitude of each harmonic source.
- α is the summation factor coefficient that is assigned according to the harmonic order as shown in table 2.2 to indirectly compensate for the phase angle of the harmonic current.
- N is the number of wind turbines in the wind farm.

Harmonic Order	α exponent value
$1 < h < 5$	1
$5 \leq h \leq 10$	1.4
$h > 10$	2

Table 2.2: The IEC α Exponent Values [16]

The IEC second summation rule assumes worst case scenario for the harmonic current injection, and hence the use of the 95th percentile. Each harmonic source in the network will be assumed to be injecting the 95th percentile of the harmonic current I_{h_n} . The α coefficient is utilized to indirectly compensate for the phase angle of the harmonic current, and thus the summation can be between arithmetic and geometric depending on the harmonic order as seen in table 2.2. The resulting harmonic current I_h is the sum of all harmonic currents from all harmonic sources under assessment. This current represents the harmonic current distortion coming from the OWPP. In addition to this current, there is a background harmonic distortion that should be added to compute the harmonic distortion at the PCC.

2.1.6. Harmonic Emission from a Wind Turbine Converter and its Random Behavior

Wind turbine harmonics can be classified into three categories as presented in figure 2.2:

1. **Baseband Harmonics:** These are the harmonics that WT injects at low frequencies such as the 5th and 7th harmonics. They are usually impacted by the grid distortion to a certain degree, and therefore this impact has to be decoupled in order to analyze baseband harmonics in harmonic studies [10].
2. **Switching Harmonics:** These are integer multiple of the switching (carrier) frequency of the Pulse Width Modulation of the converter [10].

3. **Sideband Harmonics:** These are the harmonics that appear around the switching frequency, and its integer multiples, of the converter, i.e. $f_{sw} \pm nf_0$ Hz where f_{sw} is the switching frequency, f_0 is the fundamental frequency, and $n=1, 2, 3$, etc. They are impacted by the modulation ratio m_f of the converter [10]. The sideband harmonics are dependent on the active and reactive power in addition to the fundamental voltage [10].

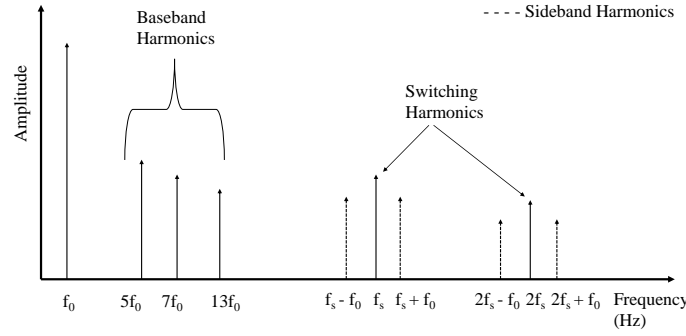


Figure 2.2: Harmonics Categories

In this thesis, it is assumed that harmonics appear in their natural sequence as follows and shown in table 2.3:

- Positive sequence: $3h+1$
- Negative sequence: $3h+2$
- Zero sequence: $3h$

Harmonic Order	1	2	3	4	5	6	7	8	9	10	11	12	13
Harmonic Sequence	Positive	Negative	Zero	Positive	Negative	Zero	Positive	Negative	Zero	Positive	Negative	Zero	Positive

Table 2.3: Harmonic Sequence

[28]

The primary delta side of the WT step-up transformer traps the flow of triplen zero-sequence harmonics into the system and thus they are usually not analyzed in harmonic studies [24, 29]. Moreover, in general, even harmonics can appear if there is asymmetry between the half-waves, i.e. between the positive and negative halves of a cycle [30]. The waveform produced by the PWM is expected to have a perfect half-wave symmetry, which would lead to cancellation of even harmonics. However, it is seen in the literature that manufacturing's tolerance can impact the firing angle of the switches and could create even harmonics [28]. Specifically, as the switches are not perfectly the same, the voltage drop across them may differ, making the converter to inject even and odd harmonics [18]. Even harmonics have been measured in real wind farms as shown in [19, 22, 31, 32], thus, and despite their potential low magnitude, should be considered in harmonic studies. Furthermore, even if the WT harmonic emission at even orders is low, the potential for amplification and, therefore, for grid code non-compliance, persists.

Wind Turbine harmonics can be further classified into characteristic and non-characteristic harmonics. The characteristic harmonics are the normal harmonics generated by the converter in balanced networks [10]. They are dependent on the converter topology and switching patterns, and they are correlated among WTs by the modulation technique of the Pulse-Width Modulation (PWM) of the converter [10]. On the other hand and due to imbalance in the network, non-characteristics harmonic can be emitted by the WTs converters into the network [10]. The operating point and control scenarios of each individual converter determine the non-characteristic harmonics that are associated with the Phase Locked Loop (PLL) and control loops of the converter that are directly impacted by the imbalance in the network [10].

Earlier works on harmonic studies represented the converter of the wind turbine by an ideal current source that injects constant harmonic current into the OWPP and then harmonic distortion at the PCC is measured. This modelling approach was widely used when the power system was dominated by load-commutated converters and diode rectifiers where this assumption was a valid simplification [29]. In particular, using a constant current source can be a valid simplification in cases in which the non-characteristic harmonics are negligible. The current source, in this case, represents the characteristic harmonics, which are the harmonics that the converter will inject regardless of the voltage distortion or imbalance at its terminals. In the case of wind turbine converters, however, it has been shown that the non-characteristic harmonics can be considerable. Depending on the voltage distortion at its terminals, the converter might generate different harmonics [13]. It was demonstrated afterwards that earlier harmonic studies of wind farms that implemented a constant current source to represent the converter behavior did not produce accurate results [10]. On the contrary, it has been proven in the literature that it is necessary to include an impedance in parallel to the current source, making a Norton equivalent (or, alternatively, a Thévenin equivalent can be used).

The impedance is fundamentally a linearized input-to-output relationship of the converter, where the input is the distorted or unbalanced voltage and the output is the current that the converter generates as a response [13]. This impedance varies with frequency, which means that it is recommended to represent the converter with a Thévenin or Norton equivalent circuit as shown in figure 2.3 for each harmonic order to accurately represent the converter [29, 33].

The impedance represents the dynamic behavior of the WT converter, and therefore, it depends on numerous factors, like the control loops in the converter [13]. The impedance can be extended to represent other parameters such as the filters, the different sides of the converter (grid and rotor sides), series reactor or transformers depending on the modelling approach for the harmonic study [33, 34]. In this thesis, the impedance will only represent the WT converter input-to-output relationship between the converter and the network.

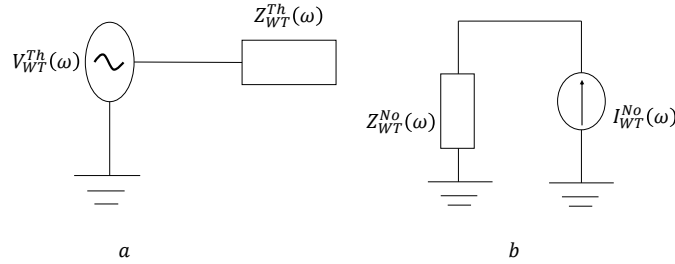


Figure 2.3: a) WT Thévenin Equivalent b) WT Norton Equivalent

In [18] an ideal current source with random magnitude drawn from its probability distribution function was placed at the high voltage side of the transformer in the analyzed OWPP to account for the stochastic nature of the harmonic current in the harmonic study. The authors state that the exclusion of the frequency-dependent impedance from the converter model could lead to problems caused by the current source inability to adapt to changes in the short circuit impedance and to overcome this limitation a parallel impedance of the converter has to be included in the model [18]. Moreover, the harmonic current emission from the converter is not independent from the grid's impedance and this assumption is not well founded for wind farms, and therefore the parallel impedance in the model would account for the grid's impedance impact on the harmonic current. The reason behind this is that when the grid impedance changes, the voltage at the terminal of the wind turbine changes, which leads to changing the current emitted into the network. This impact is compensated for by including the impedance in the converter model [33].

A typical full-scale back-to-back converter utilizes a two-level three-phase Voltage Source Converter (VSC) technology as shown in figure 2.4. The rotor side converter is responsible for maximizing the power extraction, controlling the active power and reactive power [25]. The grid side converter is responsible for controlling the DC link voltage and reactive power [25]. The PWM filter is responsible of minimizing the switching related harmonics injected into the network by the converter, and can have several configurations such as

LCL filter or inductor with several trap filters in parallel.

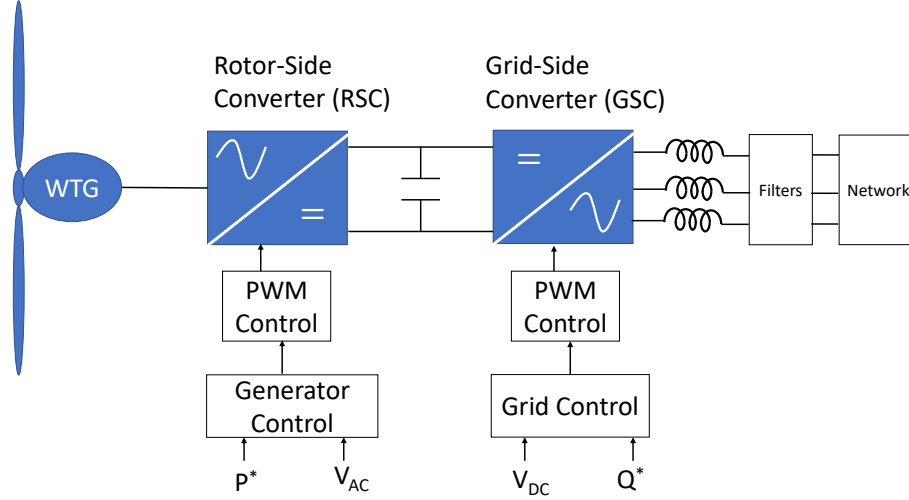


Figure 2.4: Wind Turbine Generator Back-to-Back Converter [25]

The switching process of each phase leg of the converter is controlled by the PWM control that utilizes a sinusoidal reference signal compared to triangular carrier waveform [10]. One of the commonly used PWM method is the asymmetrically regular sample pulse-width-modulation for triangular carrier signal that results in a remarkable harmonics cancellation between the phase legs [10]. The author in [10] derived the converter's voltage for one of the three-phase legs of the Thévenin equivalent based on Fourier series theory for the asymmetrically regular sample pulse-width-modulation as shown in equation 2.14. The first term in equation 2.14 represents the fundamental component and baseband harmonics that are integer multiple of the fundamental frequency [10]. The second term represents the switching harmonic and its integer multiple of the carrier frequency [10]. The last term represents the sideband harmonics [10]. $M = 2V_0/V_{DC}$ is the modulation index where V_0 is the converter output voltage and V_{DC} is the DC link voltage between the two VSC converters, and the frequency ratio is $m_f = \omega_c / \omega_0$ [10]. Both the modulation index and frequency ratio impact the magnitude of the harmonics generated by the asymmetrically samples pulse-width-modulation [10]. When the fundamental voltage at the terminals of the converter changes, the modulation index has to adapt and therefore the harmonics change (although not linearly with the change in the fundamental voltage). Moreover, the fundamental frequency tends to vary overtime due to changes in generation and demand while the carrier frequency is mostly kept constant, which leads to variation in the magnitude of harmonics [10, 20]. In addition, the fundamental frequency variation results in variation in the magnitude of the sideband harmonic [10]. Therefore, it is clear that pulse-width-modulation can lead to random harmonic current injection by the converter.

As the network parameter or configuration is changing over time, the fundamental voltage change, which lead to varying harmonic from the converter. Moreover, it is observed that changing the operating point (i.e. the output power of the converter), whether it is small or big, of the wind turbine would lead to adjusting the modulation index M , and hence it would result in different harmonic injection by the converter [10]. Therefore, the current source in the Norton equivalent in figure 2.3 ought to be represented by a random behavior to capture the statistically varying harmonics [10, 18, 19, 22, 35].

$$\begin{aligned}
V_{az}(t) = & \frac{2V_{DC}}{\pi} \sum_{n=1}^{\infty} \frac{1}{\left[n \frac{\omega_0}{\omega_c}\right]} J_n\left(n \frac{\omega_0}{\omega_c} \frac{\pi}{2} M\right) \sin\left(n \frac{\pi}{2}\right) \cos(n [\omega_0 t + \theta_0]) \\
& + \frac{2V_{DC}}{\pi} \sum_{m=1}^{\infty} \frac{1}{m} J_0\left(m \frac{\pi}{2} M\right) \sin\left(m \frac{\pi}{2}\right) \cos(m [\omega_c t + \theta_c]) \\
& + \frac{2V_{DC}}{\pi} \sum_{m=1}^{\infty} \sum_{n=-\infty, n \neq 0}^{\infty} \frac{1}{\left[m + n \frac{\omega_0}{\omega_c}\right]} \left[J_n\left(\left[m + n \frac{\omega_0}{\omega_c}\right] \frac{\pi}{2} M\right) \sin\left([m + n] \frac{\pi}{2}\right) \cos(m [\omega_c t + \theta_c] + n [\omega_0 t + \theta_0]) \right]
\end{aligned} \tag{2.14}$$

Equation 2.14 represents only one specific modulation technique. However, different modulation techniques could also result in random harmonic as the modulation index would impact the magnitude of the harmonics. However, there are other sources of harmonics caused by the converter such as the dead-time. The dead-time of the converter is defined as the small time period where both the upper and lower IGBT in the converter are not conducting simultaneously [36]. The dead-time is required to avoid short circuit in the DC link between the two VSC converters as shown in figure 2.4; however, it creates harmonic distortion by deviating from the fundamental voltage waveform [36]. A typical dead-time is in the range between 1 and 5 μs [37]. The dead-time pulses can generate odd baseband harmonics ($6h \pm 1$) in the positive- and negative-sequence for three-phase inverter [37], and their phase angles are linearly linked to the phase of the fundamental current [18]. There are many control techniques in the literature to compensate for the dead-time problem; however, as seen in [37], many of these techniques do not fully eliminate the harmonic distortion in the output voltage [37].

In light of the above, harmonic emissions from WTs cannot be represented on a deterministic basis, i.e. the 95th percentile, and both the magnitude and phase angle of the harmonic current present a random behavior [20, 22]. Moreover, it has been shown in the literature based on measurement campaigns that the magnitude and the phase angles are indeed statistically random variables [10, 16, 18, 19, 22, 35], and they should be represented by a probability distribution function. Therefore, the magnitude and phase angle of the harmonic currents will be represented by statistically random variables in this thesis to determine the harmonic distortion at the PCC of an offshore wind farm.

Recent literature has shown that different operating points of the wind turbine would create different harmonic spectrum for each harmonic order [10, 31]. The operating points are divided into different power bins from 0% to 100% rated power for harmonic studies. When the wind turbine is operating at 50% rated power, for example, then the harmonic current is expected to be different than the harmonic current for full rated power. The harmonic current of each operating point will be statistically random based on the above explanation. Therefore, when considering a specific power bin, then harmonics will have a random behavior represented by their PDFs due to the varying fundamental voltage and fundamental frequency, thus the current source of the Norton equivalent in figure 2.3 would be assigned different PDFs for the magnitude and phase angle based on the operating point of the wind turbine in the harmonic study.

A major assumption of the Thévenin and Norton equivalent modelling is system linearity. However, recent literature has shown that a non-linear behavior appears in the power electronic converters that is categorized in the frequency coupling phenomenon. Frequency coupling is created around the fundamental frequency due to the PLL and converter control loops, and around the switching frequency due to the PWM [13]. Frequency coupling happens when one particular frequency leads to the appearance of other frequencies in the network caused by the system nonlinearities, which in turn will induce other frequencies as well creating a coupling loop in the network [13, 29]. The impact of the frequency coupling phenomenon on the harmonic distortion at the PCC of an OWPP has not yet been included in any harmonic emissions studies, to the best knowledge of the author. Therefore, it will be included in this thesis to determine its level of influence on the harmonic distortion and whether it has a big impact at the OWPP level.

2.1.7. IEC Summation Rule Criticism

IEC second summation rule outlined in equation 2.13 makes two major assumptions when calculating harmonic distortion:

1. The representation of the harmonic current magnitude is based on the worst case scenario, i.e. the 95th percentile, hence it is deterministic.
2. The representation of the harmonic current phase angle by the α exponent is sufficient in the harmonic study, and hence it is also deterministic.

Therefore, these two assumptions result in wind turbines injecting into the OWPP the same magnitude of harmonic current without accurately representing any phase displacement, which would interact with different parallel and series resonance points of the OWPP. Eventually the harmonic current would be either amplified or diminished when measured at the PCC. Nonetheless, these two main assumptions lead to inaccurate harmonic distortion at the PCC as proved in the literature where harmonic currents were measured and compared to the IEC summation rule [10, 16–18, 33].

Phase Angle of WTs Harmonic Current

The harmonic current is a complex variable with both magnitude and phase angle, however the latter is represented by the α exponent in the IEC summation rule. The α exponent values shown in table 2.2 describe different scenarios under the IEC summation rule. For lower order harmonics, IEC summation rule assumes that the harmonics are more likely to be in phase, and therefore an α exponent of 1 is assigned, and higher values are assigned for higher harmonics dictating phase displacement probability [17]. Nonetheless, this representation has led to inaccurate harmonic distortion estimation at different OWPP after comparing it to actual harmonic distortion from measurements [10, 16–18, 33]. In [17] a new more relaxed α exponent is proposed for all harmonics greater than the 5th harmonic while maintaining the same α exponent for lower harmonics as in table 2.2 to increase the accuracy of the IEC summation rule. Other α exponents are suggested in [34], harmonics lower than the 5th harmonic order are more likely to have an exponent value greater than 1. While the α exponent does not change from the IEC value for harmonic orders between the 5th and the 10th harmonics, and a lower exponent is assigned for harmonic orders higher the 10th harmonic, i.e. around 1.2 to 1.8 [34]. The reassigning of new α exponent values could prove to yield good results at determining the harmonic distortion; however, different power electronic topologies and control scenarios might result in different probability distribution functions for the harmonic magnitude and phase angles, and thus it is unclear how the proposed different exponents would have to be adjusted to consider the statistical variation of the magnitude and the phase angle for each converter. Even if new literature proposes a new set of exponents, it is unclear whether these exponents would be valid for the wide extension of converter possibilities. Therefore, it seems a more practical and reliable approach to directly use the magnitude and phase angle PDFs of each particular converter in the harmonic studies.

Deterministic Behavior Versus Random Behavior

The current source in the Norton equivalent circuit shown in figure 2.3 is used to represent the injection of the harmonic current of the converter into the network. Although, the Fourier analysis in equation 2.1 suggests that harmonics are always thought of as a steady-state concept where they are periodically repeated. However, the fundamental current and voltage change over time due to changing parameters and network configurations that lead to time-varying harmonics [20]. More specifically, PECs high frequency switching and nonlinear behavior result in time-varying operation and thus time-varying harmonic currents [19, 21]. Moreover, the background grid frequency is continuously changing, within the controlled threshold, based on generation and demand that eventually impact the control loops of PECs and causes the fundamental and non-fundamental currents to vary over time [13]. Therefore, harmonic emissions from WTs should not be represented on a deterministic basis, i.e. the 95th percentile, and both the magnitude and phase angle of the harmonic current will be random variables as shown in the literature [10, 18, 19, 22, 35]. Moreover, the use of the exponent in lieu of the actual phase angle assumes that harmonic current are more likely to add up since it is based on arithmetic sum. However, as the phase angles are continuously changing based on their random behavior, there could be WTs with opposing phase angles that lead to harmonic cancellation [16]. This effect is called the Summation and Cancellation Effect where harmonic currents can add up or cancel out. However, this effect can only be fully realized if the phase angles are considered in the calculations. It is noteworthy to remember that the sum of harmonic vectors with time varying angles is either smaller or equal

to their arithmetic sum [18], and thus the final harmonic distortion at the PCC could be lower than what IEC would yield. Therefore, the magnitude and phase angle of the harmonic currents will be represented by statistically random variables in this thesis to determine the harmonic distortion at the PCC of the OWPP.

2.2. Statistics Fundamentals

The work on this thesis is based on probability theory, therefore there are few statistics concepts that should be explained to provide insights on the method and results of the thesis. First, different probability distribution functions will be explained. Second, the law of large numbers will be discussed. Third, the central limit theorem will be explained. Last, Monte Carlo approach will be presented.

2.2.1. Probability Distribution Functions (PDFs)

The complex harmonic currents of WTs have different random behavior as seen in the literature, and the most common PDFs seen in [10, 16, 18, 19, 22, 35] for the magnitude and phase angle of the harmonics are:

1. Uniform Distribution [38]: A continuous random variable has a uniform distribution on the interval $[\alpha, \beta]$ if its probability distribution function f is:

$$f(x) = \frac{1}{\beta - \alpha} \text{ for } \alpha \leq x \leq \beta \quad (2.15)$$

The outcome of the uniform function is completely arbitrary between the interval bounds and it has the same likelihood while it has zero probability outside the bounds. The distribution is donated by $U(\alpha, \beta)$.

2. Normal Distribution [38]: It is also called the bell curve and it is characterised by its mean μ and its standard deviation σ , its probability distribution function f is:

$$f(x) = \frac{1}{\sigma \sqrt{2\pi}} e^{-\frac{1}{2} \left(\frac{x-\mu}{\sigma}\right)^2} \text{ for } -\infty \leq x \leq \infty \quad (2.16)$$

The normal distribution in figure 2.5 shows that data around the mean μ has a higher probability of occurrence. Also, approximately 65% of the values taken from the normal distribution fall within one standard deviation σ from the mean μ while 95% of the values fall within two standard deviations and 99.7% are within three standard deviations [38].

Therefore, the magnitude and phase angle of the harmonic current injected by the wind turbines will not be assigned one deterministic value, but they would be drawn randomly from their probability distribution functions to perform the harmonic emission study and determine the harmonic distortion at the PCC of an OWPP in this thesis.

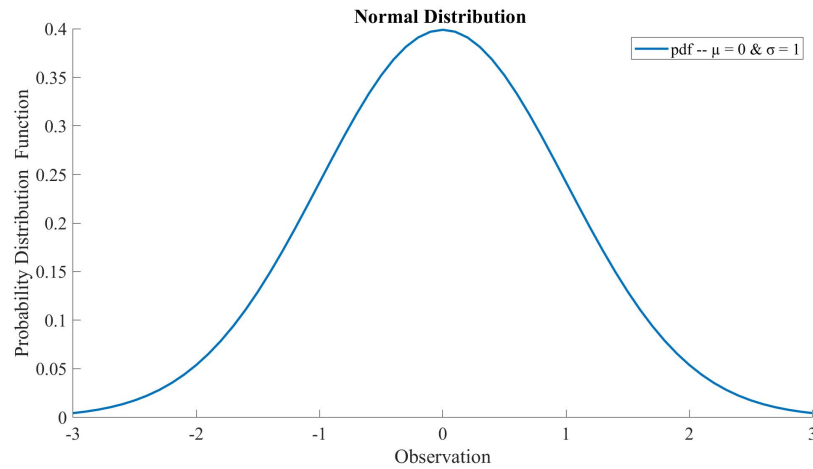


Figure 2.5: Normal Distribution

2.2.2. Law of Large Numbers

Many experiments and simulations involving random variables with the same conditions could result in different outcomes caused by the random variation [38]. It has been known that more accurate results are obtained when the experiments are repeated a number of times and the average of all repetitions is used to represent the outcome of the experiment [38]. The law of large number states if \bar{X}_n is the average of n independent random variables with mean μ and variance σ^2 then for any $\varepsilon > 0$ [38]:

$$\lim_{n \rightarrow \infty} P(|\bar{X}_n - \mu| > \varepsilon) = 0 \quad (2.17)$$

Therefore, as the number of repetitions n increases then the probability for the average to be within a certain distance of the true mean increases [38]. In this thesis, a large number of simulations will be performed to randomly draw the magnitude and the phase angle of the harmonic currents of the wind turbines to determine the harmonic distortion at the PCC in each iteration. Then, the mean can be averaged from all the repetitions which according to the law of large numbers would be very close to the true mean.

2.2.3. Central Limit Theorem

The Central limit theorem states that for a large number of independent identically distributed random variables X_1, \dots, X_n with finite variance, the average \bar{X}_n approximately has a normal distribution, regardless of the probability distribution of the X_i [38]. If μ is the mean and the standard deviation is σ for each of the X_i , for $n \geq 0$, then the resulting probability distribution function Z_n is [38]:

$$Z_n = \sqrt{n} \frac{\bar{X}_n - \mu}{\sigma} \quad (2.18)$$

$$\lim_{n \rightarrow \infty} F_{Z_n}(a) = \Phi(a) \quad (2.19)$$

Therefore, the probability distribution function Z_n converges to the normal distribution. In this thesis, as the number of harmonic estimation repetitions increase then regardless of the type of probability distribution functions used for the magnitude and phase angle of the harmonic currents of the wind turbines then the resulting means of the harmonic distortion at the PCC would have a normal distribution.

Both the central limit theorem and the law of large numbers are the basis of the method of this thesis. The resulting harmonic distortion at the PCC is foreseen to have a normal distribution with a mean μ that is very close to the expected mean subject to having a very high number of repetitions.

2.2.4. Monte Carlo Simulation

Monte Carlo simulation is viewed as one of the most important numerical methods used in statistical engineering to solve problems of probabilistic nature and can be applied to many engineering disciplines [39]. In a Monte Carlo simulation, random samples will be drawn from the probability distribution functions of the stochastic variables and results will be recorded [39]. Therefore, the probability distribution functions of the random variables has to be known; i.e. the PDFs of the magnitude and phase angles of the harmonic currents of the wind turbines in this thesis.

In each repetition, independent random samples of the magnitude and the phase angle of the harmonic currents will be drawn from their respective PDFs and assigned independently to each wind turbine in the OWPP. Then, the harmonic load flow is executed to measure the harmonic distortion at the PCC. Afterwards, another set of independent random samples will be taken and assigned to the WTs to measure the harmonic distortion at the PCC. The results from each repetition will be within some statistical error that is predefined in the study [39]. The result of the Monte Carlo is accurate and will yield the result along with the probability of each outcome [39]. However, Monte Carlo simulation has one major disadvantage that is the computational difficulties of the time-intensive simulations needed to increase the accuracy of the results [39].

The main question in the Monte Carlo simulation is how many repetitions are sufficient to achieve the desired accuracy and to ensure that both the central limit theorem and law of large numbers can be used as the basis to explain the results. To answer the question, a pre-defined statistical error "E" and confidence level "Z_c" of the mean μ have to be set. The statistical error can be chosen as low as desired while the confidence level is set from table 2.4 in a way to guarantee that the mean has a very low error and its confidence is very high. Then, a minimum number of iterations is also set, i.e. 1,000 iterations to perform the simulations and acquire the results. Afterwards, the mean μ and standard deviation σ are calculated from the simulations and

used in equation 2.20 [40] to determine the number of iterations "N" required to achieve the pre-defined statistical error and confidence level. Lastly, the Monte Carlo simulation is performed for the calculated number of iterations "N" and the results are analyzed.

$$N = \left(\frac{100 \times Z_c \times \sigma}{\mu \times E} \right)^2 \quad (2.20)$$

Confidence Level %	99.7	99	98	96	95.5	95	90	80	68	50
Z_c	3	2.58	2.33	2.05	2	1.96	1.645	1.28	1	0.6745

Table 2.4: Confidence Level for Normal Distribution Random Variables
[40]

3

Modelling of the OWPP for Harmonic Studies

3.1. Wind Turbine Harmonic Sources Literature Review

This section will provide an overview of the probability distribution functions of the magnitude and phase angle of harmonic currents in the literature, and the PDFs that will be used in this thesis.

3.1.1. WTs Harmonic Currents PDFs

In [18] a measurement campaign was performed at Burbo Banks offshore wind farm to measure the harmonic currents of one full-scale PEC in a 3.6 MW wind turbine. The measurements were performed at the high voltage side of the step-up transformer of the wind turbine. It was found that the harmonic current magnitude and phase angle for the 5th harmonic order have a normal distribution while it was a log-normal for the 7th harmonic order [18]. However, the authors state that the shape of the PDFs were likely to be affected by the distortion from the main grid and should be used with care on other systems [18].

In [19] measurements were performed at the medium voltage collection point of a wind farm that revealed that different harmonic orders have different probability distribution functions. The magnitude of the 3rd and the 5th harmonic orders have a Rayleigh distribution and the 7th harmonic order has a Rice distribution, thus the author suggested representing all harmonic orders with a Stacy distribution based on analytical works [19]. The phase angles were found to follow a normal distribution for the 3rd and the 5th harmonic order, and a uniform distribution $U(0,360^\circ)$ for the 7th harmonic order [19].

In [22] measurements were performed for many wind turbines of different types and sizes at the low voltage and medium voltage sides to discover that different harmonics have different probability distribution functions, however in general the magnitude PDF can be represented by a Weibull distribution for all harmonic orders and then by adjusting the shape factor k , the actual PDF of a particular harmonic order can be obtained. For example, the magnitude of the 5th harmonic order has a normal distribution with a $k \approx 5$. The phase angle of low-order harmonics tend to be synchronized to the fundamental voltage waveform while the high-order harmonics would have more random phase angles, thus the low frequency phase angles can be characterised with a normal distribution while the higher order harmonics would tend to have uniformly-distributed phase angles $U(0,360^\circ)$ [22].

In [35] harmonic currents at the medium side of a type 3 wind turbine transformer were measured to determine the probability distribution functions, the author performed a chi-square goodness-of-fit with 95% significance level as a threshold to determine if the phase angle of the harmonic current is uniformly distributed. The phase angles of inter-harmonics and switching frequency have a uniform distribution while the remaining lower order harmonics tend to have a non-uniform distribution.

The author in [10] had done an extensive measurements campaign to measure the harmonic currents at different points of the system including the low voltage side of wind turbines at three different wind farms:

- Burbo Bank wind farm which is located around 6.4 km from the shore and has 25 wind turbines rated at 3.6 MW and is connected to the PCC by a 33 kV submarine export cable.
- Avedøre Holme wind farm is located 10 meters from the shore and has 3 wind turbines rated at 3.6 MW.

- Gunfleet Sands II wind farm is located around 7 km from the shore and consists of 18 wind turbines rated at 3.6 MW connected by 33 kV submarine cables to the offshore transformer substation.

The probability distribution function of the 5th harmonic order magnitude at Avedøre Holme and Gunfleet Sands is very close to Rayleigh distribution which indicate that the real and imaginary part of the current have normal distribution [10]. Approximation of the mean μ and standard deviation σ of the magnitude for the 5th and 7th harmonic order for the three wind farms are presented in tables 3.1 to 3.3. It is noted that Burbo Bank wind farm has higher emissions compared to Gunfleet Sands II since it is located near a consumption center that has a higher background distortion than the other two wind farms [10].

Harmonic Order	Magnitude Mean (%)	Magnitude Standard Deviation (%)
5 th Harmonic	1.23	0.48
7 th Harmonic	0.56	0.059

Table 3.1: Avedøre Holme Wind Farm
[10]

Harmonic Order	Magnitude Mean (%)	Magnitude Standard Deviation (%)
5 th Harmonic	1.75	0.37
7 th Harmonic	1.00	0.296

Table 3.2: Burbo Bank Wind Farm
[10]

Harmonic Order	Magnitude Mean (%)	Magnitude Standard Deviation (%)
5 th Harmonic	0.311	0.148
7 th Harmonic	0.286	0.126

Table 3.3: Gunfleet Wind Farm
[10]

The authors in [31] measured the harmonic currents and voltages of type 4 WT with 3.6 MW rated power and full-scale back-to-back converter at Anholt offshore wind farm. Some of the measurements points are the low voltage and medium voltage sides of the wind turbine transformer. The measured voltages and currents were post-processed according to IEC 61000-4-7 for all power bins 0% to 100% rated power and presented in box plots, and summarized as following [31]:

- Lower order characteristic harmonics such the 5th and 7th have the biggest distortion.
- The harmonic current magnitudes and phase angles vary over the different power bins.
- Non-multiple of 3 odd harmonics are strongly impacted by the fundamental frequency.
- Switching high order harmonics have a uniform phase angle distribution $U(-180^\circ, 180^\circ)$ with a mean $\mu \sim 0$.
- The magnitudes of the harmonic currents tend to have a normal distribution with different means and standard deviations. This same observation can be made to the phase angles distributions, except the switching high order harmonics.

As these observations are impacted by the voltage distortion of the external grid, it is necessary to decouple the impact the grid harmonic distortion from the WT distortion. The authors in [31] performed the decoupling by utilizing the WT Converter Harmonic Model (CHM), which is modelled as a Thévenin equivalent circuit. The voltage source represents the voltage distortion of the converter while the impedance is a frequency-dependent impedance that represents the control loops, the emission of the WT, and the relationship between the background distortion and the WT distortion. The emission of the WT is impacted by the background distortion and this relationship is essentially represented by the frequency-dependent impedance. The main findings of the converter's emission are:

- Harmonic orders such the 5th and 7th have deterministic phase angles with narrow variation while the even harmonics have more scattered variation.
- Switching high order harmonics have a uniform phase angle distribution $U(-180^\circ, 180^\circ)$ with a mean $\mu \sim 0$.
- The magnitude of the different harmonic orders vary with the power rating and they could be approximated by normal distribution.

The CHM model provides the emission of the converter solely without the impact of the background grid emission, and due to the precise measurements procedure in [31], it is decided to utilize these harmonic emission measurements for this thesis and they are shown in section 3.1.2.

3.1.2. Chosen WTs and their harmonic PDFs

Wind Turbine Generators (WTG) shown in figure 3.1 are classified into four major types based on their connection to the rotor, converter topology and type of generator deployed and they are summarized as follow [25]:

- **Type 1: Fixed Speed WT with Squirrel Cage Induction Generator (SCIG):** This is known as "The Danish Concept" WT, and it utilizes an asynchronous generator that is connected to the grid with a soft-starter and step-up transformer [25]. The speed of the turbine is nearly fixed to the electrical grid frequency with 1% allowed variation [25]. This WT type has a low efficiency.
- **Type 2: Limited Speed WT with Wound Rotor Induction Generator (WRIG):** This type of WT provides the possibility to adjust the speed of the WT up-to 10% by altering the variable resistor in the rotor circuit [25].
- **Type 3: Variable Speed with partial-scale converter:** This type of WT has two connections to the grid; one by a partial-scale converter at the rotor side and another directly through the stator [25]. This type is widely used in the wind farms, however its limited capability for fault-ride through and the required and expensive gearbox makes it less suitable for offshore wind farms applications [25].
- **Type 4: Variable Speed with full-scale converter:** This type of wind turbine has a full-scale power electronic converter connected to a synchronous generator, which can be of different type: Wound Rotor Synchronous Generator (WRSG), Permanent Magnet Synchronous Generator (PMSG) or SCIG [25]. This type of WT provides fault-ride through capabilities, can operate at different wind speed and has high efficiency, which are the main reasons behind its increasing deployment in offshore wind farms [25].

In light of the above, it was decided to select a type 4 wind turbine with a full-scale back-to-back converter for the modelling of the wind turbine in the OWPP in this thesis. The WT converter will be modelled by a Norton equivalent for the harmonic domain in this thesis as recommended in [33] and explained in section 2.1.6. Moreover, as previously seen in section 3.1.1, there are different PDFs to represent the harmonic currents statistical variation. However, the only source that provides the harmonic current statistical variation at the converter side of a full-scale back-to-back converter is seen in [31]. Furthermore, it is clear in [31] that the authors also took into account the effect of the background harmonics at the WT terminals, which was decoupled by using the converter impedance. Therefore, it was decided to extract and use the data from the measurements shown in [31] represented by PDFs of the harmonic emissions by the wind turbine. In particular, [31] gives information about the different PDFs for different power bins. In this thesis, it was decided to focus in one operating point (full power production) although the methodology and methods shown here can be applied for other power bins.

As explained earlier in chapter 2, harmonic resonance analysis is vital in understanding the possible amplification of harmonics as there could be various peaks and dips along the frequency spectrum. In [12, 41, 42] it was shown that resonance points are seen at lower frequencies due to the high capacitance of the submarine cables and the highly inductive transformers within the OWPP, which increase the probability of amplification of low order harmonics. These amplified low order harmonics could require OWPP developers to install filters to mitigate their negative impacts. However, filters designed for low order frequencies can be more complex and expensive than the ones designed for higher order harmonics [13]. Low order harmonics filters are often single-tuned filters that are used to filter a harmonic at a specific frequency, which makes

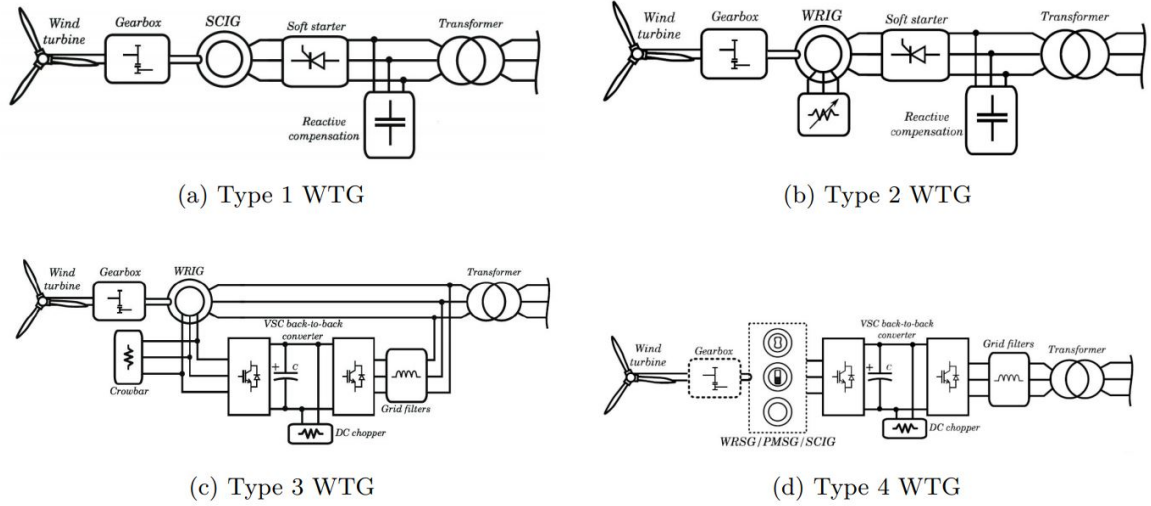


Figure 3.1: Wind Turbine Generator Types
[25]

re-tuning very challenging [28]. On the other hand, high order harmonics are usually filtered by damped filters as a group since the damped filters can be tuned in between specific harmonics [28]. Damped filters can result in high losses due to their remarkably high resistance compared to the single-tuned filters, and thus they are rarely used for low order harmonics near the power frequency [28]. Furthermore, it is seen in [31] that higher order harmonics tend to have uniformly-distributed phase angles $U(-180^\circ, 180^\circ)$, which indicates a higher probability of harmonic cancellation in the OWPP compared to the low order harmonics. Therefore, the high order harmonics will not be studied in this thesis due to the above-mentioned reasons, and only low order harmonics will be analyzed. Moreover, as seen in table 3.4, and as it was explained in section 2.1.6 with regard to the even harmonics, the 8th harmonic presents a much lower magnitude than the other harmonics, and has a higher standard deviation of the phase angle. This is due to the fact the non-characteristic harmonics are caused to a great deal by the asymmetry in the dead-time error pulses, non-linearity of the switching devices and voltage drop over the semi-conductor [18]. In spite of the low magnitude and high standard deviation of the 8th harmonic, it is decided to include it along with the 5th and 7th harmonics to be studied in the thesis. The harmonic emission limit for the 8th harmonic set by IEC 61000-3-6:-2008 as presented in table 2.1 is very low, and thus, despite the low magnitude, a grid code non-compliance is still probable especially if the 8th harmonic is near a parallel resonance point. Finally, the 8th harmonic has certain properties in comparison to the 5th and 7th harmonics, in particular the very high standard deviation of the phase angle, that makes it an interesting study subject in a thesis based on statistical methods. The parameters of the probability distribution functions for the 5th, 7th and 8th harmonics are presented in table 3.4.

Harmonic Order	Mean Value of The Magnitude in RMS (A)	Mean Value of The Harmonic Current Magnitude over Fundamental Current (%)	Standard Deviation of The Magnitude (%)	Mean Value of The Phase-Angle (°)	Standard Deviation of The Phase-Angle (°)
5 th Harmonic	28.9	0.81	0.17	-12.76	10.76
7 th Harmonic	23.5	0.65	0.12	-40.94	13.42
8 th Harmonic	6.0	0.17	0.08	-52.79	94.93

Table 3.4: The Harmonic Current PDFs Parameters

The probability distribution functions of the different harmonics (as a percent of the fundamental current) are presented in figure 3.2 while their phase angles are presented in figure 3.3.

The results of the Monte Carlo simulation are compared to another simulation performed with the IEC summation law using the 95th percentile of the magnitude for each harmonic order. The 95th percentile of each harmonic order is calculated using equation 3.1 based on normal distribution and are presented in table 3.5:

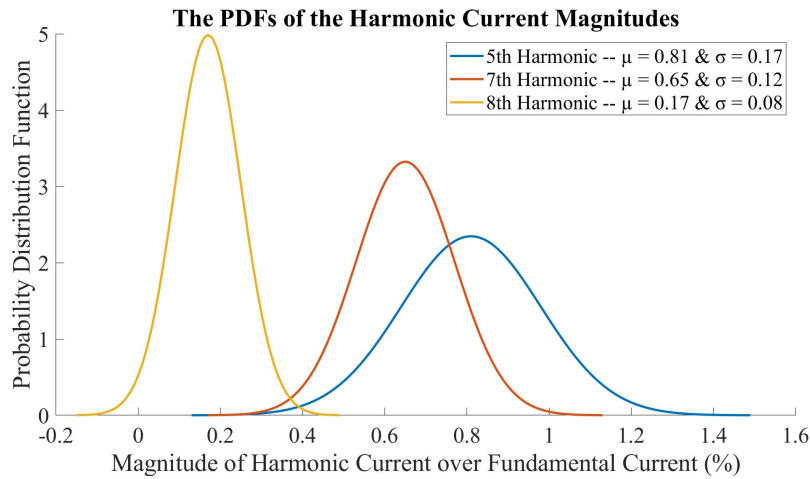


Figure 3.2: The PDFs of the Harmonic Current Magnitude

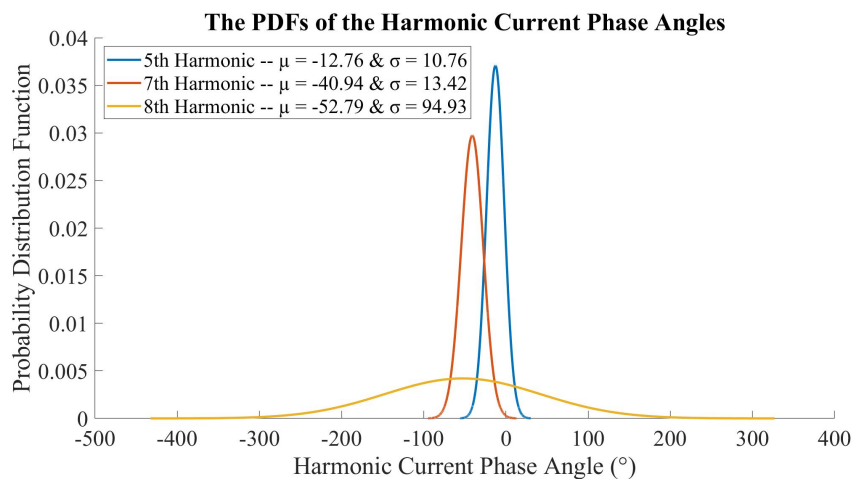


Figure 3.3: The PDFs of the Harmonic Current Phase Angles

$$x = \mu + z \times \sigma \quad (3.1)$$

where x is the 95th percentile, $z = 1.645$ for the 95th percentile, μ is the mean and σ is the standard deviation.

Harmonic Order	95 th Percentile of the magnitude as I_h/I_f (%)
5 th Harmonic	1.090
7 th Harmonic	0.847
8 th Harmonic	0.302

Table 3.5: The 95th Percentile of the Magnitude the Harmonics

3.2. Offshore Wind Power Plant Design Basis and Modelling

This section will provide the Offshore Wind Power Plant design basis, layout and the modelling in DlgSilent PowerFactory for harmonic study. The OWPP consists of 89 WTs and each WT has a full-scale back-to-back power electronic converter, each WT has a step-up transformer to step the voltage from 690 V to 33 kV and then the WTs are connected radially by array cables. The wind turbines are divided into 12 groups and each group has 7 to 8 wind turbines. The WTs groups are divided into two main groups, each of which is connected to one side of the 33 kV offshore substation. The array cables are connected to an offshore substation

where the voltage is stepped-up to 110 kV using two parallel three-windings 33/110 kV transformers. Then two 110 kV HVAC submarine cables each of a total length of 45 km connect the offshore substation to an onshore busbar. Then two 110 kV HVAC underground cables each of a total length of 45 km connect to the Point of Common Coupling. Therefore, the 110 kV transmission system expands 45 km offshore and 45 km onshore. The schematic shown in figure 3.4 is very close to the model built in PowerFactory, and shows the main components with their voltage ratings and length of the export cable systems.

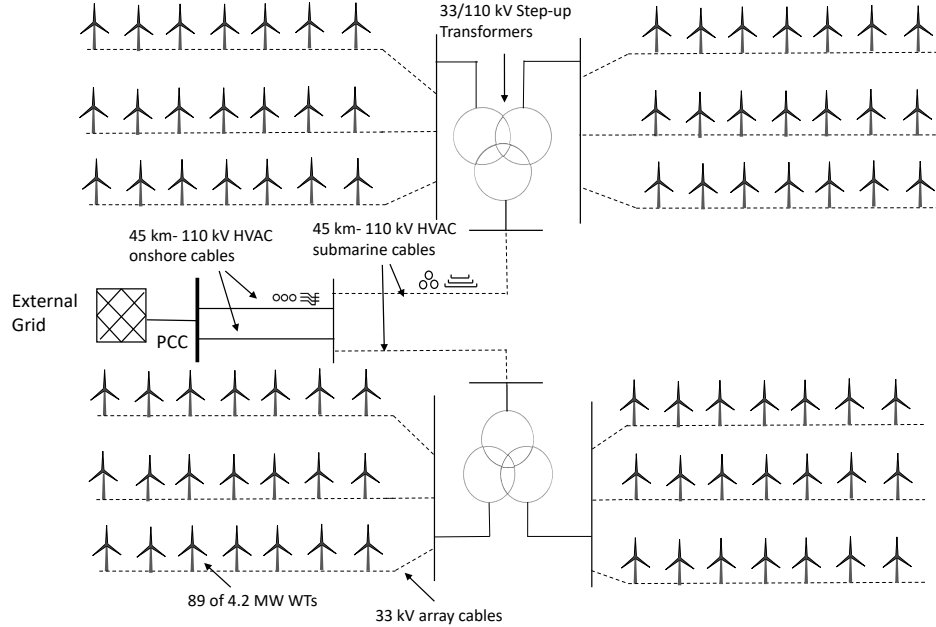


Figure 3.4: Offshore Wind Power Plant Schematic

An example of the model of group 1 that has 7 wind turbines is shown in figure 3.5. Each WT has several filters in parallel. The array cable is then connected to the offshore substation shown in figure 3.6 where the voltage is stepped up to 110 kV and the offshore submarine cables are laid to the onshore busbar shown in figure 3.7. Two parallel onshore cables are laid from the onshore busbar to the PCC where the external grid is connected in figure 3.7.

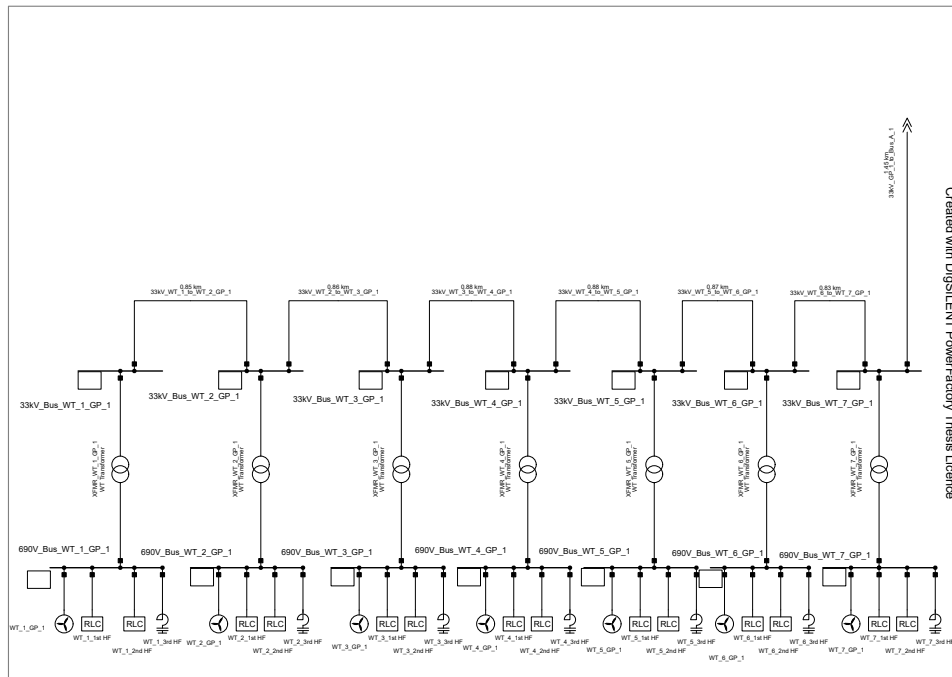


Figure 3.5: Single Line Diagram of Group 1 WT's

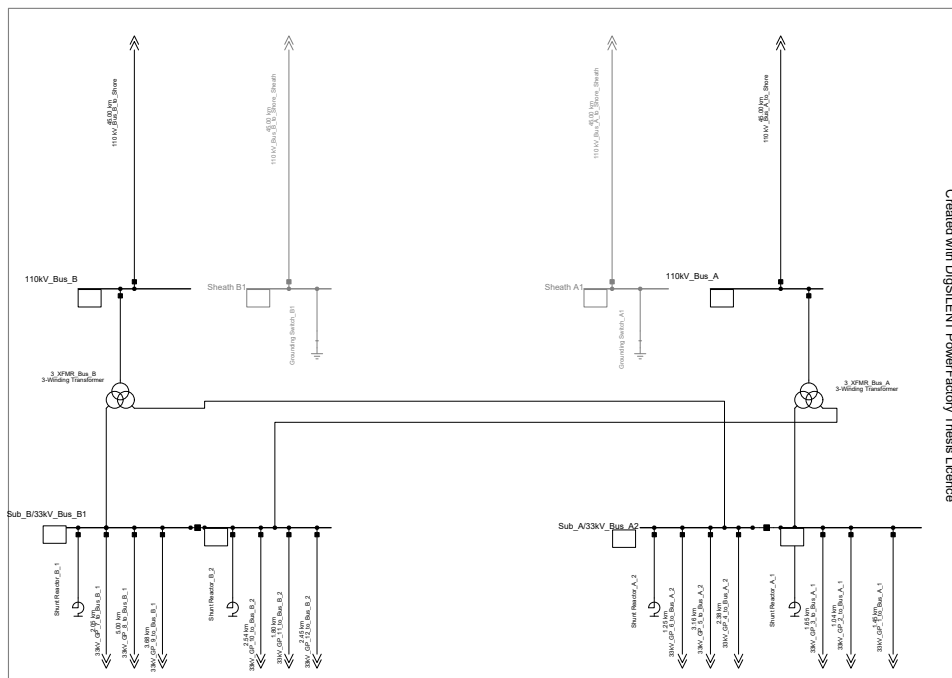


Figure 3.6: Single Line Diagram of Offshore System

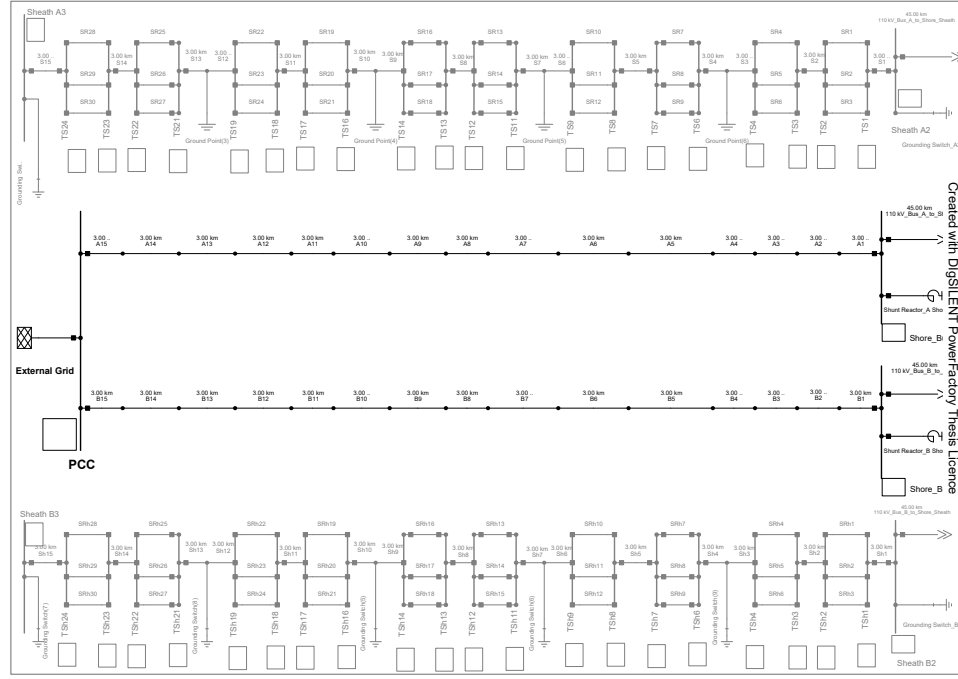


Figure 3.7: Single Line Diagram of Onshore System

3.2.1. Wind Turbines

There are 89 wind turbines in the Offshore Wind Power Plant and their electrical details are presented in table 3.6. They are modelled using the static generator element *ElmGenStat* in PowerFactory for three-phase system. The switching frequency of the WT converter is 2.5 kHz.

Parameter	Nominal Apparent Power (MVA)	Nominal Active Power (MW)	Nominal Reactive Power (Mvar)	Rated Current (kA)	Rated Voltage (V)
WTG	4.2	4.2	0	3.514	690

Table 3.6: WTG Parameter

PowerFactory provides many local-controllers options for the load flow analysis. The Constant Q option is used in this model that allows setting up the active and reactive power set points [43]. The reactive power is set to zero Mvar since IEC 61400-21:2008 requires zero reactive power injection by the wind turbines during harmonic analysis [31]. The static generator is modelled for harmonic analysis using Norton Equivalent for the positive, negative and zero sequences, although the zero-sequence was not modelled since zero-sequence currents would be trapped by the step-up transformer and thus they are not expected to present a problem, as shown in figures 3.8, 3.9 and 3.10, respectively.

The impedance is frequency-dependent and represents the converter impedance only in this thesis since the filters are modelled separately in the model, and this modelling approach is the most accurate representation of the wind turbine as recommended by CIGRE [29]. PowerFactory provides three options to model the frequency-dependent impedance [27]:

1. Frequency Polynomial Characteristic (ChaPol) [27]:

This option allows the user to use one of two defined equations 3.2 and 3.3 to model the impedance for higher frequencies by adjusting two scale parameters "a" and "b" to account for the frequency-dependency.

$$y(f_h) = (1 - a) + a \times \left(\frac{f_h}{f_1} \right)^b \quad (3.2)$$

$$y(f_h) = 1 + a \times \left(\left(\frac{f_h}{f_1} \right) - 1 \right)^b \quad (3.3)$$

where f_h is the harmonic frequency and f_1 is the fundamental frequency.

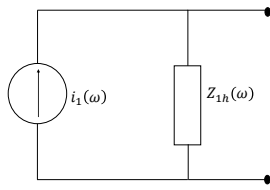


Figure 3.8: WT Positive Sequence

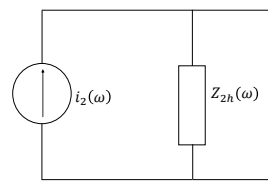


Figure 3.9: WT Negative Sequence

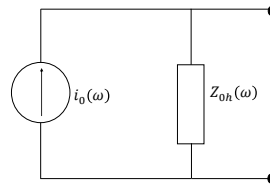


Figure 3.10: WT Zero Sequence

2. Vector Characteristic (ChaVec) with Frequency Scale [27]:

This option allows the user to define the impedance as a continuous characteristic with a pre-defined frequency scale. This option will be used to be able to model the frequency-dependent impedance of the converter for higher frequencies. A scale is created for frequency range and then two vector characteristics are created for the resistance and reactance of an offshore full-scale back-to-back converter impedance that is utilized in the model as shown in figure 3.11; this is the impedance of the Norton equivalent model of the converter. The frequency-dependent impedance shown in figure 3.11 was calculated in the same way as it was done in [44], i.e. with an analytical model of the WT converter taking into account its current control and PLL. As explained in [44], the control parameters significantly affect the shape of the impedance curve; however, in [44] the impedance has been compared and adjusted for similarity to the impedance given by a real WT manufacturer. Also, it is worth mentioning that the WT in [44] has the same characteristics (e.g. power rating and topology) as the WT studied in this thesis. Only a few parameters have been re-adjusted in between [44] and the impedance used in this thesis. Therefore, this impedance is considered valid for the present study. PowerFactory allows creating separate impedances for each sequence as shown in figures 3.8, 3.9 and 3.10 for the Norton Equivalent circuits. However, it is assumed that the impedances of the different sequences are equal. This assumption is based on the fact that the WT current control is typically based on a specific type of strategy, called double synchronous reference frame current control, that is symmetrical in both sequences. Therefore, since the current control is dominant in the frequency range that is studied in this thesis, the differences in between the positive and the negative sequence impedances are negligible. Similar assumptions have also been considered in literature as seen in [45].

3. Matrix Characteristic (ChaMat)[27]:

This option allows the user to define a matrix parameter characteristic as a continuous characteristics with two pre-defined scales.

The current spectrum is defined in PowerFactory using harmonic source *typHmccur* for the Norton Equivalent current source, and the harmonic current can be entered according to three options [27]:

- **Balanced Phase Correct:** The magnitude and phase angle of the positive and negative sequence harmonic injection at odd and integer harmonic orders can be defined for balanced and unbalanced harmonic load flow [27].

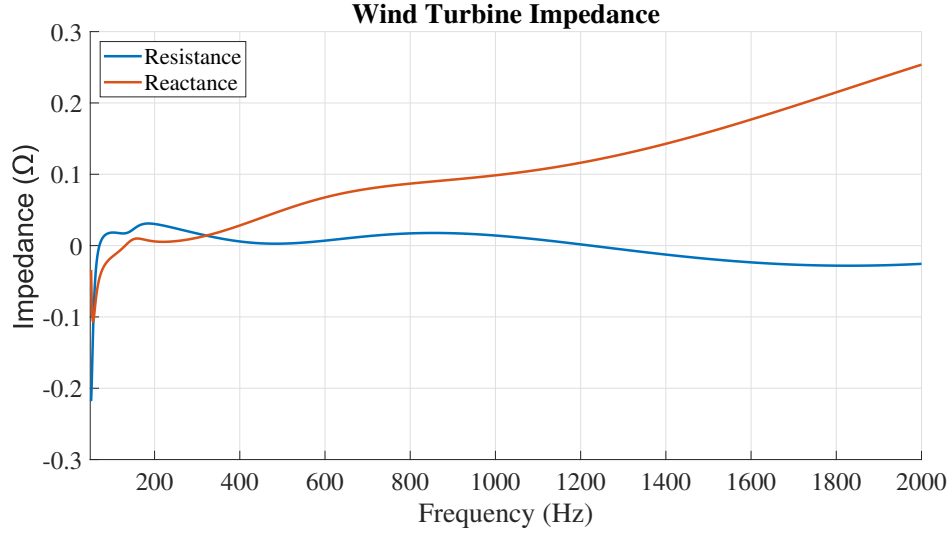


Figure 3.11: Wind Turbine Impedance
[44]

- **Unbalanced Phase Correct:** The magnitudes and phase angles for all phases of the harmonic injections at integer and non-integer harmonic orders can be defined for balanced and unbalanced harmonic load flow [27].
- **IEC 61000 Harmonic Source:** The magnitude of harmonic injections at integer and non-integer harmonic orders can be defined for a harmonic load flow based on IEC summation rule in equation 2.13.

The unbalanced phase-correct method will be used in this thesis to be able to define the harmonic injections at all phases for the defined integer harmonics for the Monte Carlo method (proposed method in the thesis) while the IEC 61000 harmonic source will be used for the IEC summation rule method. The actual harmonic current of a phase-correct current source is calculated for each frequency by [27]:

$$I_h = k_h \times e^{\Delta\varphi_h} \times I_1 e^{h \cdot \varphi_1} \quad (3.4)$$

where I_h is the harmonic current at frequency f_h , I_1 is the fundamental current, φ_1 is the fundamental phase angle and the other parameters for phases a, b and c, respectively are [27]:

$$k_h = \frac{I_{ah}}{I_{a1}} \quad (3.5)$$

$$\Delta\varphi_h = \varphi_{ah} - h \times \varphi_{a1} \quad (3.6)$$

$$k_h = \frac{I_{bh}}{I_{b1}} \quad (3.7)$$

$$\Delta\varphi_h = \varphi_{bh} - h \times \varphi_{b1} \quad (3.8)$$

$$k_h = \frac{I_{ch}}{I_{c1}} \quad (3.9)$$

$$\Delta\varphi_h = \varphi_{ch} - h \times \varphi_{c1} \quad (3.10)$$

There is a unique harmonic source for each one of the 89 wind turbines in the model. The k_h and $\Delta\varphi_h$ variables will have to be entered for each harmonic source that is assigned to each individual wind turbine to inject the phase correct harmonic with a magnitude and phase angle. The probability distribution functions of the harmonic magnitude have been changed to the k_h ratio as seen in figure 3.2 while the $\Delta\varphi_h$ will be calculated in the Python code, will be explained in details at a later stage, from figure 3.3 and the fundamental phase angles of each wind turbine and then will be assigned to each harmonic current source.

3.2.2. Pulse Width Modulation (PWM) Filters

Filters are used for harmonic mitigation. They are basically a combination of inductive, capacitive and resistive components chosen with the consideration to be tuned at a particular frequency by forming a resonant circuit [29]. There are several PWM shunt filters connected in parallel to each wind turbine in order to minimize its harmonic emission, especially at switching-harmonics orders. Both *ElmFilter* and *ElmShnt* models from PowerFactory are used in the OWPP model. They are all modelled using 3PH-Y technology. The filters can also be modelled for higher frequencies by adding a frequency-dependent impedance, however this is not widely performed in the literature [29] and thus will not be performed in this thesis.

3.2.3. Wind Turbine Transformer

Each wind turbine has a step-up transformer as shown in figure 3.5 to step the voltage to a higher voltage level to increase the efficiency and lower the power losses in the system. The wind turbine transformer specifications are presented in table 3.7. The transformer is modelled in PowerFactory using *ElmTr2* model. The transformers represent inductive elements in the system along the frequency spectrum and they can interact with capacitive elements such as the submarine cables to create series or parallel resonance points [29], thus their accurate modelling in the frequency domain is essential for harmonic analysis and estimation. The primary delta side of the transformer traps the flow of triplen zero-sequence harmonics into the system and thus they are usually not analyzed in harmonic studies [24, 29]. The transformer vector group representation is important in the harmonic domain since they can introduce phase shifts to harmonic voltages and currents [29]. On the other hand, it is safe to neglect the transformer stray capacitances in the harmonic domain design for frequencies below 4 KHz as well as the magnetizing branches of the transformer where the transformer core is assumed to be operating in the linear region [29].

Technology	Rated Power (MVA)	Primary Side Voltage (V)	Secondary Side Voltage (kV)	Vector Group
Two-Winding Three-Phase System	4.65	690	33	DYN11

Table 3.7: Wind Turbine Transformer Specification

There are five different models proposed in [29] to model the power transformers for harmonic studies with examples and approximate ratings. The wind turbine transformer can be best modelled using a simple impedance as per Model 2:IEEE Std.399 shown in figure 3.12 [29]. This modelling approach is also recommended in [20, 46].

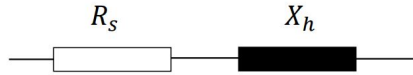


Figure 3.12: Power Transformer Model in Frequency Domain [29]

The transformer resistance and reactance are calculated as per the following equations, respectively [29]:

$$R_S(h) = R_{DC} (1 + Ah^B) \quad (3.11)$$

$$X_h = 2\pi f_n L_\sigma \quad (3.12)$$

where [29] recommends using 0.1 and 1.5 for A and B, respectively.

The input data for the above equations are the transformer DC resistance R_{DC} and the leakage reactance at fundamental frequency [29]. The leakage inductance L_σ is assumed to be constant over the frequency spectrum while the resistance is modelled using equation 3.11 to account for skin effect, winding eddy current losses and other losses such as core clamps and magnetic shield [47]. The DC resistance, the impedance and the reactance are approximated by the following equations [47]:

$$R_{DC} = \frac{\Delta P_{cu} U_N^2}{S_N^2} \quad (3.13)$$

$$Z_T = \frac{\Delta U_Z U_N^2}{S_N} \quad (3.14)$$

$$Z_T = \sqrt{R_{DC}^2 + X_T^2} \quad (3.15)$$

Where P_{cu} is the copper losses, U_N is the nominal voltage, S_N is the nominal apparent power, U_Z is the short circuit voltage, and X_T is the leakage reactance at fundamental frequency. It is clear from equation 3.13 that the resistance of the wind turbine transformer increases with frequency with respect to the value of the R_{DC} , thus an example for this frequency-dependent resistance is shown in figure 3.13 (This graph is scaled to show the trend of the frequency-dependent resistance for the WT transformer).

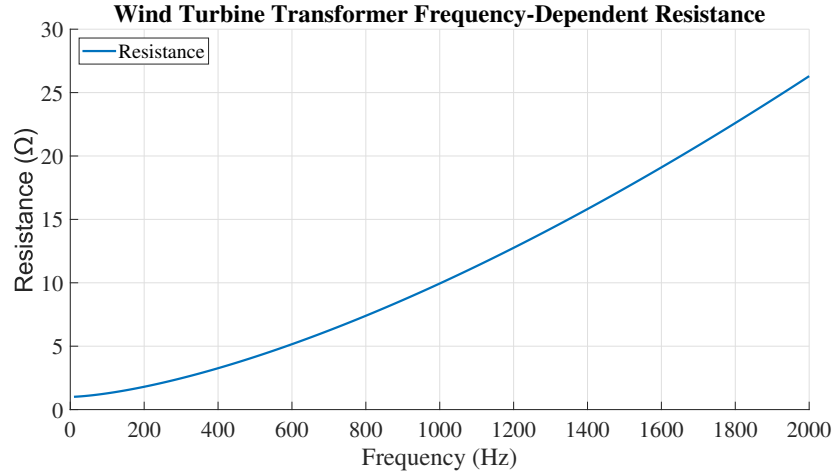


Figure 3.13: WT Transformer Frequency-Dependent Resistance (Example)

3.2.4. Array Cables

There are three types of AC array cables used in the OWPP. The wind turbines are connected in radial formation, which means that the farthest wind turbine, the first WT in the group, will require a smaller array cable compared to the closest wind turbine, the last WT in the group, which would require to carry more current and hence requires a larger cable. Thus, the cables' conductor cross section increases as more WTs are connected in the radial. For example, in figure 3.5 the first four array cables have the same cross section, the fifth has a larger cross section and the last two have the largest cross sections. This would allow the cables to carry more current as more WTs are connected in the group.

PowerFactory uses different models to model the lines and cables based on the available cable's information. These types are line (*TypLine*), tower (*TypTow*), a tower geometry (*TypGeo*) and cable definition (*TypCabsys*) [27]. The main differences are:

- *TypLine* uses electrical parameters directly to define the cable or line. An example of an electrical parameter would be the equivalent resistance per km [27].
- *TypTow* and *TypGeo* have two options: geometrical parameters and electrical parameters modes. The electrical parameters will be calculated by PowerFactory if the geometrical option is selected. These types are usually used for overhead lines. For example, the equivalent resistance per km is an input when the electrical parameter mode is chosen while the conductor's size is an input when the geometrical parameter mode is selected [27].
- *TypCabsys* requires the definition of the complete cable system including the geometry, the cable's construction, characteristics of all layers and the definition of the coupling between the phases [27].

The model choice of the array cables is very important since it does not only influence the results of the power flow, but it also has a high impact on the harmonic study due to the cables' high reactance that could cause resonance points at lower frequencies [29, 44]. Modelling the cable's with high accuracy can be difficult

at the design stage due to unavailability of final manufacturers' data-sheets of selected cables, construction and laying configuration [29], thus the design of the array and export cables used in the thesis are based on manufacturer's data-sheets to increase the accuracy of the study. The main factors of cables' design that influence harmonic studies are:

- Cable length has the greatest effect on the magnitude and frequency of the resonance peaks and as length increases, the capacitances increases which result in downward shift in the resonance points [29].
- The design characteristics of the cables such as the thickness of the core conductor and insulation [29].
- The layout of the cable on the sea bed or in trenches largely impact the frequency and resonance points [29].
- The sheath bonding type and number of cross-bonding points impact the sequence impedance [29].
- The choice between lumped or distributed model to represent the cable impacts the accuracy of the model in the frequency domain where the latter model proved to provide higher accuracy [15, 29].

In addition to the above points, the impedance of AC cables at higher frequency is different than the impedance at 50 Hz mainly due to losses that are characterized in two phenomena:

1. **Skin Effect:**

The skin effect is a result of nonuniform current distribution over the conductor of the cable. The current tends to be concentrated on the surface of the conductor as the frequency increases due to electromagnetic induction [48]. This concentration of current is similar to the reduction of the cross-section of the cable, which results in increase in the resistance as the frequency increases [48].

2. **Proximity Effect:**

The proximity effect occurs when two or more conductors are next to each other and at least one of them is energized and has AC current [48]. This AC current will impact the distribution of the current on the other conductor(s) by inducing eddy current opposing the original current [48]. The proximity effect increases the resistance as the frequency increases [48]. In the study performed in [49], the proximity effect of three-core submarine cables was found to be significant and thus should be considered when determining the harmonic impedance.

Therefore, it is very crucial to design the cables in accordance to the influencing factors listed above and the skin and proximity effects to model the behavior of the cables at higher frequencies for harmonic studies.

When *TypLne* is chosen to model the array cables, then a frequency-dependent impedance has to be created using one of the three options outlined in section 3.2.1 to account for the skin and proximity effects of the cables. In [50], the author chose to model the subsea cables using this approach by including the frequency-dependent resistance after calculating the proximity and skin effects using the imperial formulas in [48]. However, the author states that the accuracy of the model would improve if the cable inductance is modelled as frequency-dependent to account for the decreased inductance with the increase in frequency, but this was not performed due to time-constraint [50]. In [32, 34], the authors modelled the cables using the *TypLne* with distributed parameter and added the frequency-dependent impedance using equation 3.2 to account for the skin and proximity effects. The authors performed sensitivity analysis to determine the A and B coefficients, and decided on $A = 1$ and $B = 0.8$ [32].

On the other hand, when a *TypCabsys* is used to model the cables, then the cables' geometry, conducting layers, insulation layers and semiconducting layers will be used by PowerFactory to calculate the electrical parameters of the cables based on the standard electromagnetism equations, Maxwell's equations, and the more complex cable modelling method to automatically calculate the frequency-dependent impedance and admittance matrices and used by various simulations functions in PowerFactory [27, 50, 51]. Thus, it was decided to model the array and export cables using *TypCabsys*, which has two sub-types:

- Parallel single-core cable (*TypCab*) that is used for underground HVAC cables [51].
- Multi-core/Pipe-type cable (*TypCabmult*) that are used for submarine cables in pipes [51].

The multi-core option of the *TypCabmult* could be used to model the array cables, however the model currently only includes the skin effect when calculating the impedance while the proximity effect is not considered due to the assumption of uniform current distribution in the conductors [51]. In contrast, the pipe-type uses a system of three-single cores cables in a pipe to calculate the impedance and the admittance matrices [51]. The pipe-type cable system requires the definition of the conducting layers, insulation layers, semiconductor layers, the shape and diameter of the core, the number of phases, the pipe definition and the conductor coordinates as shown in figures 3.14, 3.15 and 3.16.

Multicore/Pipe Cable Type - Equipment Type Library\300 mm2 Single core cable.TypCabmult

Basic Data

Description: 300 mm2 Single core cable

Version: 33. kV

Load Flow: Pipe-type

Short-Circuit VDE/IEC: No. of phases: 3

Short-Circuit Complete: Core

Short-Circuit ANSI: Shape: Compact

Short-Circuit IEC 61363: Outer diameter: 20.4 mm

Short-Circuit DC: Frequency characteristic (Ohm/km)

Simulation RMS

Simulation EMT

Cable Analysis

Power Quality/Harmonics

Reliability

Hosting Capacity Analysis

Optimal Power Flow

Conducting layers:

	Exists	Material	Resistivity (uOhm*cm)	Relative Per...	Thickness mm	Filling Factor %	DC-Resista... Ohm/km
Conductor	<input checked="" type="checkbox"/>	Aluminium	2.8264	1.	10.2	91.7998	0.09419801
Sheath	<input checked="" type="checkbox"/>	Copper	1.7241	1.	0.2	100.	0.7108754
Armour	<input type="checkbox"/>	Steel	13.8	1.	2.	100.	0.

Insulation layers:

	Exists	Material	Dielectric Los...	Relative Perm...	Thickness mm	Filling Factor %
1 (Insulation)	<input checked="" type="checkbox"/>	XLPE (> 18/30...	0.	3.	8.	
2 (Oversheath)	<input checked="" type="checkbox"/>	PE (HD/LD)	0.	2.3	2.	
3 (Serving)	<input type="checkbox"/>	Unknown	0.02	3.	1.	

Semiconducting layers:

	Exists	Thickness mm	Advanced	Resistivity uOhm*cm	Relative Permeab...	Relative Permittiv...
Core Outer	<input checked="" type="checkbox"/>	0.5	<input checked="" type="checkbox"/>	1000000	1.	3.4
Ins. Outer	<input checked="" type="checkbox"/>	0.5	<input checked="" type="checkbox"/>	1000000	1.	3.4

Advanced definition of semi-conducting layers

Figure 3.14: *TypCabmult* Array Cable-General

Modelling the pipe-type cable requires the definition of a single core cable without armor and serving (sheath). The armor thickness is defined by the pipe thickness while the outer serving (sheath) is used for the insulation thickness [51] shown in figure 3.15. The polar coordinates for each core are calculated based on the radius per phase (r). For a trefoil arrangement, which is a typical arrangement for submarine cables [48], the distance from the center of the trefoil arrangement shown in figure 3.16 to the center of each single core cable is calculated according to the below equation [51]:

$$R = \frac{2 \times r}{\sqrt{3}} \quad (3.16)$$

The conductor shape can be selected from three options: Compact, Hollow, and Segmental in PowerFactory. Many submarine cables have stranded conductors that are made from round wires [52]. Solid conductors are not usually used for large cross sections due to skin and proximity effects, however the segmented or stranded conductors are used to minimize these effects, which then require a larger cross section area than actually stated by the cable's data sheet [48]. Therefore, the cable resistance should be corrected to account for the empty spaces between the stranded/segmented wires of the conductor [38], which would alter the filling factor of conductors that are formed from compressed round wires. The filling factor of a typical stranded submarine cable could be up to 92% [52]. The filling factor is related to the DC resistance of the cable and is calculated by PowerFactory after specifying the DC resistance. Therefore, it is necessary to correct the DC resistance for all submarine cables using the following equations [48]:

$$\rho = \rho_{Sol} \times \frac{\pi R^2}{S} \quad (3.17)$$

Multicore/Pipe Cable Type - Equipment Type Library\300 mm2 Single core cable.TypeCabmult

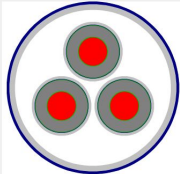
Basic Data	General	Multicore common outer layers	Pipe definition	Conductor coordinates
Description	Outer radius	0.06195	m	
Version	Thickness	2.	mm	
Load Flow	Insulation thickness	4.	mm	
Short-Circuit VDE/IEC	Resistivity	20.	uOhm*cm	
Short-Circuit Complete	Rel. permeability	1.		
Short-Circuit ANSI	Fill: rel. permittivity	2.3		
Short-Circuit IEC 61363	Ins. rel. permittivity	2.3		
Short-Circuit DC				
Simulation RMS				
Simulation EMT				
Cable Analysis				
Power Quality/Harmonics				
Reliability				
Hosting Capacity Analysis				
Optimal Power Flow				

Figure 3.15: *TypCabmult* Array Cable-Pipe Definitions

Multicore/Pipe Cable Type - Equipment Type Library\300 mm2 Single core cable.TypeCabmult

Basic Data	General	Multicore common outer layers	Pipe definition	Conductor coordinates
Description	Polar coordinates of cores:			
Version	Magnitude 1	Magnitude 2	Magnitude 3	
Load Flow	1	0.026	0.026	
Short-Circuit VDE/IEC				
Short-Circuit Complete				
Short-Circuit ANSI				
Short-Circuit IEC 61363				
Short-Circuit DC				
Simulation RMS				
Simulation EMT				
Cable Analysis				
Power Quality/Harmonics				
Reliability				
Hosting Capacity Analysis				
Optimal Power Flow				

Note: Magnitudes are in [m]


Figure 3.16: *TypCabmult* Array Cable-Conductor Coordinates

$$R_{DC} = \frac{\rho}{S} \quad (3.18)$$

Where R is the radius of the conductor, S is the cross-section of the conductor and ρ_{sol} is the resistivity of the conductor. The corrected DC resistance will indirectly correct the filling factor in the cable model.

The semiconductor layers between the conductor and insulation, and between the insulation and metallic screen are required to ensure a cylindrical electric field and to avoid formations of gaps to prevent partial discharge [48]. In addition, they are required to avoid local stress on the insulation by the conductor that would reduce the dielectric strength of the insulation [52]. The material of the semiconductor layers should be similar to one of the insulation's material [48]. The most used insulation material for submarine cables is Cross-Linked Polyethylene (XLPE), and thus the semiconductor layers would be semi-conductive XLPE made from enhanced extrudable polymers with high conductivity [48, 52]. Since the semiconductor layers are considered as part of the insulation, their permittivity is required to be corrected as per the below equation [48]:

$$\varepsilon = \varepsilon_{Ins} \times \frac{\ln\left(\frac{R_2}{R_1}\right)}{\ln\left(\frac{b}{a}\right)} \quad (3.19)$$

where ε_{Ins} is the insulation permittivity with a typical value between 2.3 to 2.5, R_2 is the radius over the insulation including the semi-conductors and conductor layers, R_1 is the conductor radius, b is the outer-radius of the insulation including the conductor radius, and a is the inner-radius of the insulation that includes the conductor and the first semi-conductor layer [48]. The 33 kV three-core-array cables are modelled in the OWPP in PowerFactory based on submarine cables obtained from [53] and shown in table 3.8 using the pipe-type cables (*TypCabmult*) after correcting the DC resistance of the conductor and permittivity of the semiconductor layers.

Layer (radius in mm)	Material	3C-300 mm ²	3C-400 mm ²	3C-800 mm ²
Conductor	Aluminum	10.2	11.6	16.85
Conductor Screen	Semi-Conductor XLPE	0.5	0.5	1
Insulation	XLPE	8	8	8
Insulation Screen	Semi-Conductor XLPE	0.5	0.5	1
Magnetic Sheath/Screen	Copper	0.2	0.2	0.4
Over Sheath	HDPE/LDPE	2	2	2
Aarmor	Steel	2	2	2
Outer Sheath/Serving	PVC	4	4	4
Outer Diameter		123.9	129.9	154.4

Table 3.8: 3 Core Array Cables' Specifications [53]

3.2.5. Three-Winding Transformer

There are two parallel three-phase three-winding transformers in the OWPP to further step up the voltage from 33 kV to 110 kV to reduce the power losses and increase the efficiency in the system as shown in figure 3.6. The three-winding transformer specifications are presented in table 3.9. The two secondary sides are identical, thus this type of transformer is called "Double-Secondary Transformer" [54]. Moreover, the grounded primary Wye connection with the Delta double-secondaries are advantageous in trapping the triplen zero-sequence harmonic and voltage transients [54]. The transformers are modelled in PowerFactory using *ElmTr3* model, and they, along with the WTs transformers, represent the main inductive elements in the system. The transformers are modelled for linear saturation and three limb core, hence no magnetizing impedance is modelled. The magnetizing branch can be neglected under normal conditions unless the transformer saturation is a primary concern in the study [54].

Parameter	Transformer Primary Side	Transformer Secondary Side	Transformer Tertiary Side
Rated Voltage (kV)	110	33	33
Rated Power (MVA)	290	145	145
Vector Group	YN0	D1	D1

Table 3.9: Three-Winding Transformer Specification

The three-winding transformer can be modelled for harmonic analysis similar to the WT two-winding transformer shown in figure 3.12. The resistance and reactance between the primary and secondary sides, and between the two secondary sides are calculated using equations 3.13 and 3.15 from the full load losses and impedance voltages of the transformer, respectively. Then, equations 3.11 and 3.12 are utilized to model the frequency-dependent impedances of the transformer between the primary and secondary sides and between the secondary and secondary sides. Example of frequency-dependent resistance and reactance between the primary and secondary sides that could be used in such model are shown in figures 3.17 and 3.18, respectively. While, another example of the frequency-dependent resistance and reactance between the two secondary sides are shown in figures 3.19 and 3.20, respectively. The graphs show the resistance and reac-

tance vary with frequency, and also that there is a difference between the primary-secondary and secondary-secondary sides values. The reactance varies linearly with the frequency while the resistance increases according to equation 3.11. Moreover, the losses are higher between the primary-secondary sides than between the two secondaries as seen in the resistance graphs.

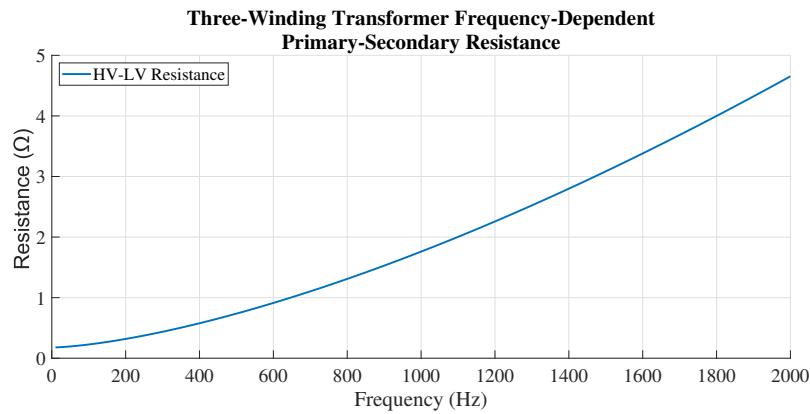


Figure 3.17: Three-Winding Transformer HV-LV Frequency-Dependent Resistance (Example)

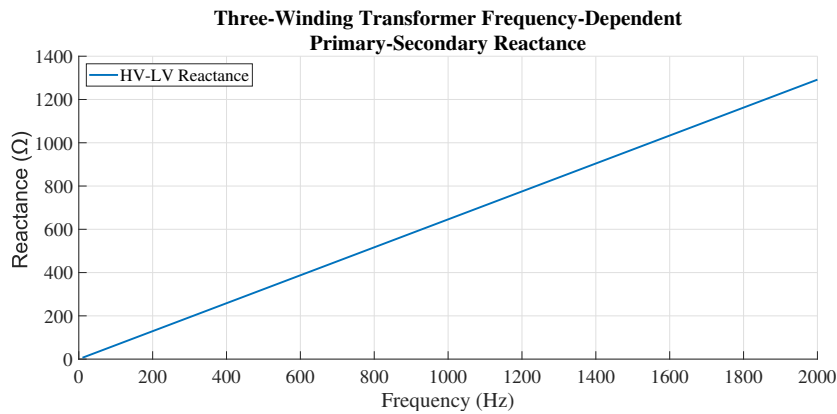


Figure 3.18: Three-Winding Transformer HV-LV Frequency-Dependent Reactance (Example)

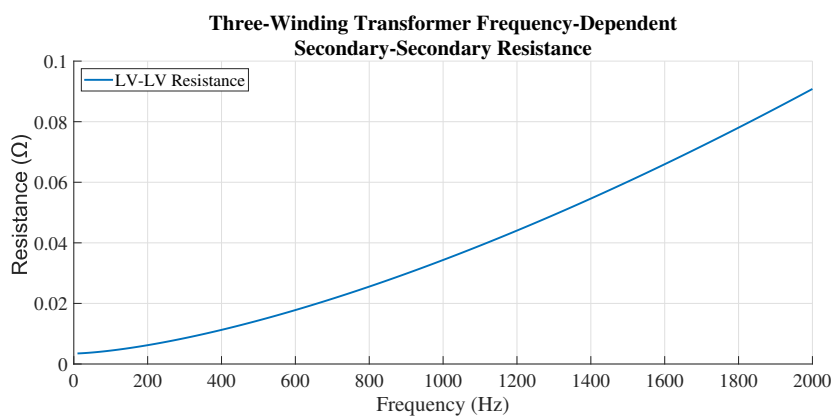


Figure 3.19: Three-Winding Transformer LV-LV Frequency-Dependent Resistance (Example)

3.2.6. Export Cable Systems

There are two export systems in the OWPP: offshore cable system and onshore cable system. The offshore cable system has two parallel 45 km each 110 kV submarine cables connecting the offshore substation to

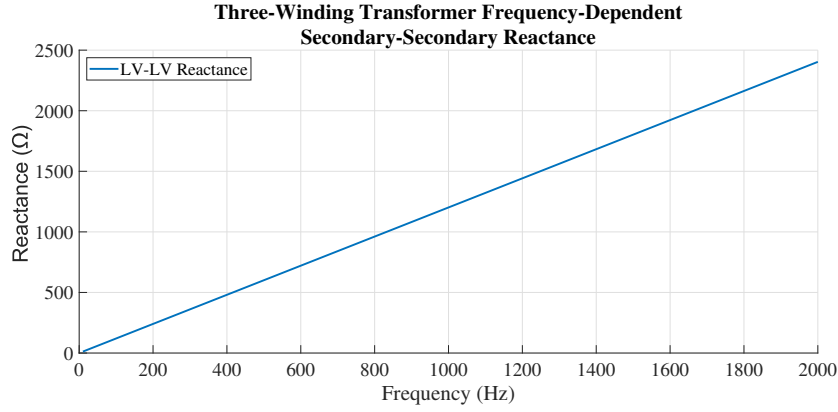


Figure 3.20: Three-Winding Transformer LV-LV Frequency-Dependent Reactance (Example)

the onshore connection point, and onshore cable system has two parallel 45 km 110 kV underground cables connecting the onshore substation to the PCC. The offshore cables are all modelled using *TypCabmult* similar to the array cables while the onshore cables are all modelled using *TypCab*. There are few differences in the modelling of the export cable systems when compared to the 33 kV array cables:

1. Single Core:

The offshore cables are modelled with three single-core cables in trefoil formation and the onshore cables are modelled with three single-core in flat formation while the array cables are modelled with three-core cable in trefoil formation. The offshore cables are usually laid in trefoil formation due to unavailability of sufficient laying corridor under the sea while the onshore cables are laid in flat formation since a larger cable corridor can be obtained [13]. The main reason behind the difference in single-core versus three-core cable is the voltage level; where medium-voltage cables are usually designed as three-core cables [52]. Moreover, the three-core cables are insulated together, thus it is easy to cause inter-phase short circuit when the insulating materials are deteriorated [55]. On the other hand, single-core cables have three separate cables each with its own insulation material, and in case of deterioration in the insulation it is rare to have an inter-phase short circuit [55]. In addition, the single-core cable of the same conductor size usually has higher current carrying capacity [55]. Therefore, it is decided to model the offshore and onshore cables with three single-core cables.

2. Segmental Conductors:

The alternating magnetic field from AC current in a conductor produces an electromagnetic force (emf) that concentrates the current flow in the skin of the conductor [48]. The current carrying capacity decrease due to this high skin effect of large conductors [48]. In segmental conductors, the emfs at the center and at the edge of the cable would partly cancel each other out due to having opposite signs, thus reducing the skin effect and increasing the cable's ampacity for large cross-sectional conductors [48]. The Milliken (segmental) conductors tend to be expensive and hence only used if the cross section of the conductor is larger than 1200 mm². The offshore and onshore cables are modelled with segmental conductors with a cross-section of 2000 mm².

3. Serving Bonding:

Circulating current in steady-state conditions in cable's core induces a voltage in the serving (sheath) of the cable, and when there is a closed loop then this circulating current can increase system losses [48]. Therefore, it is essential to reduce this circulating current and minimize the sheath's voltage to reduce the system losses. There are three different bonding techniques to overcome this problem:

- Single-end bonding where one end of the sheath is grounded and thus reducing the circulating current. However, the voltage is zero at the grounded side while the other end will have a voltage that is proportional to the length of the cable and hence increases the sheath's voltage [48]. This is recommended for short length of cables such as 3 km.

- Both-end bonding where both ends of the sheath are grounded. This technique will reduce the sheath's voltage to almost zero, however there will still be circulating current in the sheath due to the formation of a closed loop resulting in losses in the system [48].
- Cross-bonding where both ends of the sheath are grounded with transposition of the sheath in between as shown in figure 3.21. This technique will reduce the circulating current compared to both-end bonding and it will reduce the induced voltage in the sheath compared to single-end bonding [48]. The cable is divided into three minor sections and the sheath is transposed between them and then grounded at the third minor section [48]. The three minor sections form a major section, thus a cable can be divided to major sections each of which has its own three minor sections. Therefore, HVAC cables are usually installed using cross-bonding technique with a minor section of a maximum length of 3 km due to manufacturing capability limitation [48]. However, there is an exception for submarine cables where cross-bonding is impractical in the sea and both-end bonding is instead recommended and implemented [48].

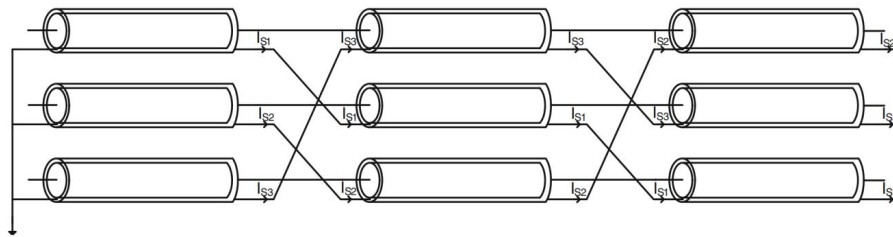


Figure 3.21: Example of a Major Section of a Cross-Bonded Cable [48]

Therefore, it is decided to model the offshore cable using both-end bonding and the onshore cable with cross-bonding technique, this approach is also performed in [56]. The offshore cable's sheath is modelled using a separate line *TypLne* model with zero impedance and then connected to the main cable using the line coupling *ElmCabsys* model in PowerFactory. The sheath is grounded from both ends using a grounding *ElmGndswt* model. This procedure is performed for the two parallel 45 km offshore cable as shown in figure 3.6. The sheath of the onshore cable is also modelled using three-phase lines *TypLne* model with zero impedance for each minor section of the cable. At the end of each minor section, the cross-bonding technique is performed by using three parallel single-phase series reactor *ElmSind* model for the transposition of the sheath's phases that now will be connected to a different phase of the three single-phase series reactor. Then, the three-phase series reactor is connected to the next sheath's minor section and the process is repeated twice to complete the major section where the system will be grounded. The line coupling *ElmCabsys* model is used to couple the sheath and the cable. The 45 km onshore cable is divided into 5 major sections, and each major section has three 3 km minor sections as shown in figure 3.7.

The magnetic field generated by each phase of the three single-core cables is exposed to the other phases' magnetic field by the transposition of the sheath, and when the cable is installed in a trefoil configuration with equal length then the induced voltage and circulating current will be almost zero [48]. However, since the onshore cable are installed in flat formation, then an unbalanced mutual-coupling between phases will most probably occur [48]. Moreover, the flat formation results in greater number of resonance peaks compared to the trefoil formation due to a higher asymmetry in the flat formation [29]. In addition, the cross-bonding results in higher magnitudes and lower resonant frequencies than both-end bonding technique where the latter would result in shifting resonance points to higher frequencies [29]. The number of major sections also impact the resonance points as increasing the number of major sections, for the same cable length, yields in shifting the resonance points to higher frequencies with an increase in the magnitude [29]. Thus, the modelling of the offshore in trefoil formation with both-end bonding and onshore cables in flat formation with cross-bonding will greatly impact the resonance behavior of the OWPP.

The technical specification of the offshore and onshore cables required to model the cables in PowerFactory are presented in table 3.10.

Layer (radius in mm)	Material	Offshore 1C-2000 mm ² Milliken	Onshore 1C-2000 mm ² Milliken
Conductor	Aluminum	28	27.2
Conductor Screen	Semi-Conductor XLPE	1.5	1
Insulation	XLPE	15.5	13
Insulation Screen	Semi-Conductor XLPE	1	1
Magnetic Sheath/Screen	Copper	1.5	1
Over Sheath	HDPE/LDPE	3	2.25
Armor	Steel	5.5	2
Outer Sheath/Serving	PVC	5	4
Outer Diameter		120	101.9

Table 3.10: Offshore and Onshore Cables Specifications
[57] [13]

3.2.7. Shunt Reactors

The capacitance of the cables is 10-20 times higher than the capacitance of an equivalent overhead line [48]. This high capacitance generates a high reactive power that leads to voltage increase in the system and reduction of the cables' ampacity [48, 56]. This high reactive power has to be consumed in order to stabilize the voltage level in the system, which is achieved by using shunt reactors [12, 48]. Shunt reactors are defined as inductive reactance capable of drawing inductive currents from the system, and are designed with an inductor and resistor in series [48, 56]. Despite the fact that shunt reactors improve the voltage profile at fundamental frequency, they actually effect the harmonic profile and thus have to be modelled for harmonic analysis [29].

The shunt reactor is modelled in PowerFactory using *ElmShnt* model. The used technology is 3PH-Y for a three-phase system. The shunt reactors are modelled with no-saturation (linear) and three-limb core. The shunt reactor can be defined using one of two methods:

- Design Parameter: rated reactive power or rated current and a quality factor [58].
- Layout Parameter: inductance and the resistance can be defined [58].

The design parameter approach is considered by estimating the reactive power using the below equation [13]:

$$Q = V^2 \times \text{Capacitance}_{\text{per km}} \times \text{cable length} \times 2\pi \times \text{frequency}_{\text{fundamental}} \quad (3.20)$$

PowerFactory will calculate the power quality from the resistance, which is calculated by dividing the losses by the square of the nominal current [56] as per the below equations:

$$I = \frac{Q}{(\sqrt{3} \times V)} \quad (3.21)$$

$$R = \frac{\text{Losses}}{I^2} \quad (3.22)$$

The estimated reactive power that needs to be consumed is approximately 214 Mvar in the OWPP. As the best location for shunt reactors is the middle of the cable as current flows from the shunt reactor into both directions [48], it is decided to divide the reactive power between two locations and to place the shunt reactors at the 33 kV busbar in the offshore substation where the array cables are terminated and at the 110 kV busbar where the offshore cables are terminated as shown in figures 3.6 and 3.7 and detailed in the shunt reactors design table 3.11. This placement method will ensure that inductive currents are drawn from the array cables, the offshore cables and the onshore cables to meet the voltage limit and improve the cables' ampacity.

Location	33 kV Offshore Substation A-1	33 kV Offshore Substation A-2	33 kV Offshore Substation B-1	33 kV Offshore Substation B-2	110 kV Onshore Connection Point A	110 kV Onshore Connection Point B
Reactive Power Rating (Mvar)	26.75	26.75	26.75	26.75	53.5	53.5
Power Quality	166.67	166.67	166.67	166.67	166.67	166.67

Table 3.11: Shunt Reactors Specifications

The modelling of the shunt reactors for harmonic analysis is performed similar to [47] where the shunt reactors are modelled for frequency analysis by including a frequency-dependent resistance that increases with frequency due to the winding eddy current losses and losses in the core while the inductance is assumed to be constant. The frequency-dependent resistance is modelled using equation 3.2 of the frequency polynomial characteristics with $a = 1$ and $b = 0.5$.

3.2.8. External Grid

The external grid is modelled in PowerFactory using *ElmXnet* model that is connected to the PCC busbar as shown in figure 3.7. The external grid is modelled as a slack (SL) bus type where it controls the voltage set point of the PCC busbar, i.e. set to 1.0 PU. The external grid is modelled as a Thévenin equivalent for harmonic analysis as shown in figure 2.3 where the impedance is frequency-dependent as shown in the example impedance in figure 3.22 while the voltage is modelled using phase-correct option where the magnitude and phase angle of the sequence voltage can be specified. The phase angle of the sequence voltage is assumed zero for all the simulations in the thesis while the magnitude is assigned a fixed value based on the harmonic order. The impedance shown in figure 3.22 provides an idea of how the grid's impedance would have several peaks and valleys and is frequency-dependent. However, a similar yet realistic frequency-dependent impedance is utilized in the model for the fixed grid cases A and C; however, it is not included in the report due to confidentiality. Many TSOs perform several simulations of the grid with N-1 and N-2 contingencies where different parts of the system are disconnected or connected to measure the impedance for different range of harmonic orders. Then, the impedance points could be plotted in a Resistance-Reactance (R-X) plot, and when a contour is drawn around all points then an impedance loci is established. This impedance loci represents the variation in the grid's impedance due to different operating scenarios. Some TSOs require wind farm developers to prove compliance for all points in the impedance loci, and this methodology will be used in cases B and D. A realistic impedance loci is used in the thesis, and it is similar to the impedance loci used in [44].

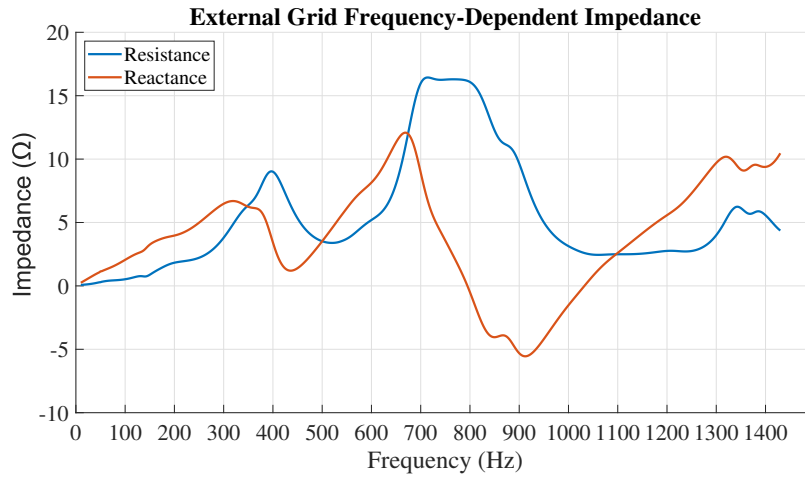


Figure 3.22: An Example of an External Grid Frequency-Dependent Impedance (similar to the impedance used in the thesis)

3.3. Simplified Model

The WT's converters are modelled as Norton equivalent in this thesis and thus they can all be aggregated to one Norton equivalent circuit while the external grid is modelled using a Thévenin equivalent. [13] shows a simplified model for the OWPP with the external grid as shown in figure 3.23. The harmonic voltage distortion at the PCC is computed using equation 3.23.

$$V_{PCC} = \frac{Z_{OWPP}}{Z_{OWPP} + Z_g} \times V_g + \frac{Z_{OWPP} \times Z_g}{Z_{OWPP} + Z_g} \times I_{OWPP} \quad (3.23)$$

The ratio that is multiplied by V_g is called the Harmonic Gain (HG) and it describes the amplification of the external grid background harmonic distortion at the PCC due to its interactions with the OWPP impedance

[13]. The ratio that is multiplied by I_{OWPP} is the equivalent impedance at PCC, which is a parallel impedance of the OWPP and grid impedance.

$$HG = \frac{Z_{OWPP}}{Z_{OWPP} + Z_g} \quad (3.24)$$

$$Z_{PCC} = \frac{Z_{OWPP} \times Z_g}{Z_{OWPP} + Z_g} \quad (3.25)$$

The simplified model demonstrates that the statistical variation of the harmonic current from the OWPP would lead to a statistical variation of the harmonic voltage at the PCC, which can be represented by a probability distribution function. Moreover, the fact that the harmonic currents are represented by their magnitudes and phase angles in the thesis means that the summation and cancellation effect could be exploited since the aggregated I_{OWPP} would be a complex current in lieu of only a magnitude of the 95th percentile in case of the IEC summation rule. Furthermore and as explained previously, the grid impedance could be represented by an impedance loci to capture its changing behavior over time. Each impedance point of the impedance loci could have different resonance points that could amplify the harmonic distortion at the PCC differently leading to a range of harmonic voltage distortions at the PCC. Therefore, this simplified model shows the importance of the impedances and their enormous impact on the harmonic amplification at the PCC. On one hand, there is a statistical variation of the PCC distortion due to the statistical variation of the I_{OWPP} , and on the other hand there is a range of harmonic distortions at the PCC due to the impedance loci, each of which would have also a statistical variation.

The harmonic distortion at the PCC depends on the harmonic voltage distortion of the grid and the aggregated harmonic current of the OWPP. However, some TSOs impose limits on the contribution of the OWPP while considering zero background distortion while others impose limits on the final distortion due to both contributions [13]. Therefore, it is vital to be able to decouple the two contributions to prove compliance in some cases.

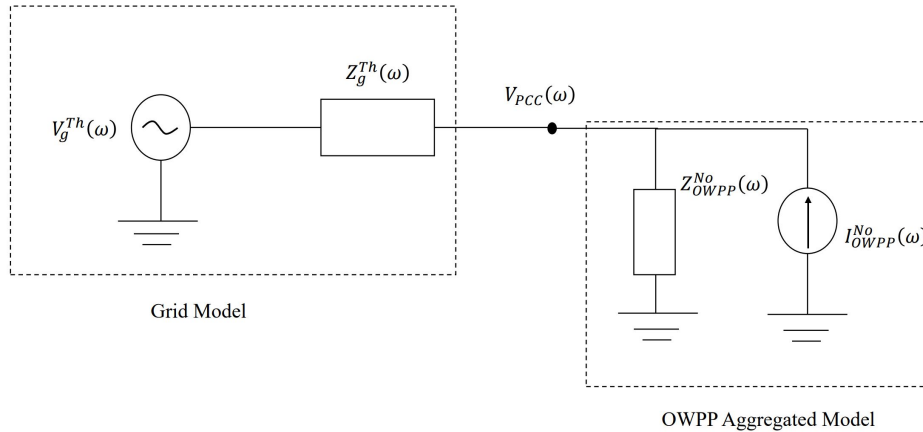


Figure 3.23: Simplified Model

[13]

3.4. PowerFactory Harmonic Analysis and Simulation

This section will provide an overview of power flow simulation, harmonic load flow simulation, frequency sweep and python scripting and interaction with the PowerFactory OWPP model.

3.4.1. Power Load Flow

Load flow is used to analyze the power system under steady-state where all variables and parameters are assumed to be constant during the analysis [27]. PowerFactory utilizes Newton-Raphson in an iterative method to solve the non-linear equations for the system [27]. The load flow calculation determines the magnitude of the voltage and its phase angle of the nodes, the magnitude of the current and its phase angle, and active and reactive power flow [27]. The nodes of the wind turbines (busbars/terminals) in the model are defined as

PQ nodes where the active and reactive power values are specified while the PCC node is specified as a slack node where the voltage magnitude is fixed. The calculations methods are:

- **AC Load Flow, balanced, positive sequence:** performs load flow calculations for a single-phase positive sequence network representation, valid for symmetrical networks [27].
- **AC Load Flow, unbalanced, 3 Phase (ABC):** performs load flow calculations for a multi-phase network representation, and it is used to analyze unbalanced 3-phase systems [27].
- **DC Load flow :** performs a DC load flow [27].

A load flow is required to be performed prior to performing harmonic load flow to calculate the fundamental current magnitudes I_1 and phase angles φ_1 at the WTs' terminals to be used in the calculations of the harmonic currents injected by the current sources of the Norton equivalent that represent the converters of the WTs as seen in equation 3.4. The cross-bonding and the flat formation of the onshore cable make the OWPP network an unbalanced system, hence an unbalanced AC load flow will be performed.

3.4.2. Harmonic Load Flow

The harmonic load flow in PowerFactory calculates harmonic voltage and current distortions at all nodes in the network by performing a steady-state network analysis at each frequency at which harmonic sources are defined [27]. Similar to the power load flow, iterative Newton-Raphson method is used [27]. The harmonic load flow can be performed as phase-correct (balanced or unbalanced) or according to IEC 61000-3-6 summation rule. If at least one harmonic source is defined as IEC 61000-3-6 then the harmonic load flow will be performed based on the summation rule [27]. The proposed method in the thesis will utilize the unbalanced phase-correct method to be able to define both the magnitude and phase angle of the harmonic currents, however the IEC method will also be performed to compare the results. PowerFactory harmonic load flow has two network representation options:

- **Balanced:** This option is used to represent symmetrical networks and balanced harmonic sources where the characteristics harmonic can be either in the positive sequence component (7th, 13th, etc) or negative sequence component (5th, 11th, etc) [27]. A single-phase (positive or negative) equivalent representation of the network is used in the analysis [27].
- **Unbalanced, 3-Phase (ABC):** This option is used to represent non-symmetrical networks, unbalanced harmonic injections or inter-harmonics [27].

Similar to the power load flow, an unbalanced 3-phase ABC option is used in the thesis to calculate the harmonic distortion of the non-symmetrical OWPP.

PowerFactory can perform harmonic load flow for a single frequency, i.e. 5th or for all frequencies for which harmonic sources are defined [27]. The single frequency option will calculate the harmonic distortion of the selected frequency only while the all frequencies option will calculate the harmonic distortion for all frequencies. A single-frequency option will be used in the thesis to calculate the distortion of each of the harmonic orders specified in the study.

3.4.3. Frequency Sweep

PowerFactory frequency sweep command is used to calculate the frequency dependent impedances for a specified frequency range [27]. The frequency sweep can be used to analyze the series and parallel resonance of the network at any terminal, and it will be used in the thesis to compute the impedance characteristics at the PCC. Similar to the harmonic load flow, two network representations are available: balanced, positive sequence and unbalanced, 3- phase (ABC), and the latter is chosen.

The frequency sweep command can provide the self-impedance values only (the diagonal elements of the impedance matrix). Thus, it was necessary to develop a separate python code to compute the whole impedance matrix in the sequence domain. The method involved adding a new current source at the PCC that injects a known harmonic current at each harmonic order (while all other harmonic sources are injection zero harmonic current), measuring the voltage distortion at the PCC for all the sequences, and then computing the impedance matrices. The results of the PCC and OWPP impedance matrices are shown in section 4.1.3.

3.4.4. Python Scripting

PowerFactory has two scripting options: Digsilent Programming Language *DPL* and Python. The DPL is a built-in programming language that is used for automating tasks in PowerFactory [27]. The same automation can also be performed by the open source programming language Python. It is decided to utilize Python to perform the Monte Carlo simulations explained in section 2.2.4 and as detailed in the following procedure and presented in the process flow chart in figure 3.24:

1. Perform an unbalanced power flow in the OWPP to get the phase angle of the fundamental current at all the wind turbines' terminals. Each wind turbine will have a different φ_{11} Since they are located at different locations in the OWPP.
2. Specify the value of the background distortion based on the harmonic order under assessment.
3. Specify the minimum number of iterations, i.e. 1,000 iterations, or the number of iterations based on the accuracy requirements.
4. Generate and assign a unique random harmonic current magnitude to each WT in the OWPP for the harmonic order under assessment from the PDF in figure 3.2.
5. Generate a unique random harmonic current phase angle for each WT in the OWPP for the harmonic order under assessment from the PDF in figure 3.3.
6. Calculate the random phase angles for all WTs using equation 3.6 based on the harmonic order and the fundamental phase angles for all phases and assign these values to the WTs.
7. Execute an unbalanced harmonic load for the harmonic order under assessment.
8. Measure and record the harmonic distortion at the PCC in an external file.
9. Repeat the procedure from step 4 to 8 till the specified number of iterations is met.

Upon completing all the steps explained above, at least 1,000 (minimum number of iterations) harmonic voltage distortion values will be available for analysis. A histogram can be constructed using these distortion values to represent the statistical variation of the voltage distortion at the PCC. The mean, standard deviation and the 95th percentile of the harmonic voltage distortion can also be computed for each harmonic order under assessment. The 95th percentile is the most interesting value since the harmonic emission limit is compared to it.

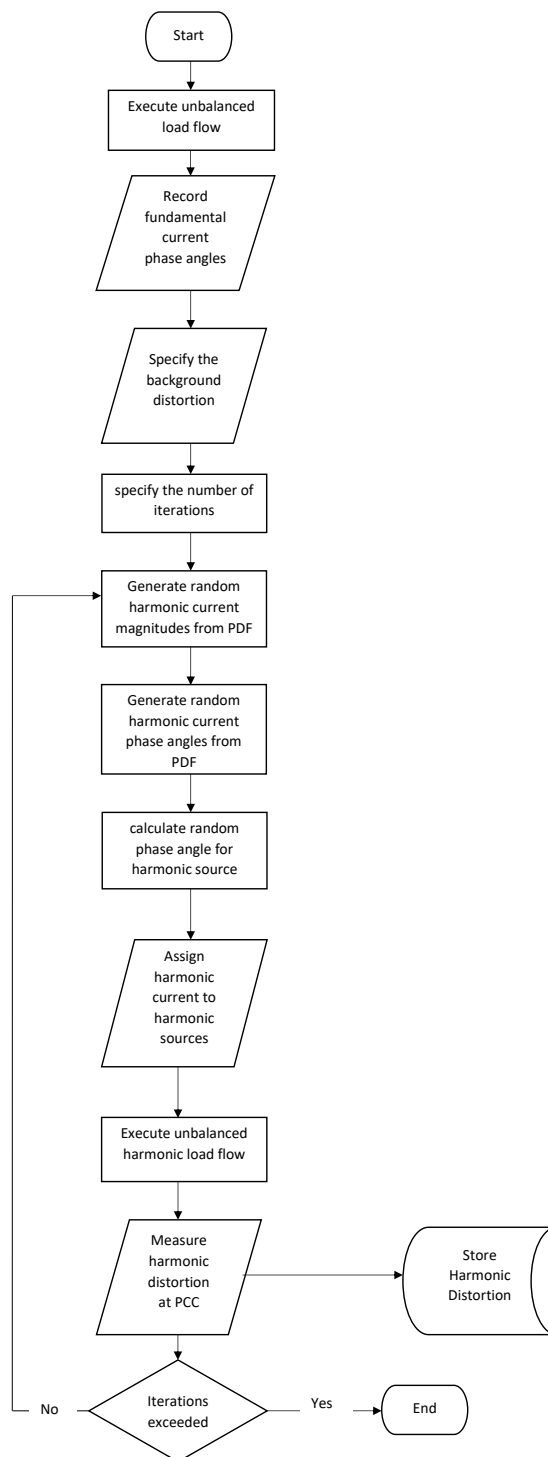


Figure 3.24: Python Script Flow Chart

4

Results and Discussions

4.1. Simulation and Network Analysis

It is imperative to analyze and understand the OWPP network prior to analyzing and discussing the results of the Monte Carlo simulations to gain a comprehensive perspective on how the results are obtained including impacting and influencing factors. This section will discuss the accuracy of the Monte Carlo simulation and the determination of the number of iterations, then it will cover the influencing factors on the final results by discussing the amplification factor, after that the results of frequency sweep will be utilized to discuss the impedance impact on the harmonic distortion and amplification at the PCC, which will be supported with hand verification for a simplified model.

4.1.1. Monte Carlo Simulation

Monte Carlo simulation was explained in section 2.2.4, and it was decided that the minimum number of iterations "N" is set to 1,000. The pre-defined statistical error "E" is set to 0.1% and the confidence level " Z_c " is set to 99.75%. As the Monte Carlo simulation always starts with the trial run with the minimum number of iterations, an approximation of the mean μ and the standard deviation σ can be computed for the harmonic voltage distortion at the PCC. Then, using the pre-defined statistical error and confidence level, the number of iterations is calculated using equation 2.20. If the number of iterations is below the minimum number of iterations, then the pre-defined statistical error and confidence level are met, and the results of this trial iteration is utilized in the study. Otherwise, the computed number of iterations would be the required number to be performed in order to meet the accuracy requirements. Increasing the number of iterations does not always yield more accurate results as the accuracy can be achieved using equation 2.20. The 5th harmonic order is simulated for different iterations using a balanced harmonic load flow and results are obtained in order to examine this hypothesis. The results are presented in table 4.1 and in figure 4.1.

Number of Iterations	Simulation Time (seconds)	Mean of HD (%)	Standard Deviation of HD (%)	95 th Percentile of HD (%)
10	44.02	1.10109	0.00334	1.10702
500	241.70	1.10079	0.00282	1.10530
1,000	477.67	1.10076	0.00317	1.10575
10,000	5,179.67	1.10089	0.00305	1.10600
50,000	51,256.12	1.10088	0.00304	1.10591

Table 4.1: 5th Harmonic Order Simulation Results

As seen in the iteration graph 4.1, the mean of the harmonic distortion in percent does not change significantly after the 1,000 iteration. Moreover, the deviation prior to the 1,000 iteration is within 0.09%. This indicates that the minimum number of iterations met the accuracy level for the 5th harmonic, and the statistical error and confidence level are within the pre-defined boundaries.

This confirms that calculating the required number of iterations based on the minimum iteration simulation is sufficient to meet the accuracy level without the need for very long and time-consuming simulations.

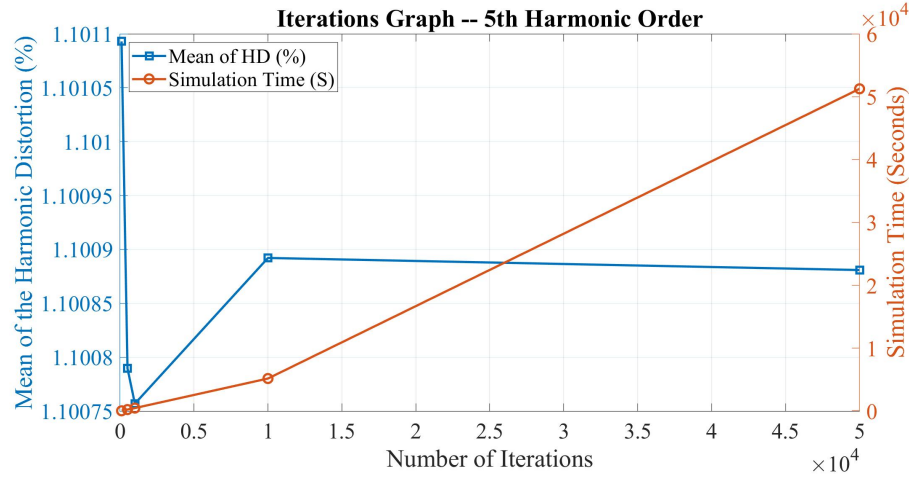


Figure 4.1: The Iteration Graph

4.1.2. OWPP Amplification Analysis

It is imperative to understand what factors play a major role in defining the harmonic distortion at the PCC prior to analyzing the results of the Monte Carlo simulations and to gain this insight an amplification factor (k) is introduced. The amplification factor is obtained by dividing the 95th percentile of the harmonic distortion (V) at the PCC by the 95th percentile of the injected harmonic current (A) as shown in equation 4.1. The 95th percentile of the harmonic distortion is measured at the PCC in Volts. While the 95th percentile of harmonic current magnitude is obtained by multiplying the 95th percentile of the harmonic current magnitude by the fundamental current of the WT, which is the 95th percentile of the current assigned to the current source of the Norton equivalent of the converter.

$$\text{Amplification Factor} = \frac{95^{\text{th}} \text{ percentile of Harmonic Distortion (V)}}{95^{\text{th}} \text{ Percentile of current magnitude (A)}} \quad (4.1)$$

The issues that will impact the amplification factors are: the OWPP network, the probability distribution function of the WT current magnitude, the probability distribution function of the WT current phase angle, and the external background distortion. In order to study the influence of each of these issues separately, four scenarios have been created. The scenarios range from the most simple (which does not include any statistical variation nor background distortion), to the most complicated (which includes all elements), hence the gradual effect of each issue is understood by seeing the incremental changes in the amplification factors. In particular, the scenarios are:

- The OWPP network and the impedance at PCC and this scenario is called "Deterministic Magnitude" since there is not any statistical variations.
- The probability distribution functions of the harmonic current magnitude and this scenario is called "Random Magnitude".
- The probability distribution functions of the phase angle of the harmonic current and this scenario is called "Random Phase Angle".
- The external grid background distortion for each harmonic order and this scenario is called "Background Distortion Impact".

These four factors and scenarios will serve as the foundation to explain and understand the final results of the different cases using the proposed probability harmonic estimation method in this thesis.

In the first scenario, the WTs are all assigned the 95th percentile of the harmonic current magnitude with zero phase angle and without any background distortion assigned to the external grid. The amplification factors shown in figure 4.2 demonstrate the network response for different harmonic orders. It shows that the 8th harmonic order will have the highest amplification factor and this could be attributed to the impedance

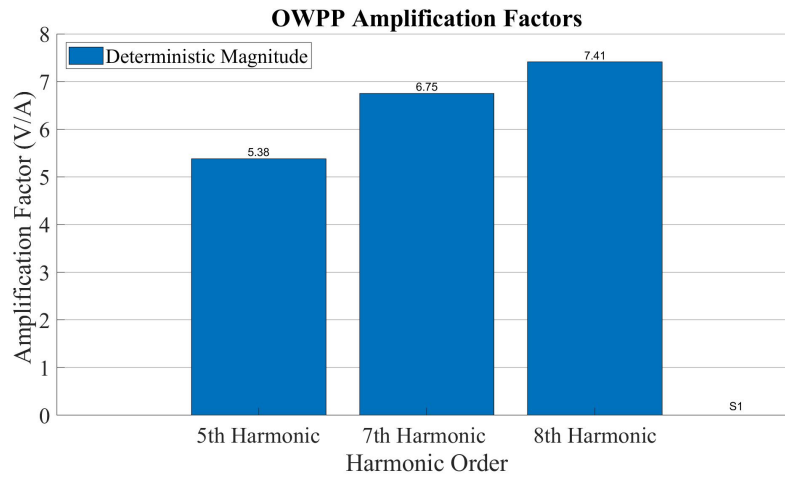


Figure 4.2: Amplification Factor- Deterministic Magnitude Scenario

at the PCC since the amplification factor is an impedance value (voltage divided by current). However, this will be explained in the next section.

The second scenario introduces statistical variation in the magnitude of the harmonic current to understand the impact of basing harmonic emission studies on the probability distribution function of the harmonics in lieu of the 95th percentile as recommended in IEC summation rule. The WTs are assigned random harmonic current magnitudes drawn from the PDF shown in figure 3.2 with zero phase angle and no background distortion. The simulation is performed for 1,000 iterations for each harmonic order, then the 95th percentile of the harmonic voltage distortion at the PCC is calculated from the results and used to calculate the amplification factors in figure 4.3 for the three harmonic orders to compare them with the deterministic magnitude scenario results. The statistical variation of the magnitude yields lower amplification factors and this is expected since now the harmonic analysis is not performed on a single value and that the WTs' converter could be injecting lower harmonic current into the OWPP. This shows that using the summation rule with only the 95th percentile could result in overestimating of the harmonic distortion at the PCC, with all other parameters assumed to be equal. It is also important to understand how the shape of the PDFs is related to the difference between the two scenarios. The difference between the scenarios is called the amplification factor error, which is the percentage change in the amplification. While the ratio of the standard deviation over the mean of the harmonic current magnitude is called the PDFs parameter ratio. The reason we are comparing to this ratio and not to the standard deviation is that the ratio can provide an insight of much the current magnitude could change by adding or subtracting the standard deviation to the mean. The standard deviation only does not indicate whether the change from the mean is statistically big or small if it is not compared to the original mean. It is concluded as presented in table 4.2 that both values have the same behavior. The 8th harmonic has the highest amplification factor error and the highest PDF parameter ratio while the 7th harmonic has the lowest values. This shows the relationship between how random the magnitude of the harmonic current to how much error could be expected in the final amplification factor results.

Harmonic Order	Amplification Factor Error (%)	Probability Distribution Function Parameter Ratio (%)
5 th Harmonic	29.4	21
7 th Harmonic	25.79	18
8 th Harmonic	62.44	47

Table 4.2: Amplification Factors-Random Magnitude

The third scenario introduces the statistical variation of the phase angle of the harmonic current to understand how harmonic currents could cancel out due to opposing phase angles that is not fully considered in IEC summation rule. The WTs' harmonic sources are now assigned random phase angles drawn from the phase angle PDF shown in figure 3.3 in addition to the random harmonic current magnitude taken from its PDF in figure 3.2 but without any background distortion. The simulation is performed for 1,000 iterations for

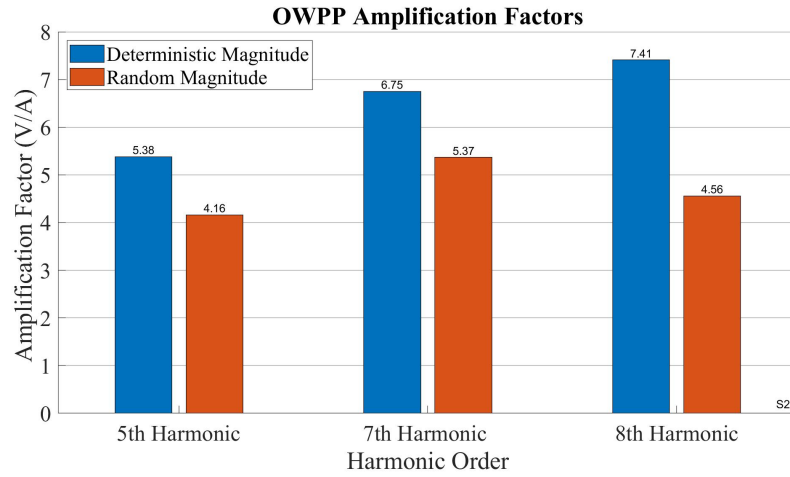


Figure 4.3: Amplification Factor- Random Magnitude Scenario

each harmonic order, then the 95th percentile of the harmonic voltage distortion at the PCC is calculated from the results and used to calculate the amplification factors. The variation of the phase angles leads to different cancellation impact for the harmonic orders when compared to the second scenario, i.e. random magnitude. It is shown in figure 4.4 that the biggest change in the amplification factor is seen in the 8th harmonic that indicates a high cancellation effect that is attributed to the highest standard deviation of the harmonic current phase angle. The amplification factor error is consistent with the trend of the phase angle standard deviation as shown in table 4.3. Therefore, it can be concluded that the standard deviation of the phase angle of the harmonic current could indicate how much harmonic current cancellation and amplification factor error would be expected in the OWPP.

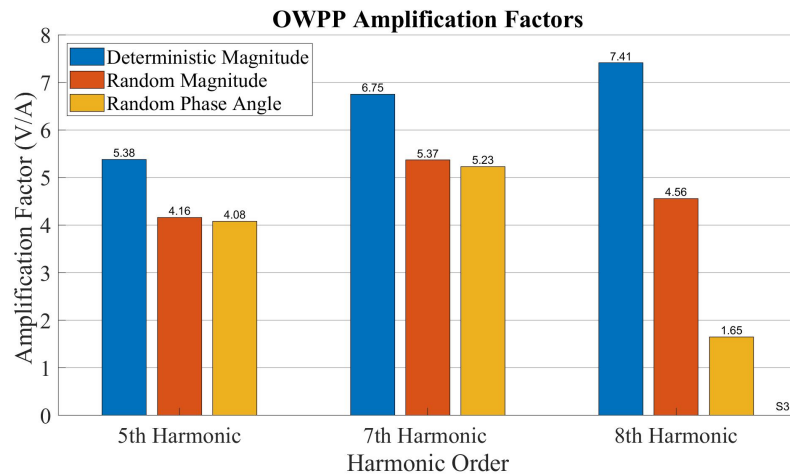


Figure 4.4: Amplification Factor- Random Phase Angle Scenario

Harmonic Order	Amplification Factor Error (%)	Standard Deviation of The Phase Angle (°)
5 th	1.81	10.76
7 th	2.66	13.42
8 th	176.34	94.93

Table 4.3: Amplification Factors-Random Phase

The fourth scenario accounts for the external grid distortion and demonstrates its impact on the amplification factors of the OWPP. The WTs are assigned random harmonic current magnitude and phase angles

drawn from their PDFs and the background distortions shown in figure 4.5 are now assigned for the different harmonic orders in the external grid model. The simulation is performed again for 1,000 iterations for each harmonic order, and then the 95th percentile of the harmonic distortion is used to compute the amplification factor. The 7th harmonic has the biggest background distortion, which is expected to translate into the biggest impact on the amplification factor while the 8th has the lowest background distortion that would result in lower amplification factor. The amplification factors presented in figure 4.6 confirm the expected results. It can be concluded that there is a positive correlation relationship between the external grid distortion and the amplification factor.

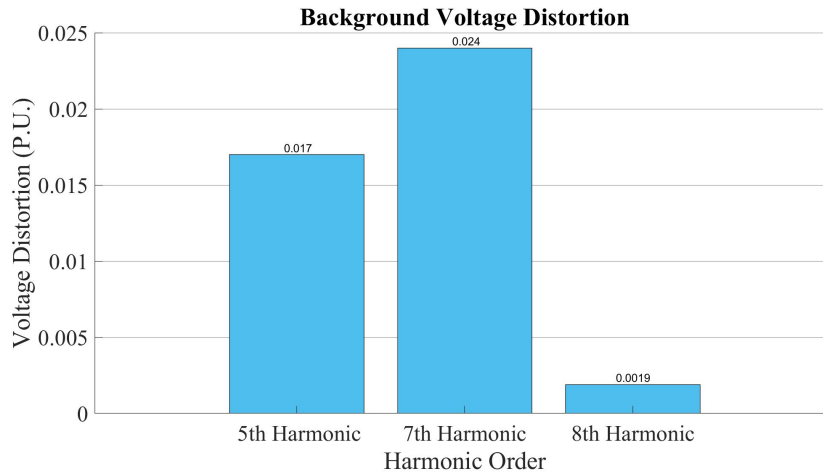


Figure 4.5: External Grid Background Distortion

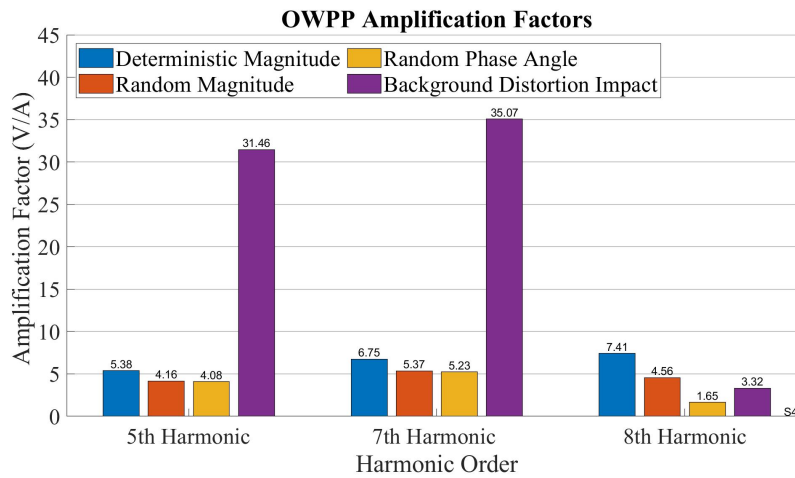


Figure 4.6: Amplification Factor- Background Distortion Impact Scenario

4.1.3. OWPP Network Analysis

In section 3.3, the simplified model was explained and equation 3.23 demonstrated that the harmonic voltage distortion at the PCC is greatly impacted by the impedances of the OWPP and external grid, and therefore so do the amplification factors. The amplification factor as a definition is voltage divided by current, which is basically an impedance. Moreover, the impedance at the PCC could result in resonance points that can amplify the harmonic distortion. Therefore, it is very important to execute a frequency sweep to obtain and analyze the impedance at the PCC.

The OWPP is an unbalanced network due to the cross-bonding and flat formation of the onshore cables, thus it is important to examine an impedance matrix to determine the coupling between the different sequence components. The zero-sequence harmonics are not analyzed since they can be trapped by the delta

winding of the WT's transformers, hence it is not included in the impedance matrix in equation 4.2 that is obtained for each frequency. Since the frequency sweep command in PowerFactory does not generate the complete impedance matrix, a separate python code was written to automate this task and to acquire the impedance matrices as explained in section 3.4.3.

$$Z_h(\omega) = \begin{bmatrix} Z_{++} \angle \varphi_{++} & Z_{+-} \angle \varphi_{+-} \\ Z_{-+} \angle \varphi_{-+} & Z_{--} \angle \varphi_{--} \end{bmatrix} \quad (4.2)$$

The magnitude of the impedance elements of OWPP impedance matrix is shown in figure 4.7 while the phase angles are shown in figure 4.8, and the main findings are:

- The diagonal impedance elements (Z_{++} and Z_{--}) are identical.
- The off-diagonal impedance elements (Z_{+-} and Z_{-+}) have almost identical values up to the 25th harmonic order after which they have minor differences, which could be attributed to the unbalanced onshore cabling system.
- The off-diagonal impedance elements are not always lower than the diagonal elements, and in fact they exceed them between 11th and 13th, and between 16th and 19th harmonic orders. This could be a result of the unbalanced mutual-coupling between the phases of the onshore cables.
- The number of major sections in the onshore cable could be the reason behind shifting the resonance points to higher frequencies with higher magnitude [29], and could explain the high parallel resonance point around the 21st harmonic order.
- The cross-bonding of the onshore cable could result in low resonant points with high magnitude while the both-end bonding would result in higher resonance points [29].
- The onshore cable is in flat formation with cross-bonding while the offshore cable is in trefoil formation with both-end bonding, thus the OWPP impedance is impacted by these factors. However, it is not part of the objective of this thesis to fully analyze each factor and its impact on the impedance.

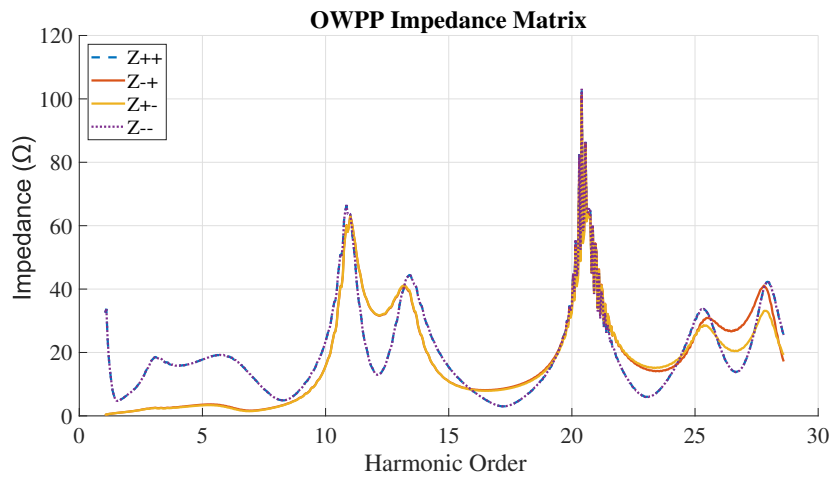


Figure 4.7: OWPP Impedance Matrix- Magnitudes

The impedance matrices of the OWPP for the 5th, 7th and 8th harmonic orders are presented in the below equations:

$$Z_{5^{th} OWPP} = \begin{bmatrix} 17.78 \angle 4.55 & 3.32 \angle 90.7 \\ 3.53 \angle -29.76 & 17.78 \angle 4.55 \end{bmatrix} \quad (4.3)$$

$$Z_{7^{th} OWPP} = \begin{bmatrix} 12.5 \angle -31.46 & 1.5 \angle 95.29 \\ 1.67 \angle -32.11 & 12.5 \angle -31.46 \end{bmatrix} \quad (4.4)$$

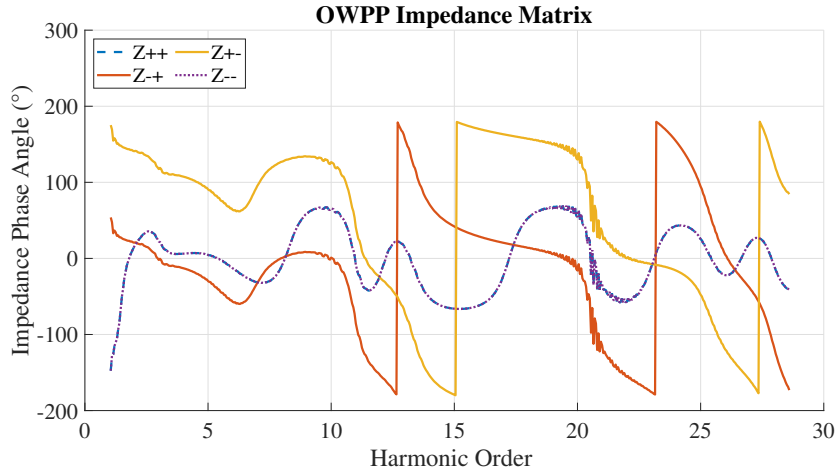


Figure 4.8: OWPP Impedance Matrix- Phase Angles

$$Z_{8^{th}OWPP} = \begin{bmatrix} 5.44 \angle -9.37 & 2.75 \angle 127.12 \\ 2.84 \angle 0.51 & 5.44 \angle -9.37 \end{bmatrix} \quad (4.5)$$

The off-diagonal impedance of the 5th and 7th are relatively low compared to the diagonal impedance while the off-diagonal impedance of the 8th harmonic order is relatively high compared to the diagonal impedance, which indicates that analyzing the harmonic distortion based on the diagonal impedance only may not be sufficient.

The equivalent impedance at PCC is the parallel impedance of the OWPP and grid impedances as seen in equation 3.25. The magnitudes of the elements in the impedance matrix are shown in figure 4.9 while the phase angles are shown in figure 4.10, and the main findings are:

- The diagonal impedance elements (Z_{++} and Z_{--}) are identical.
- The off-diagonal impedance elements (Z_{+-} and Z_{-+}) have almost identical values up to the 25th harmonic order after which they have minor differences, which could be attributed to the unbalanced onshore cabling system.
- The off-diagonal impedance elements are not always lower than the diagonal elements, and in fact they exceed them between 12th and 13th, and between 16th and 18th harmonic orders, which has a small difference in the deviation behavior when compared to the OWPP impedance. This also could be as a result of the unbalanced mutual-coupling between the phases of the onshore cables.
- The PCC impedance is lower than the OWPP impedance in general as seen from a lower magnitude of the parallel resonance points especially the highest parallel resonance point around the 21st harmonic of the OWPP that became a low series resonance at the PCC.

The impedance matrices at the PCC for the 5th, 7th and 8th harmonic orders are presented in the below equations:

$$Z_{5^{th}PCC} = \begin{bmatrix} 10.37 \angle 34.32 & 1.16 \angle 151.25 \\ 1.24 \angle 30.78 & 10.37 \angle 34.32 \end{bmatrix} \quad (4.6)$$

$$Z_{7^{th}PCC} = \begin{bmatrix} 10.65 \angle -11.4 & 1.08 \angle 136 \\ 1.21 \angle 8.59 & 10.65 \angle -11.4 \end{bmatrix} \quad (4.7)$$

$$Z_{8^{th}PCC} = \begin{bmatrix} 4.83 \angle -6.67 & 2.08 \angle 136 \\ 2.14 \angle 9.34 & 4.83 \angle -6.67 \end{bmatrix} \quad (4.8)$$

The PCC impedance directly impacts the amplification factor and the amplification of harmonic currents at the PCC since the PCC impedance ratio is multiplied by I_{OWPP} as seen in the simplified model in section

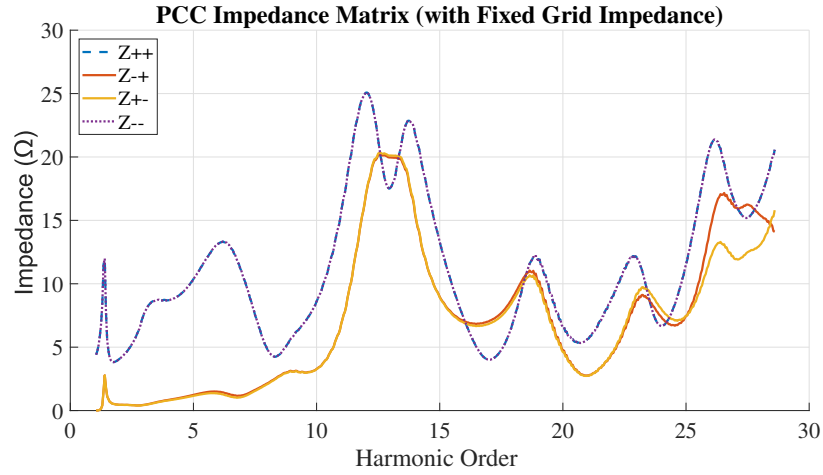


Figure 4.9: PCC Impedance Matrix- Magnitudes

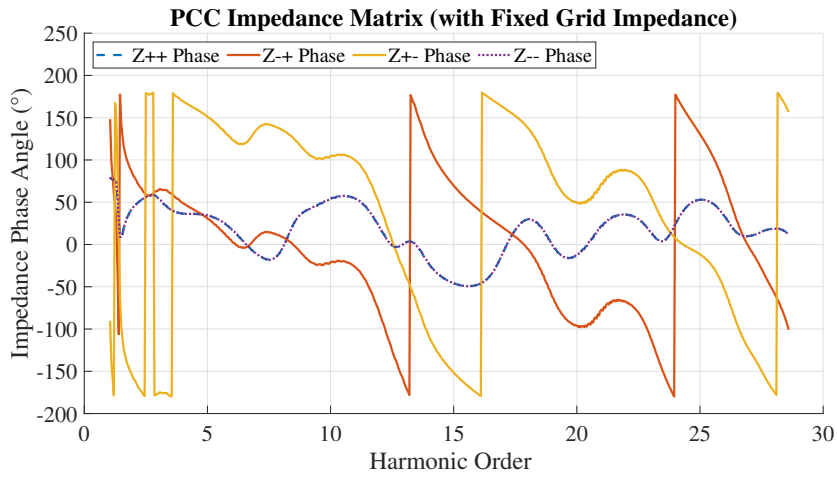


Figure 4.10: PCC Impedance Matrix- Phase Angles

3.3 and equation 3.23. The 5th and 7th harmonic orders have a relatively high and equal impedance matrices, which indicates that the harmonic distortion would be high. On the other hand the 8th harmonic order has a lower impedance matrix that indicates the harmonic distortion could be lower in magnitude at the PCC. Nonetheless, the PCC impedance matrices are not aligned with the results obtained for the amplification factors for the deterministic magnitude. To illustrate, in figure 4.2 it can be seen that the 8th harmonic order has the highest amplification factor, however it also has the lowest impedance matrix at the PCC. This could be explained by looking at the simplified model in figure 3.23. The current source in the Norton equivalent represents the emission by the entire OWPP. This current source, however, is not equal to one of the WT current sources scaled (i.e. multiplied by the number of WTs in the OWPP) but, rather, it depends also on the impedance of the network in the OWPP. A simplified network shown in figure 4.11 is used to further explain this concept, which has two parallel WTs that are injecting harmonic current into the network and then harmonic voltage distortion is measured at the PCC. The aggregation of this simple model can be obtained as shown in figure 4.12 and the Z_{OWPP} and I_{OWPP} are calculated as per the below equations [13]:

$$Z_{OWPP} = \frac{Z_{WT} + Z_{Network}}{2} \quad (4.9)$$

$$I_{OWPP} = \frac{2 \times Z_{WT}}{Z_{WT} + Z_{Network}} \times I_{WT} = f(Z_i) \times I_{WT} \quad (4.10)$$

Equation 4.10 demonstrates that the aggregated harmonic current I_{OWPP} is a product of the wind turbine current and an impedance function, i.e. $f(Z_i)$. It is also known that when there is not any background voltage

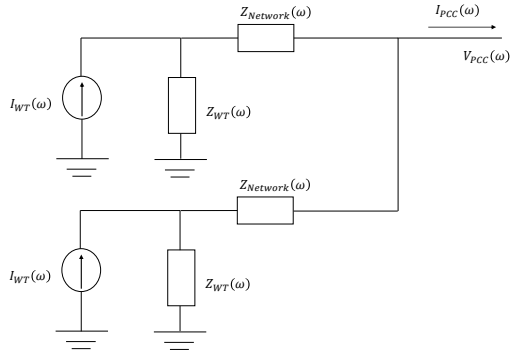


Figure 4.11: Simple Wind Farm Model

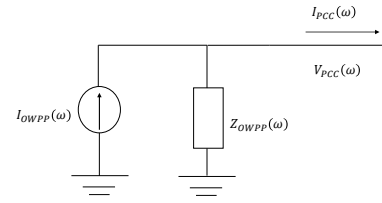


Figure 4.12: Aggregated Simple Wind Farm Model

distortion, then equation 3.23 is simplified to:

$$V_{PCC} = \frac{Z_{OWPP} \times Z_g}{Z_{OWPP} + Z_g} \times I_{OWPP} \quad (4.11)$$

The voltage distortion at the PCC is a product of the equivalent impedance at the PCC and the aggregated harmonic current of the OWPP which now becomes:

$$V_{PCC} = \frac{Z_{OWPP} \times Z_g}{Z_{OWPP} + Z_g} \times f(Z_i) \times I_{WT} \quad (4.12)$$

Therefore, the amplification factor in equation 4.1 does not only equal the equivalent impedance at the PCC. However, it is the product of the equivalent impedance and the network impedance function $f(Z_i)$ as demonstrated in equation 4.13 and further presented in figure 4.13 which explains the inconsistencies between the PCC impedance and the deterministic magnitude amplification factor. To put it another way, the fact that the PCC impedance at the 8th harmonic is very low in comparison to the other harmonics, but the amplification factor for the 8th harmonic is higher than the other harmonics, is explained by the fact that the aggregated emission from the OWPP I_{OWPP} also depends on the impedance of the network. Therefore, it is not enough to analyze the PCC impedance in order to predict which harmonics will have higher amplifications from the WT to the PCC, but, rather, the amplification factors need to be analyzed. A simple model of 7 WTs is used to verify and confirm this approach as shown in appendix A.1.

$$\text{Amplification Factor} = Z_{PCC} \times f(z_i) \quad (4.13)$$

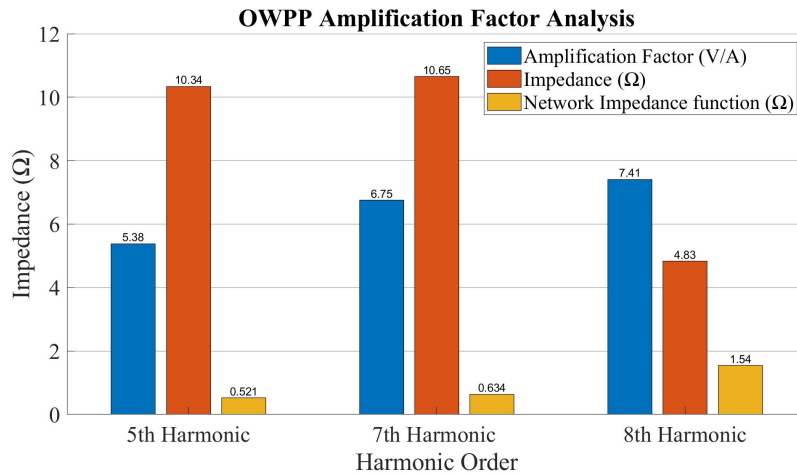


Figure 4.13: OWPP Amplification Analysis

4.2. Case A (linear and fixed grid impedance)

4.2.1. Background

Case A is implemented to answer the first research question, which inquires on how the harmonic grid compliance result is compared when harmonic studies are performed based on probability theory versus the summation law. The probability distribution function of magnitudes and phase angle of harmonic orders presented in section 3.1.2 are utilized in this case. A simple, yet a realistic and fixed background impedance is included in the model for this case as seen the example in figure 3.22. There are four simulation scenarios for each harmonic order:

1. **Scenario 1:** This scenario is the proposed Monte Carlo method in the thesis, and the background harmonic distortion is included in the simulation.
2. **Scenario 2:** This is IEC summation rule with the background harmonic distortion.
3. **Scenario 3:** This is the Monte Carlo method without the background harmonic distortion.
4. **Scenario 4:** This is IEC summation rule without the background harmonic distortion.

As previously mentioned in section 2.1.4, some TSOs require wind farms developers to prove compliance without considering the distortion from the background grid while others require compliance with the grid distortion. Therefore, the two situations are considered and analyzed in this thesis.

4.2.2. Simulation Results

5th Harmonic Order

The required number of iterations to achieve an accuracy level that has a confidence interval (CI) of 99.75% and error in the mean equal to 0.1% is calculated by using the mean and standard deviation of the minimum iteration run, i.e., 1,000 iterations with equation 2.20:

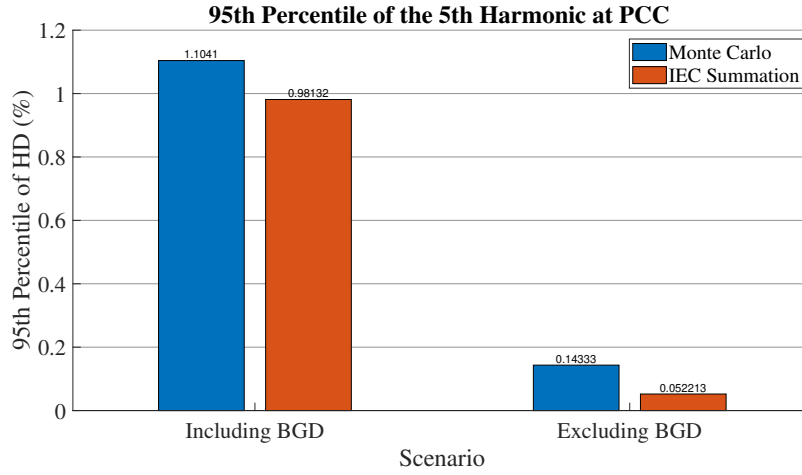
$$N = \left(\frac{100 \times Z_c \times S}{\mu \times E} \right)^2 = \left(\frac{100 \times 3 \times 0.00323}{1.09902 \times 0.1} \right)^2 = 78 \text{ iterations}$$

The accuracy level can be achieved with 78 iterations only, hence the simulated 1,000 iterations results are used for discussion and analysis. The results of the different scenarios for the 5th harmonic are presented in table 4.4. The results of the 95th percentile of the harmonic distortion in percentage are presented in figure 4.14 for all scenarios.

Scenario	1	2	3	4
Parameter	1,000 iterations	1 iteration	1,000 iterations	1 iteration
Mean of Harmonic Distortion (%)	1.09902	N/A	0.13821	N/A
Standard Deviation of Harmonic Distortion (%)	0.00323	N/A	0.00313	N/A
95 th Percentile of Harmonic Distortion (%)	1.10413	0.98132	0.14333	0.052213
Mean of Harmonic Distortion (V)	1,208.92	N/A	152.03	N/A
95 th Percentile of Harmonic Distortion (V)	1,214.54	1,079.45	157.66	57.43

Table 4.4: 5th Harmonic Order Scenarios' Results

Scenario 2 demonstrates that the IEC summation rule will underestimate the Monte Carlo method scenario 1 by approximately 12.5%. This shows that the assumed exponent in the IEC rule does not appropriately represent the actual phase angle of the harmonic current nor does only using the 95th percentile of the harmonic current magnitude. Moreover, figure 4.14 shows for this specific OWPP under assessment and the specific PDFs that were assumed for the 5th harmonic, that the IEC exponent assumes that the cancellation effect is higher than reality. This could be attributed to the fact that the assigned phase angle PDF for the 5th harmonic order (based on measurements as explained in section 3.1.2) has a relatively low standard deviation, which leads to a strong summation effect of the harmonics that might have been underestimated by the IEC exponent. The variation in the phase angle of the 5th harmonic is expected to be low due to the fact that low harmonics tend to be synchronized to the fundamental voltage waveform as explained in sections 3.1.1 and 2.1.6. Therefore, it is expected that for other wind farms with similar WT configurations that the IEC summation rule also underestimates the distortion at the PCC for the 5th harmonic.

Figure 4.14: The 95th Percentile of the 5th Harmonic Order

Although the harmonic emission limit is set to 2% as shown in section 2.1.4 and neither of the scenario is exceeding it, it is noteworthy to mention that the Monte Carlo method, scenario 1, provides more accurate results since it considers the statistical variation of the harmonic current in the network while IEC summation rule does not.

The difference between the first two scenarios and last two scenarios presented in figure 4.14 is expected as the background harmonic distortion has a higher contribution to the overall harmonic distortion as seen from the amplification factor in scenario 4 in figure 4.6.

Excluding the background harmonic distortion from scenarios 3 and 4 demonstrate that statistical variation of the harmonic current has a great impact on the final distortion level at the PCC. The IEC summation rule in scenario 4 underestimates the harmonic distortion by 174% when compared to the Monte Carlo method in scenario 3. These two scenarios exemplify the summation effect in the final harmonic distortion value more than the first scenarios. The proper representation of the phase angle of the injected harmonic by the WT leads to a higher harmonic distortion than IEC summation rule, and therefore excluding it could lead to major errors.

The IEC harmonic distortion limit drops from the high 2% Planning level (L_{hHV}) to a 0.65% Individual Harmonic Emission (E_{uhi}) when the background harmonic distortion is not considered. Neither of the scenarios without the background harmonic distortion violate the Individual Harmonic Emission limit. However, the tremendous error between these two last scenarios suggest that IEC summation rule can lead to a significant underestimation of the harmonic distortion. Moreover, the Monte Carlo results are in line with the findings from actual measurements where IEC underestimates lower order harmonic [10, 16–18].

Histogram 4.15 shows the distribution of the harmonic distortion percentage of the 5th harmonic at PCC. It is observed that there is not a big difference between the mean and 95th percentile values. Hence, with the accuracy level of the mean it can be concluded that the 5th harmonic will be lower than 1,214.54 V 95% of the time. An OWPP filter designed based on the IEC results is expected to underestimate the harmonic distortion and could lead to quality and safety matters.

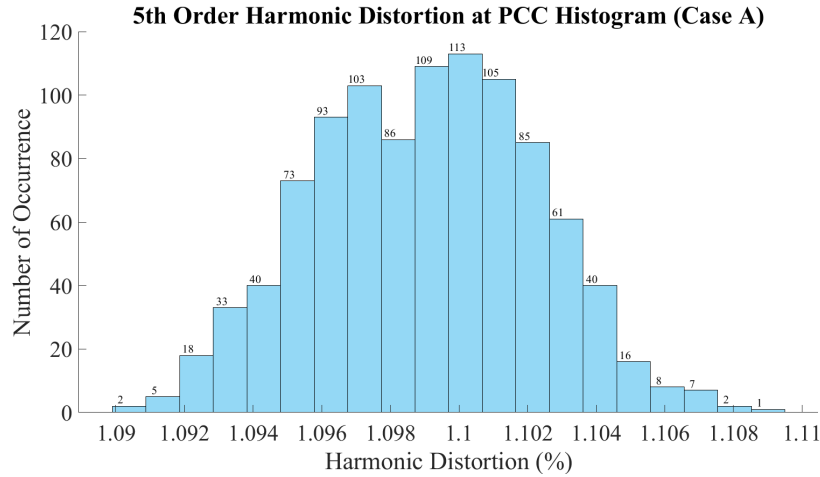
7th Harmonic Order

The number of iterations required for the accuracy level of CI of 99.75% and statistical error in the mean of 0.1% will be:

$$N = \left(\frac{100 \times Z_c \times S}{\mu \times E} \right)^2 = \left(\frac{100 \times 3 \times 0.00315}{0.95126 \times 0.1} \right)^2 = 99 \text{ iterations}$$

The accuracy level could be achieved with a number lower than the starting iteration number, i.e., 1,000. Thus, the 1,000 iterations results are used for the analysis. The results of the different scenarios for the 7th harmonic are presented in table 4.5. The results of the 95th percentile of the harmonic distortion in percentage are presented in figure 4.16 for all scenarios.

Similar to the 5th harmonic order, IEC summation rule underestimates Monte Carlo scenario 1 by approximately 10%, which demonstrates the necessity to include the statistical variation of the magnitude and

Figure 4.15: The 5th Harmonic Order Histogram

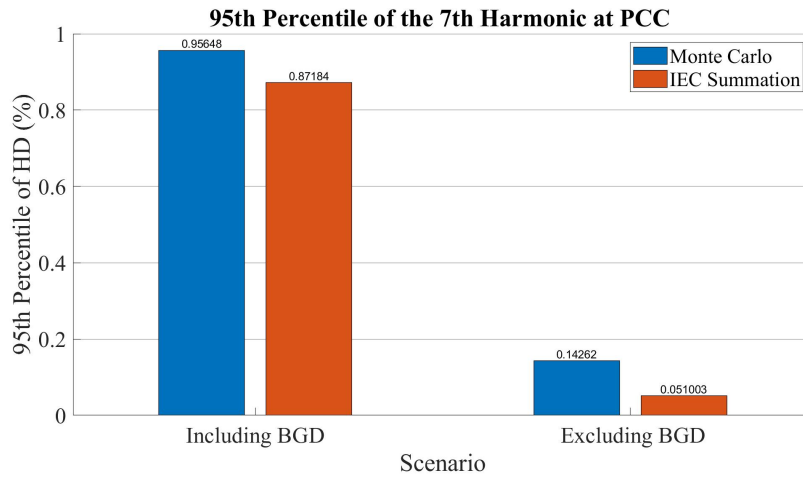
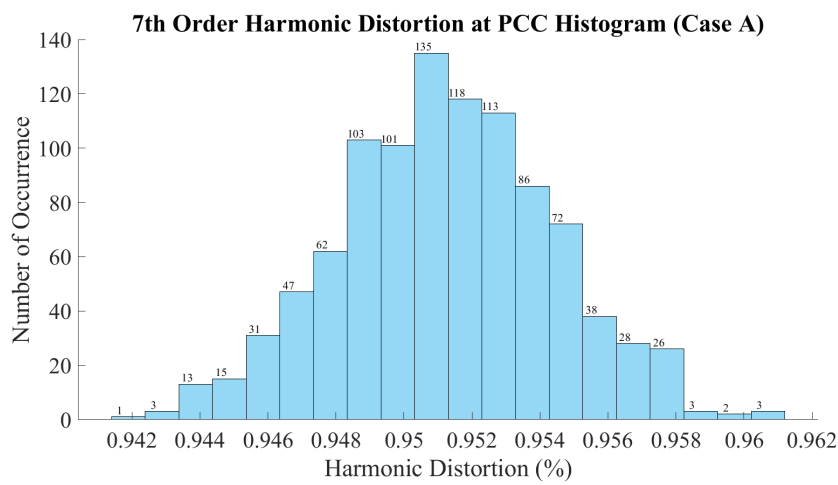
Scenario	1	2	3	4
Parameter	1,000 iterations	1 iteration	1,000 iterations	1 iteration
Mean of Harmonic Distortion (%)	0.95126	N/A	0.13802	N/A
Standard Deviation of Harmonic Distortion (%)	0.00315	N/A	0.00287	N/A
95 th Percentile of Harmonic Distortion (%)	0.95648	0.87184	0.14262	0.05100
Mean of Harmonic Distortion (V)	1,046.39	N/A	151.82	N/A
95 th Percentile of Harmonic Distortion (V)	1,052.12	959.02	156.89	56.10

Table 4.5: 7th Harmonic Order Scenarios' Results

phase angle of the harmonic currents in the harmonic study. The IEC voltage distortion limit is met in both cases. However, the summation effect of the injected harmonic is underestimated in the IEC rule in scenario 2 while it is clearer that harmonic currents are added up in scenario 1 leading to higher harmonic distortion at the PCC.

The summation effect of the harmonic can be clearly seen in scenarios 3 and 4 when the background harmonic distortion is taken out. The 95th percentile of the harmonic distortion is 180% in scenario 4 than it is for scenario 3. The underestimation of the harmonic distortion is obvious due to the exclusion of the phase angle in the harmonic calculations. The phase angles of the injected harmonic lead to addition of the harmonic current, hence resulting in a higher harmonic distortion at the PCC. Although, the IEC harmonic limit is met in all cases, but there is a probability of underestimating the harmonic distortion using IEC summation rule that could lead to inaccurate filters design.

Histogram 4.17 presents the harmonic distribution in percentage of the 7th harmonic at the PCC. It is observed that the mean and 95th percentile values are very close to each other, which are shown in figure 4.16 and table 4.5. It can be safely concluded that the 7th harmonic distortion will not exceed 1052.15 V for 95% of the time. The results of the Monte Carlo are consistent with the findings from actual measurements of OWPP that shows IEC summation rule underestimating harmonic distortion for low order harmonic [10, 16–18].

Figure 4.16: The 95th Percentile of the 7th Harmonic Order ScenariosFigure 4.17: The 7th Harmonic Order Histogram

8th Harmonic Order

The number of iterations required for the accuracy level of CI of 99.75% and statistical error in the mean of 0.1% will be:

$$N = \left(\frac{100 \times Z_c \times S}{\mu \times E} \right)^2 = \left(\frac{100 \times 3 \times 0.00344}{0.02661 \times 0.1} \right)^2 = 150,728 \text{ iterations}$$

The reason behind the high number of iterations could be the low mean of HD percentage. The lower the mean, the more iterations required to achieve the desired accuracy. This could also be due to the fact that the phase angle probability distribution function is wider than the 5th and 7th harmonics'. This means that more values can be drawn from the PDF increasing the required number of iterations to achieve the accuracy level.

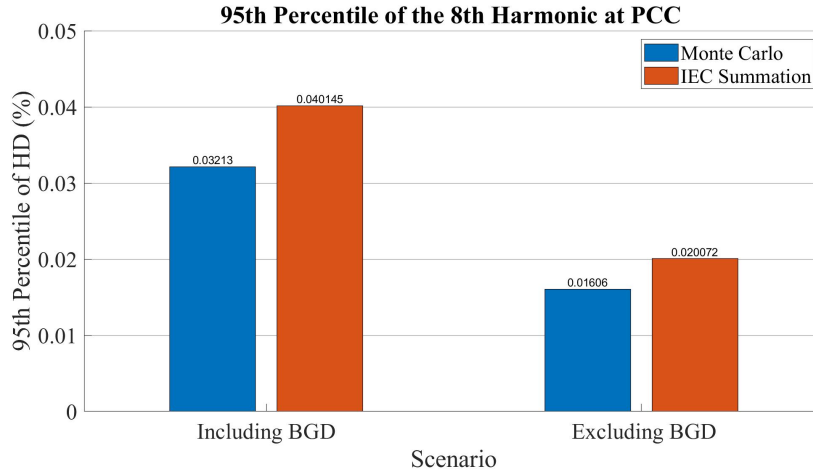
The required number of iterations is considerably large and time-consuming since the accuracy level is very strict. Thus, it was decided to lower the error in the mean to 0.5% with CI of 99.75%. The number of iterations required for the new accuracy level is:

$$N = \left(\frac{100 \times Z_c \times S}{\mu \times E} \right)^2 = \left(\frac{100 \times 3 \times 0.00344}{0.02661 \times 0.5} \right)^2 = 6,029 \text{ iterations}$$

The results of the different scenarios for the 8th harmonic are presented in table 4.6. The results of the 95th percentile of the harmonic distortion in percentage are presented in figure 4.18 for all scenarios.

Scenario 2, IEC summation rule, overestimates the harmonic distortion of the 8th harmonic from scenario 1 by approximately 25%. This could mean that the exponent used in IEC in lieu of the actual phase angle is

Scenario	1	2	3	4
Parameter	6,029 iterations	1 iteration	6,029 iterations	1 iteration
Mean of Harmonic Distortion (%)	0.02648	N/A	0.01088	N/A
Standard Deviation of Harmonic Distortion (%)	0.00339	N/A	0.00302	N/A
95 th Percentile of Harmonic Distortion (%)	0.03213	0.04015	0.01606	0.02007
Mean of Harmonic Distortion (V)	29.13	N/A	29.27	N/A
95 th Percentile of Harmonic Distortion (V)	35.35	44.16	35.48	22.08

Table 4.6: 8th Harmonic Order Scenarios' ResultsFigure 4.18: The 95th Percentile of the 8th Harmonic Order Scenarios

higher than it should be leading to higher harmonic distortion at the PCC. The phase angle PDF of the 8th harmonic shown in figure 3.3 is wider than the previous harmonic orders, which increases the likelihood of harmonic cancellation leading to a lower harmonic distortion at the PCC as presented in scenario 1 results.

The harmonic distortion limit set by IEC is met in all cases. However, the phase-correct Monte Carlo method presents an opportunity for optimization in the OWPP design since IEC overestimates the harmonic distortion that could be missed otherwise.

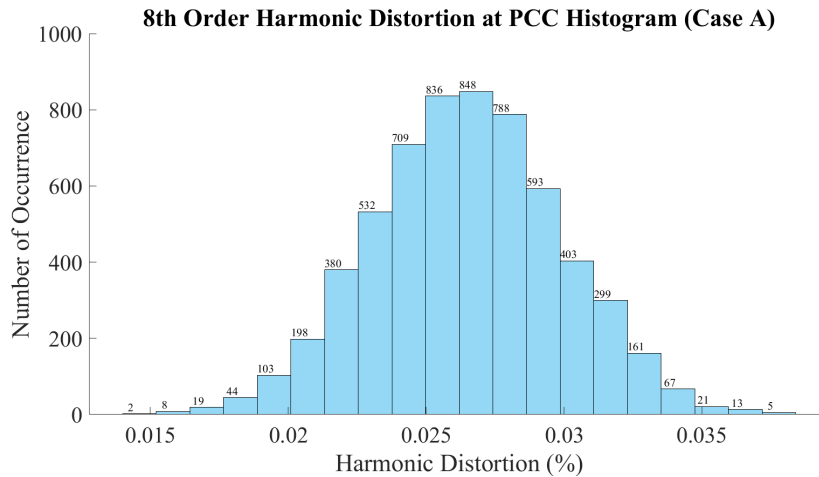
Similarly, scenario 4 overestimates the harmonic distortion by approximately 25% compared to scenario 3. The cancellation effect is not taken into consideration in the IEC summation rule that results in higher harmonic distortion. It is noteworthy to mention that the error between the first two scenarios and the last two scenarios is the same, which indicates that the low background harmonic distortion has limited impact to this harmonic order since it is approximately 10 times lower than the other harmonic's background distortion as seen in figure 4.5.

Histogram 4.19 presents the harmonic distribution in percentage of the 8th harmonic at the PCC. It can be concluded that the 8th harmonic distortion will not exceed 35.35 V for 95% of the time.

4.2.3. Case A Conclusion

As seen in figure 3.2 the PDF of the 5th harmonic has the highest mean of harmonic current magnitude over fundamental current and highest standard deviation, the 7th harmonic order has the second highest while the 8th harmonic order has the lowest values. Also, in figure 3.3, the 5th harmonic order has the lowest standard deviation for the phase angle, the 7th harmonic order has a higher standard deviation while the 8th harmonic order has the highest standard deviation. The results obtained from this case are consistent with these two trends:

- The 5th harmonic order has the highest harmonic distortion due to higher magnitude and lower possibility of cancellation of harmonics.
- The 7th harmonic order has the second highest harmonic distortion in line with the PDFs parameters.
- The 8th harmonic order has the lowest harmonic distortion due to the lower magnitude and higher

Figure 4.19: The 8th Harmonic Order Histogram

probability of harmonic cancellation.

These findings are also true due to the fact the impedance of the 5th and 7th harmonic orders at the PCC as seen in figure 4.9 are very close to each other thus the impedance amplification has a similar impact to the two harmonic orders. In contrast, the 8th harmonic order is near a resonance point that explains the diminishing of the harmonic distortion.

The main conclusions and findings of case A can be summarized as:

1. The network amplification factor is very important to determine the network behavior and the harmonic distortion level at the PCC.
2. The deterministic harmonic current could lead to errors by overestimating the amplification of the network, thus the magnitude variation should be taken into consideration.
3. The indirect compensation for a deterministic phase angle could lead to errors in estimating the harmonic distortion.
4. The distortion from the grid could amplify the final harmonic distortion at the PCC.
5. Harmonic studies based on the random behavior of the current magnitude and phase angle would exploit the cancellation/summation effect more than the traditional IEC method.
6. Harmonic studies based on probability theory provide a closer results to the expected results than IEC does, hence the uncertainty in grid-compliance is lower.

4.3. Case B (linear and variable grid impedance)

4.3.1. Background

Case B is implemented to answer the second research question, which inquires on the how the variation of grid impedance impacts the harmonic distortion level at the PCC. To answer the question, harmonic emission studies are performed based on the proposed probability method in this thesis and with IEC summation rule while the grid impedance is being changed. The background impedance is constantly changing due to the connection and disconnection of equipment, etc. The background impedance is represented by an impedance loci that is drawn in a scatter plot of resistance versus reactance. The impedance loci is usually a hexagon graph that represents different impedance operating points for each harmonic order, and the worse operating points are usually located at the boundary of the impedance loci [59]. Thus, equally-spaced points are taken between the six points of the impedance loci and a total of twenty impedance points are used for this case as shown in figure 4.20. Harmonic studies are performed for each point of the impedance loci for all of the 5th, 7th and 8th harmonic orders, separately. There are two main scenarios in this case: Monte Carlo and IEC summation rule. Similar to case A, the number of iterations is computed from the minimum number of iterations using equation 2.20 to achieve the accuracy level. A total of 140 harmonic analysis simulations are executed in PowerFactory to obtain the final results for this case.

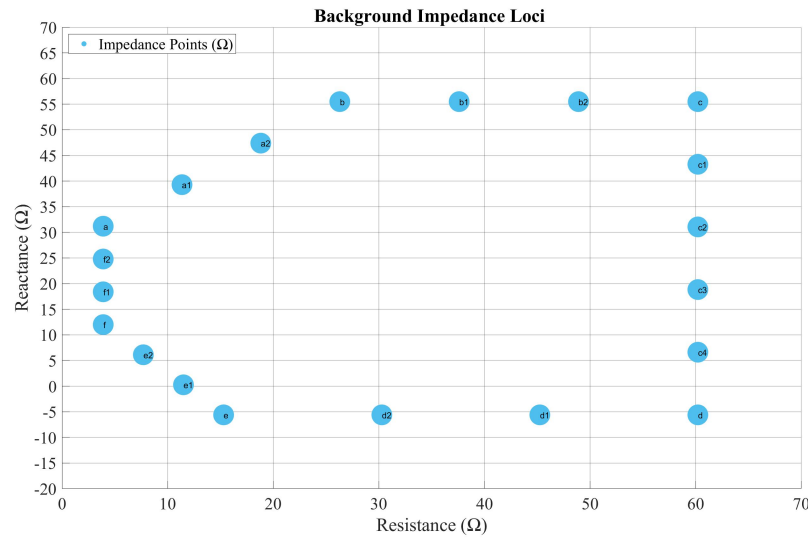


Figure 4.20: Background Impedance Loci- Case B
[13]

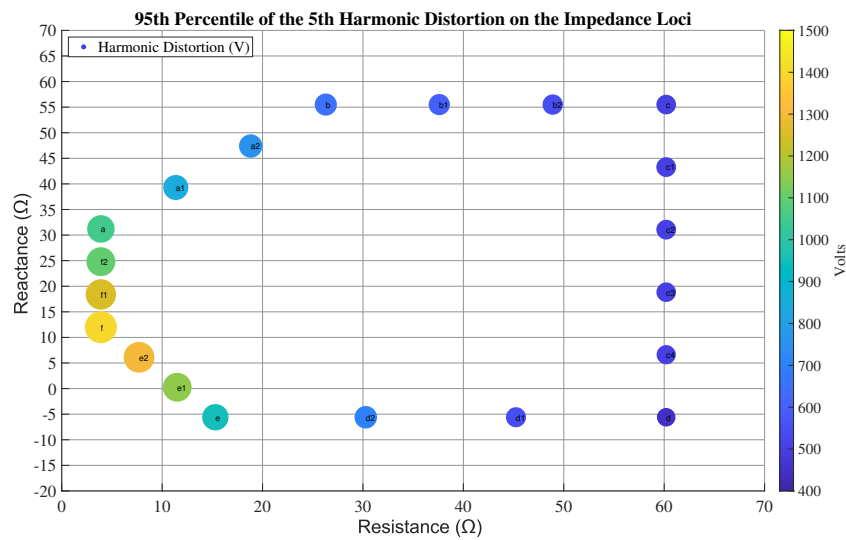
4.3.2. Simulation Results

5th Harmonic Order

The results of the harmonic studies for all the impedance loci points for the 5th harmonic order are presented in table 4.7 for the Monte Carlo method and the 95th percentile of the harmonic distortion for all the impedance loci points are presented in figure 4.21. The required iterations to achieve the accuracy level of 0.1% error in the mean with a confidence level of 99.75% is accomplished with the minimum number of iterations. It is evident from figure 4.21 that the variation of the background impedance has a significant impact on the final harmonic distortion level at the PCC. The lowest harmonic distortion is obtained at point "d" and the highest harmonic distortion is obtained at point "f" with a difference of approximately 940 V for the 95th percentile. This enormous difference indicates the necessity for harmonic studies to include the variation of the background impedance since assuming a fixed impedance, at point "d" for example, would lead to a high error.

The results obtained from the Monte Carlo method are compared to IEC summation rule and presented in table 4.8, and the 95th percentile of harmonic distortion for both scenarios are presented in figure 4.22. The 95th percentile of the harmonic distortion for all the impedance loci points are presented in figure 4.23 for the IEC summation rule. IEC summation rule resulted in underestimating the harmonic distortion compared to

Impedance Loci Point	Monte Carlo Method					
	Mean of HD (%)	Standard Deviation of HD (%)	95 th Percentile of HD (%)	Mean of HD (V)	95 th Percentile of HD (V)	Required Iterations
a	0.95304	0.00424	0.95981	1048.34	1055.79	178.40
a1	0.78972	0.00449	0.79730	868.69	877.03	290.48
a2	0.68455	0.00443	0.69145	753.01	760.59	376.65
b	0.61151	0.00469	0.61942	672.66	681.36	529.98
b1	0.56274	0.00446	0.57017	619.01	627.19	566.17
b2	0.51914	0.00420	0.52629	571.05	578.92	590.34
c	0.48089	0.00451	0.48825	528.98	537.08	790.18
c1	0.48708	0.00433	0.49435	535.78	543.79	711.61
c2	0.48721	0.00411	0.49445	535.93	543.89	639.87
c3	0.47905	0.00398	0.48580	526.96	534.38	620.41
c4	0.46041	0.00381	0.46710	506.45	513.81	616.78
d	0.43044	0.00370	0.43653	473.49	480.19	664.32
d1	0.50627	0.00347	0.51188	556.90	563.07	423.54
d2	0.63594	0.00298	0.64071	699.54	704.78	198.09
e	0.89263	0.00246	0.89672	981.90	986.39	68.22
e1	1.05107	0.00198	1.05433	1156.17	1159.76	31.83
e2	1.19853	0.00179	1.20142	1318.39	1321.56	20.08
f	1.28936	0.00260	1.29384	1418.30	1423.22	36.46
f1	1.16814	0.00345	1.17376	1284.95	1291.14	78.62
f2	1.05247	0.00390	1.05881	1157.72	1164.70	123.43

Table 4.7: 5th Harmonic Order Monte Carlo Results-Case BFigure 4.21: 95th Harmonic Distortion of the 5th Harmonic Order on Impedance Loci- Monte Carlo

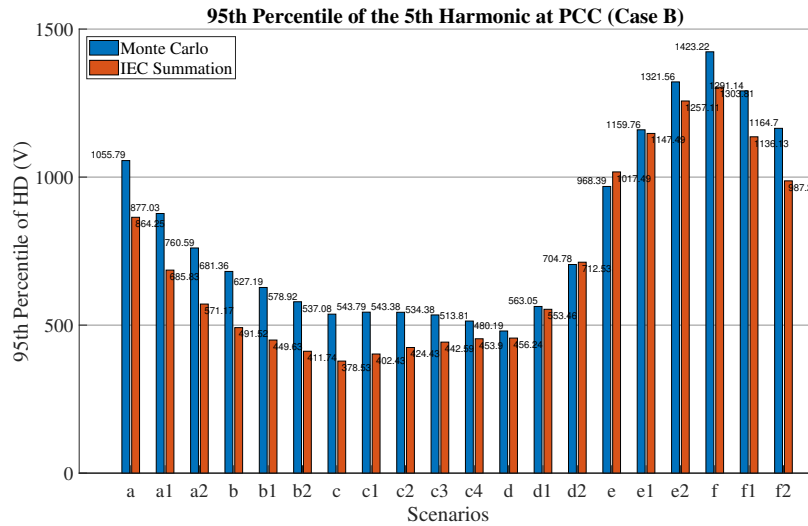
the Monte Carlo method in case A with an approximately 12.5% error. However, this is not quite true for all the points of the impedance loci of this case, points "d2" and "e" of the loci yield higher harmonic distortion with IEC summation rule than the Monte Carlo Method, while the error ranges between -3% to 30%. Therefore, the conclusion obtained from case A that IEC would underestimate harmonic distortion compared to Monte Carlo, similar to the results of actual measurements, cannot be generalized when the background impedance is changing. This establishes the requirements to perform harmonic analysis with a variable grid impedance in lieu of the fixed grid impedance approach.

The behavior and the result of the harmonic distortions at the PCC for all the impedance loci points can be explained using the simple model in section 3.3 and equation 3.23 that is reinstated here again.

$$V_{PCC} = \frac{Z_{OWPP}}{Z_{OWPP} + Z_g} \times V_g + \frac{Z_{OWPP} \times Z_g}{Z_{OWPP} + Z_g} \times I_{OWPP}$$

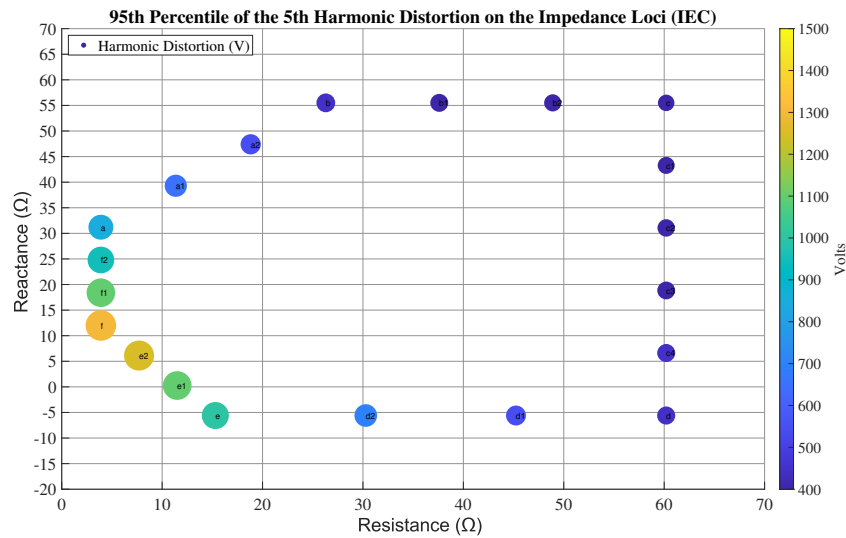
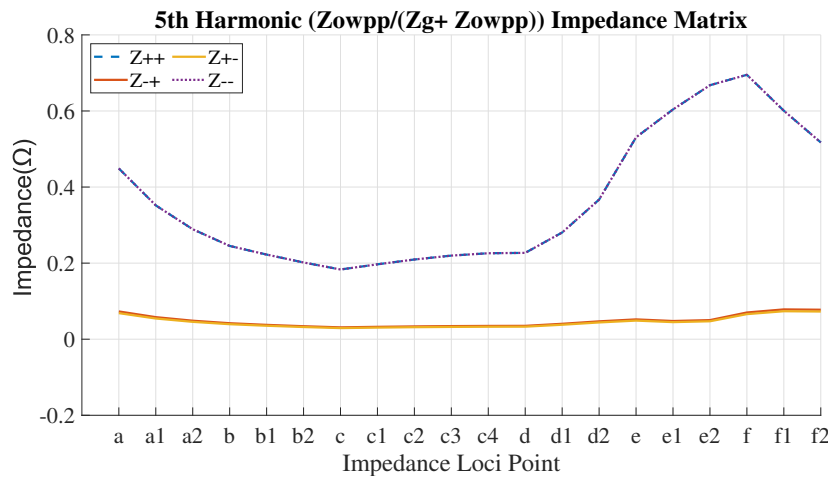
The first ratio of the equation is the harmonic gain that is multiplied by the background distortion, which will greatly impact the final distortion at the PCC as seen from scenario 4 of the amplification factor in figure 4.6, and the second ratio is the PCC impedance. Figure 4.24 shows the harmonic gain for all the impedance loci points, and point "f" has the highest diagonal impedance that explains the highest harmonic distortion at the PCC. On the other hand, point "d" has a relatively very low harmonic gain, however the lowest is at point "c". Nonetheless, the difference between the two points' impedances is considerably very small, thus

Impedance Loci Point	IEC Summation Rule		Monte Carlo VS. IEC	
	95 th Percentile of HD (%)	95 th Percentile of HD (V)	95 th Percentile of HD Difference (V)	Error (%)
a	0.78568	864.25	191.55	18.14
a1	0.62348	685.83	191.20	21.80
a2	0.51924	571.17	189.42	24.90
b	0.44683	491.52	189.85	27.86
b1	0.40876	449.63	177.56	28.31
b2	0.37431	411.74	167.18	28.88
c	0.34412	378.53	158.55	29.52
c1	0.36566	402.23	141.56	26.03
c2	0.38585	424.43	119.46	21.96
c3	0.40236	442.59	91.78	17.18
c4	0.41264	453.90	59.90	11.66
d	0.41476	456.24	23.95	4.99
d1	0.50315	553.46	9.60	1.71
d2	0.64775	712.53	-7.74	-1.10
e	0.92499	1017.49	-31.10	-3.15
e1	1.04317	1147.49	12.27	1.06
e2	1.14283	1257.11	64.45	4.88
f	1.18528	1303.81	119.41	8.39
f1	1.03285	1136.13	155.01	12.01
f2	0.89752	987.27	177.43	15.23

Table 4.8: 5th Harmonic Order Results Comparison - Case BFigure 4.22: Comparison of the 95th Harmonic Distortion of the 5th Harmonic Order between Monte Carlo and IEC methods

the harmonic distortion cannot be solely determined based on the background amplification, but the PCC impedance that is shown in figure 4.25 has to be considered and analyzed to determine the harmonic currents coming from the OWPP. Point "d" has lower PCC diagonal impedance elements compared to point "c" that indicates lower harmonic currents from the OWPP and hence a lower harmonic distortion at the PCC. It is also interesting to see that harmonic gain matrix impedance in figure 4.24 has the same trend as the harmonic distortion bar graph in figure 4.22.

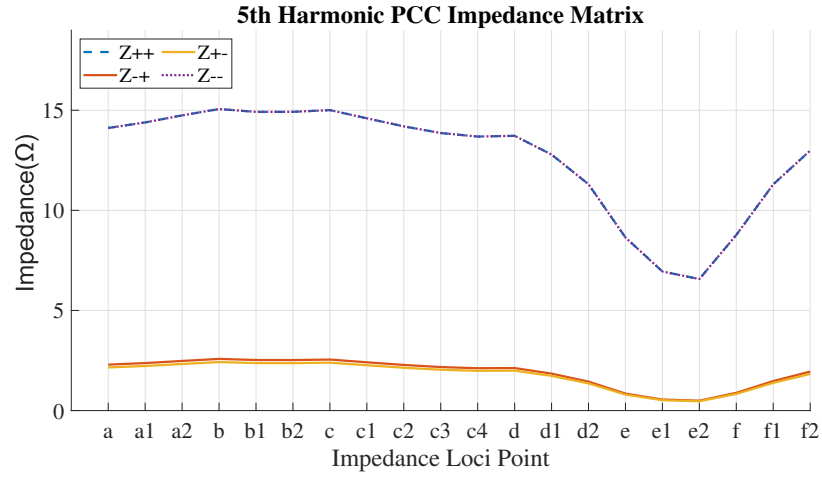
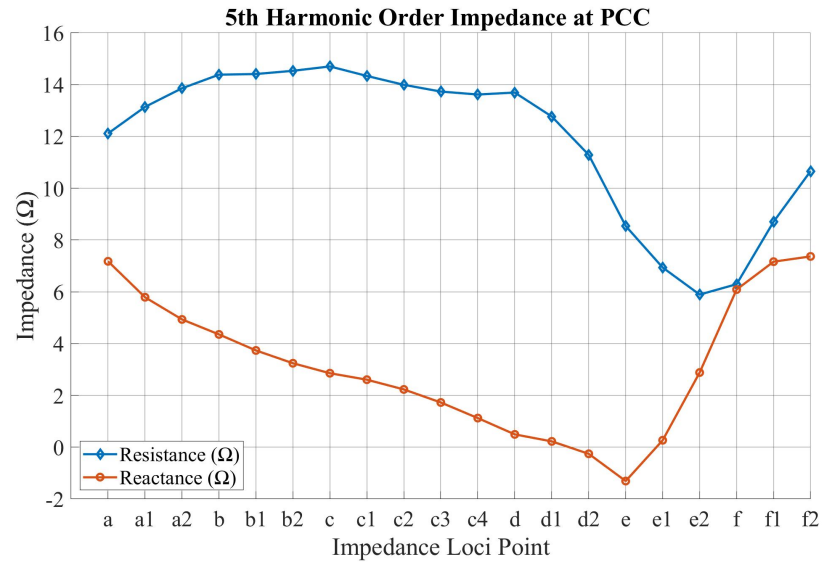
As seen in figure 4.26, the impedance at the PCC is capacitive and has low resistance at points "d2" and "e" of the impedance Loci, which could explain the reasons behind IEC overestimating the harmonic distortion compared to Monte Carlo. Moreover, the lowest positive reactance at the PCC is seen in point "d1" where the difference between the harmonic distortion of the IEC and Monte Carlo is the lowest as seen in table 4.8. Point "f" of the impedance loci has the highest 95th harmonic distortion at 1.3%, which is below the IEC limit of 2% HD planning level, thus there is no grid violation for any of the impedance loci points. However, it has been shown that the variation of the grid impedance could result in big differences between IEC and the Monte Carlo methods.

Figure 4.23: 95th Harmonic Distortion of the 5th Harmonic Order on Impedance Loci- IEC MethodFigure 4.24: The Harmonic Gain Impedance Matrix for the 5th Harmonic Order

7th Harmonic Order

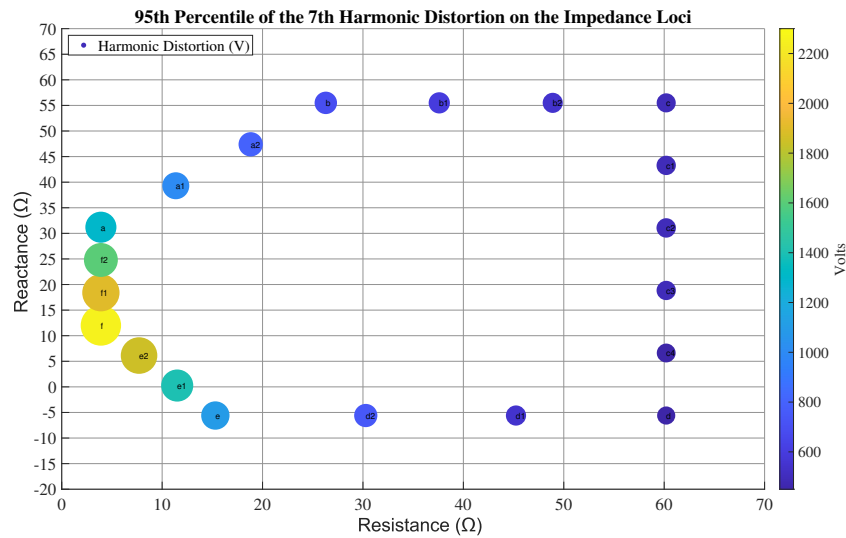
The results of the harmonic studies for all the impedance loci points for the 7th harmonic order are presented in table 4.9 for the Monte Carlo method and the 95th percentile of the harmonic distortion for all the impedance loci points are presented in figure 4.27. The required accuracy is achieved with the minimum number of iterations. Similar to the 5th harmonic, the variation of the background impedance yields great variation on the harmonic distortion at the PCC as seen in figure 4.27. The lowest harmonic distortion is seen at point "d" and the highest harmonic distortion is seen at point "f" with a harmonic voltage difference of 1,815 V for the 95th percentile. This difference is approximately twice as big compared to the 5th harmonic distortion gap between the same points. Moreover, there is an approximately 1,222 V difference between point "f" and case A result, where the former is in violation of the grid limit set by IEC. Therefore, performing harmonic study on a single fixed grid impedance could lead to major errors in determining the harmonic distortion at the PCC and the compliance to the grid code.

The results of the Monte Carlo method are compared to IEC method in table 4.10, and the 95th percentile of harmonic distortion for both scenarios are presented in figure 4.28. The 95th percentile of harmonic distortion for all impedance loci points for the IEC summation rule are presented in figure 4.29. IEC underestimates the harmonic distortion of the Monte Carlo by 10% in case A. The same behavior is obtained in this case where IEC summation rule underestimates the harmonic distortion from Monte Carlo for all impedance

Figure 4.25: The PCC Impedance Matrix for the 5th Harmonic OrderFigure 4.26: The PCC Resistance and Reactance for the 5th Harmonic Order

Impedance Loci Point	Monte Carlo Method					
	Mean of HD (%)	Standard Deviation of HD (%)	95 th Percentile of HD (%)	Mean of HD (V)	95 th Percentile of HD (V)	Required Iterations
a	1.21887	0.00353	1.22461	1340.76	1347.07	75.58
a1	0.91653	0.00345	0.92236	1008.18	1014.60	127.42
a2	0.74376	0.00330	0.74924	818.14	824.16	176.80
b	0.63253	0.00352	0.63827	695.78	702.10	278.79
b1	0.56581	0.00334	0.57146	622.39	628.61	312.78
b2	0.50686	0.00344	0.51293	557.54	564.22	415.68
c	0.45657	0.00337	0.46200	502.23	508.20	489.01
c1	0.46804	0.00344	0.47380	514.84	521.18	486.20
c2	0.47269	0.00345	0.47838	519.96	526.22	479.17
c3	0.46561	0.00360	0.47136	512.17	518.49	537.23
c4	0.44517	0.00345	0.45075	489.69	495.82	540.92
d	0.41179	0.00349	0.41744	452.97	459.18	647.17
d1	0.51071	0.00329	0.51624	561.78	567.86	372.50
d2	0.67918	0.00300	0.68407	747.10	752.48	175.67
e	1.01245	0.00229	1.01641	1113.70	1118.05	46.13
e1	1.30228	0.00213	1.30577	1432.50	1436.35	23.97
e2	1.68901	0.00200	1.69228	1857.91	1861.51	12.62
f	2.06314	0.00273	2.06753	2269.46	2274.29	15.73
f1	1.75565	0.00339	1.76113	1931.22	1937.25	33.59
f2	1.45168	0.00364	1.45748	1596.85	1603.23	56.46

Table 4.9: 7th Harmonic Order Monte Carlo Results - Case B

Figure 4.27: 95th Harmonic Distortion of the 7th Harmonic Order on Impedance Loci-Monte Carlo

Loci points except 5 points "d, d1, d2, e and e1" where it overestimates the harmonic distortion. As seen in table 4.10, the error ranges between -4.45% to 20.54%. Similar to the conclusion from the 5th harmonic order, the variation of the background impedance could result in different behavior between the Monte Carlo and the IEC methods.

Impedance Loci Point	IEC Summation Rule		Monte Carlo VS. IEC	
	95 th Percentile of HD (%)	95 th Percentile of HD (V)	95 th Percentile of HD Difference (V)	Error (%)
a	1.06014	1166.16	180.92	13.43
a1	0.77503	852.53	162.07	15.97
a2	0.61215	673.36	150.80	18.30
b	0.50719	557.91	144.19	20.54
b1	0.45492	500.41	128.20	20.39
b2	0.40819	449.01	115.21	20.42
c	0.36806	404.86	103.34	20.33
c1	0.39452	433.97	87.21	16.73
c2	0.41777	459.55	66.67	12.67
c3	0.43400	477.40	41.09	7.92
c4	0.43973	483.70	12.13	2.45
d	0.43350	476.85	-17.67	-3.85
d1	0.53867	592.54	-24.67	-4.35
d2	0.71453	785.98	-33.50	-4.45
e	1.05642	1162.07	-44.01	-3.94
e1	1.31175	1442.92	-6.57	-0.46
e2	1.64605	1810.66	50.85	2.73
f	1.94971	2144.68	129.61	5.70
f1	1.61148	1772.62	164.62	8.50
f2	1.29622	1425.84	177.38	11.06

Table 4.10: 7th Harmonic Order Results Comparison -Case B

The peak point of the harmonic gain impedance plotted in figure 4.30 explains the highest harmonic distortion at point "f" based on equation 3.23. The same reasoning of the result of the 5th harmonic PCC impedance and HG impedance is applicable to the 7th harmonic to explain the lowest harmonic distortion at point "d" as seen in figure 4.31. The trend of the harmonic distortion from figure 4.28 is aligned with the diagonal elements of the impedance matrix of the harmonic gain presented in figure 4.30, thus analyzing the impedance could indicate the behavior and the peaks of the harmonic distortion of the OWPP.

Figure 4.32 shows that IEC would overestimate the harmonic distortion when compared to Monte Carlo when the impedance at the PCC is capacitive and has low resistance as seen in points "d, d1, d2, e and e1" of the impedance Loci. Monte Carlo analysis revealed that point "f" has the highest 95th harmonic distortion

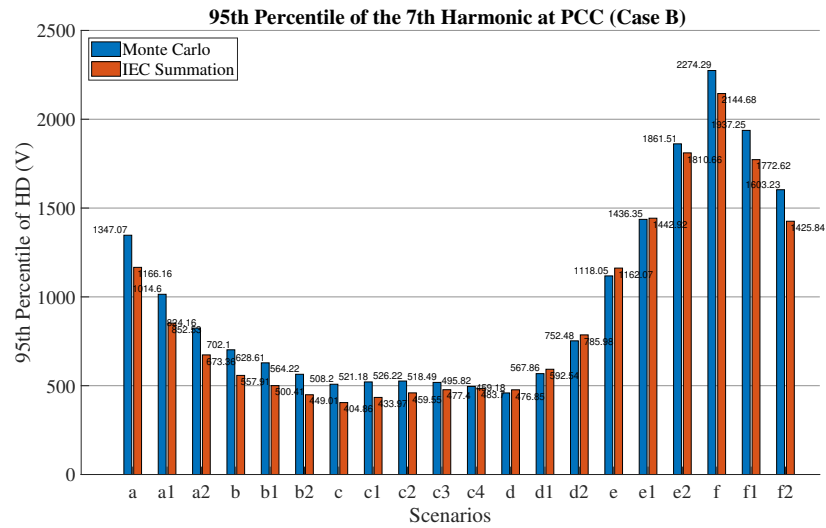


Figure 4.28: Comparison of the 95th Harmonic Distortion of the 7th Harmonic Order between Monte Carlo and IEC methods

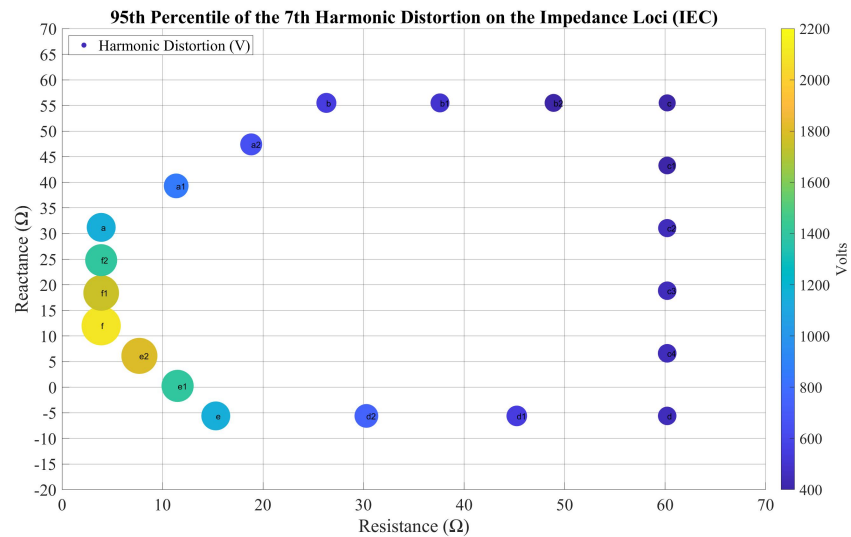
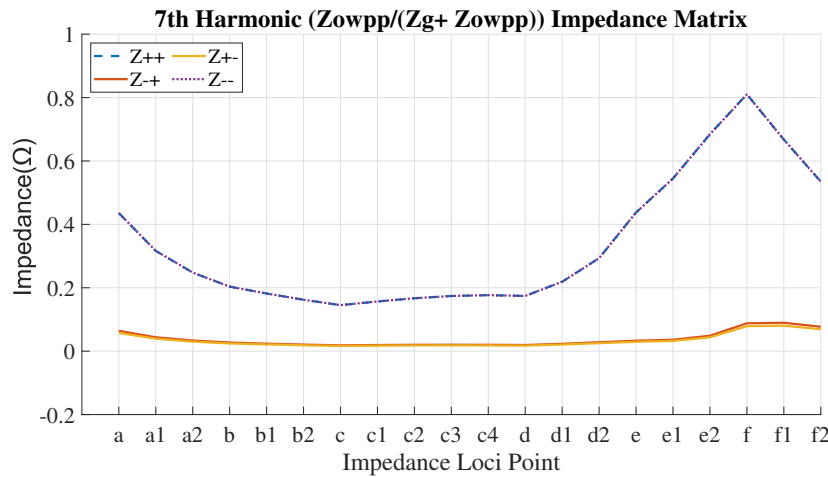
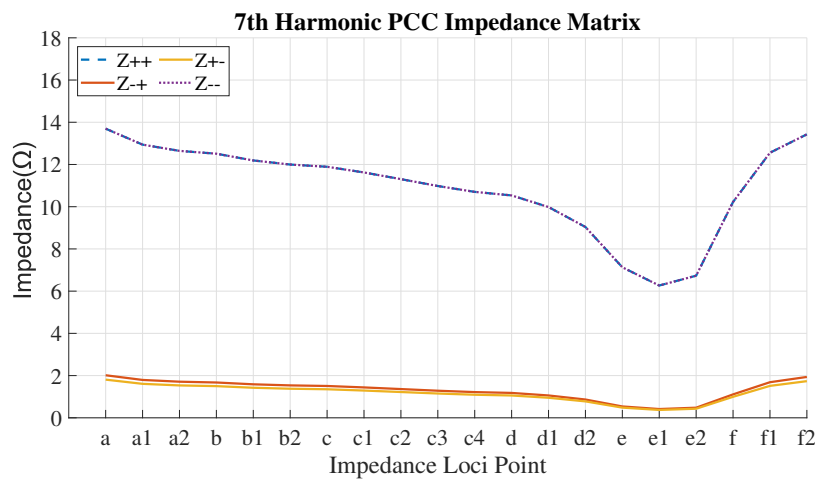


Figure 4.29: 95th Harmonic Distortion of the 7th Harmonic Order on Impedance Loci- IEC Method

at 2.06%, which violates the planning level while IEC value is 1.95% which is below the 2% limit. This error between IEC and the Monte Carlo demonstrates how IEC could prove compliance to the grid-code when the harmonic distortion could actually be higher and in violation of the code.

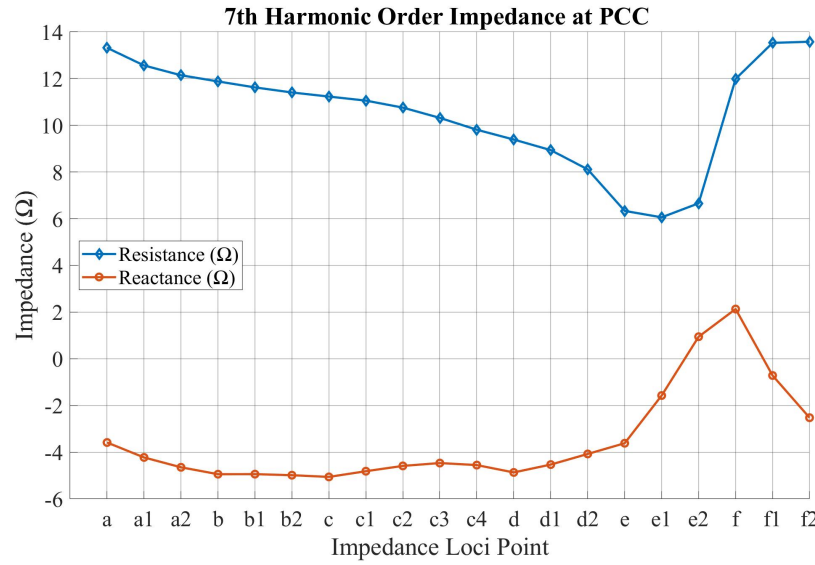
Figure 4.30: The Harmonic Gain Impedance Matrix for the 7th Harmonic OrderFigure 4.31: The PCC Impedance Matrix for the 7th Harmonic Order

8th Harmonic Order

The results of the harmonic studies for all the impedance loci points for the 8th harmonic order are presented in table 4.11. The number of iterations required to achieve the accuracy level of an error in the mean of 0.5% and confidence level of 99.75% are higher than the minimum iterations for the majority of the impedance loci points, hence the simulations were performed for the computed iterations and the results are presented in table 4.12. The 95th percentile of the harmonic distortion for all the impedance loci points are presented in figure 4.33 for the Monte Carlo method where it can be shown that the variation of the background impedance impacts the harmonic distortion. Although the distortion is not as high as the previous two harmonic orders, nonetheless the highest point "f" yields a harmonic distortion that is 5 times bigger than the lowest point "d". This difference could be missed if harmonic analysis is performed on a fixed background impedance only.

The results of the Monte Carlo method are compared to IEC method in table 4.13, and the 95th percentile of harmonic distortion for both scenarios are presented in figure 4.34. The 95th percentile of harmonic distortion for all impedance loci points for the IEC summation rule are presented in figure 4.35. IEC overestimated the harmonic distortion of the Monte Carlo by 25% in case A. The same behavior is obtained in this case where IEC summation rule overestimates the harmonic distortion from Monte Carlo for all impedance loci points except 4 points "a, f, f1 and f2" where it underestimates the harmonic distortion. As seen in table 4.13, the error ranges between -84% (overestimated) to 4.65% (underestimated).

The highest harmonic distortion is seen at point "f" of the impedance loci, however this is not the highest diagonal element impedance of the harmonic gain as seen in figure 4.36 that has the highest impedance at point "e2". Unlike the previous two harmonic orders where the off-diagonal elements are not quite as

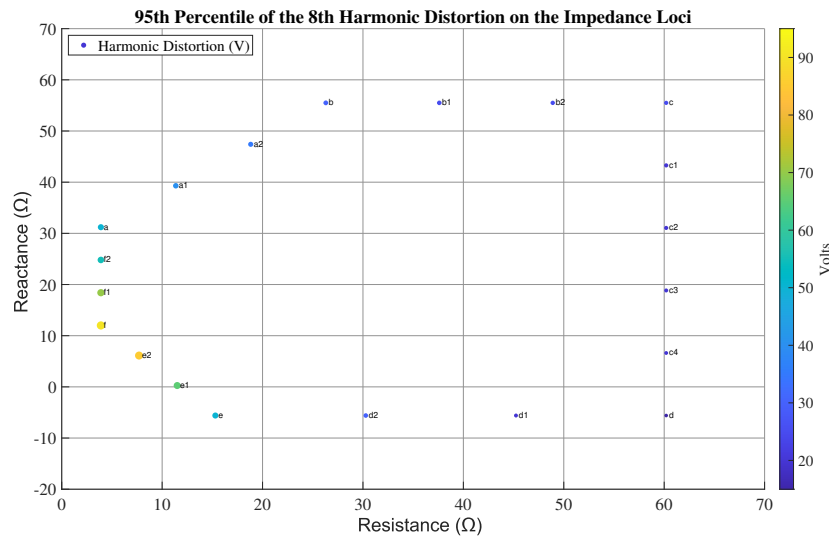
Figure 4.32: The PCC Resistance and Reactance for the 7th Harmonic Order

Impedance Loci Point	Monte Carlo Method					
	Mean of HD (%)	Standard Deviation of HD (%)	95 th Percentile of HD (%)	Mean of HD (V)	95 th Percentile of HD (V)	Required Iterations
a	0.04106	0.00393	0.04770	45.17	52.47	3,302.49
a1	0.03238	0.00382	0.03855	35.61	42.40	5,007.91
a2	0.02708	0.00377	0.03363	29.79	36.99	6,985.49
b	0.02344	0.00371	0.02940	25.79	32.34	8,993.44
b1	0.02097	0.00373	0.02734	23.07	30.08	11,373.82
b2	0.01877	0.00371	0.02491	20.65	27.40	14,098.34
c	0.01692	0.00369	0.02303	18.61	25.33	17,116.76
c1	0.01665	0.00366	0.02269	18.31	24.96	17,408.04
c2	0.01606	0.00372	0.02212	17.66	24.33	19,332.74
c3	0.01480	0.00358	0.02065	16.28	22.72	20,998.21
c4	0.01316	0.00355	0.01898	14.48	20.88	26,233.70
d	0.01067	0.00344	0.01639	11.74	18.03	37,368.53
d1	0.01448	0.00338	0.01982	15.93	21.80	19,624.51
d2	0.02204	0.00316	0.02716	24.24	29.88	7,408.57
e	0.04211	0.00280	0.04687	46.32	51.56	1,592.78
e1	0.05916	0.00254	0.06311	65.07	69.42	662.60
e2	0.07751	0.00262	0.08172	85.26	89.89	412.67
f	0.07995	0.00345	0.08560	87.95	94.16	669.62
f1	0.06010	0.00375	0.06593	66.11	72.52	1,399.84
f2	0.04843	0.00367	0.05465	53.28	60.11	2,071.28

Table 4.11: 8th Harmonic Order Monte Carlo Results - Case B

Impedance Loci Point	Monte Carlo Method					
	Mean of HD (%)	Standard Deviation of HD (%)	95 th Percentile of HD (%)	Mean of HD (V)	95 th Percentile of HD (V)	Required Iterations
a	0.04113	0.00378	0.04733	45.24	52.06	3,302.49
a1	0.03229	0.00373	0.03840	35.51	42.24	5,007.91
a2	0.02700	0.00368	0.03304	29.70	36.34	6,985.49
b	0.02345	0.00368	0.02941	25.80	32.35	8,993.44
b1	0.02097	0.00363	0.02688	23.07	29.57	11,373.82
b2	0.01876	0.00365	0.02470	20.63	27.17	14,098.34
c	0.01685	0.00363	0.02285	18.54	25.13	17,116.76
c1	0.01647	0.00363	0.02265	18.12	24.92	17,408.04
c2	0.01588	0.00358	0.02174	17.47	23.91	19,332.74
c3	0.01467	0.00359	0.02051	16.13	22.56	20,998.21
c4	0.01300	0.00354	0.01884	14.30	20.72	26,233.70
d	0.01088	0.00346	0.01664	11.97	18.31	37,368.53
d1	0.01436	0.00339	0.02002	15.79	22.02	19,624.51
d2	0.02198	0.00321	0.02732	24.18	30.06	7,408.57
e	0.04214	0.00273	0.04661	46.35	51.27	1,592.78
e1	0.05916	0.00254	0.06311	65.07	69.42	662.60
e2	0.07751	0.00262	0.08172	85.26	89.89	412.67
f	0.07995	0.00345	0.08560	87.95	94.16	669.62
f1	0.06031	0.00355	0.06628	66.34	72.90	1,399.84
f2	0.04851	0.00366	0.05435	53.36	59.78	2,071.28

Table 4.12: 8th Harmonic Order Monte Carlo Accuracy Results-Case B

Figure 4.33: 95th Harmonic Distortion of the 8th Harmonic Order on Impedance Loci-Monte Carlo

Impedance Loci Point	IEC Summation Rule		Monte Carlo VS. IEC	
	95 th Percentile of HD (%)	95 th Percentile of HD (V)	95 th Percentile of HD Difference (V)	Error (%)
a	0.04563	50.20	1.87	3.58
a1	0.03874	42.62	-0.38	-0.89
a2	0.03469	38.16	-1.81	-4.99
b	0.03211	35.32	-2.96	-9.16
b1	0.03084	33.92	-4.35	-14.73
b2	0.02971	32.68	-5.51	-20.28
c	0.02875	31.62	-6.49	-25.82
c1	0.02936	32.30	-7.38	-29.63
c2	0.02996	32.95	-9.04	-37.79
c3	0.03044	33.48	-10.92	-48.42
c4	0.03069	33.76	-13.04	-62.95
d	0.03066	33.72	-15.42	-84.23
d1	0.03393	37.32	-15.29	-69.45
d2	0.04046	44.50	-14.44	-48.06
e	0.05754	63.29	-12.02	-23.45
e1	0.07017	77.18	-7.77	-11.19
e2	0.08316	91.47	-1.58	-1.76
f	0.08243	90.67	3.49	3.70
f1	0.06319	69.51	3.39	4.65
f2	0.05231	57.54	2.24	3.75

Table 4.13: 8th Harmonic Order Accuracy Results Comparison - Case B

high, the highest harmonic distortion cannot be anticipated based on the diagonal impedance only. The off-diagonal impedances of point "f" are higher than point "e2", which explains the highest harmonic distortion. In scenarios where the off-diagonal impedance is not very high, then conclusions can be made based on the diagonal impedance only. However, the 8th harmonic results show that this approach might not be accurate at all times. It is true that it indicates one of the highest harmonic distortion point of the impedance loci, however it is not the highest. The lowest harmonic distortion is at point "d" which has a combination of one of the lowest harmonic gain and PCC impedance as shown in figures 4.36 and 4.37, respectively, this is the same behavior seen in the 5th and 7th harmonic orders. Similar to the previous two harmonic orders, the trend seen in the diagonal impedance in figure 4.36 is very close to the trend of harmonic distortion in figure 4.34.

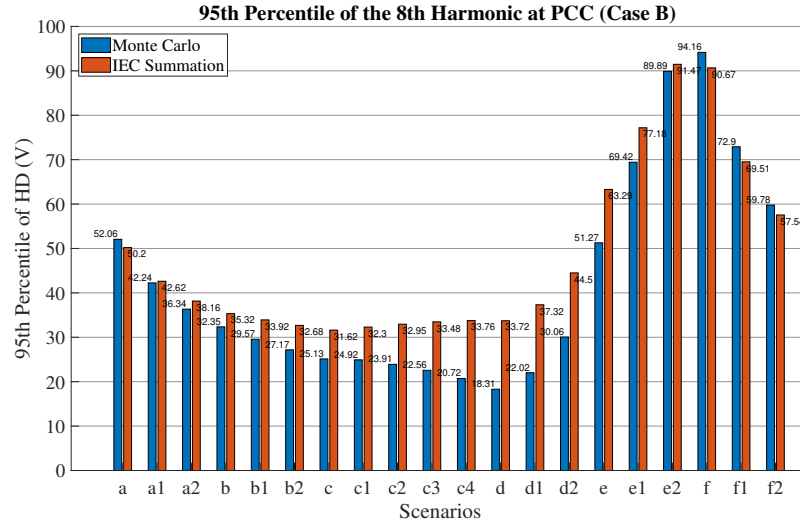


Figure 4.34: Comparison of the 95th Harmonic Distortion of the 8th Harmonic Order between Monte Carlo and IEC methods

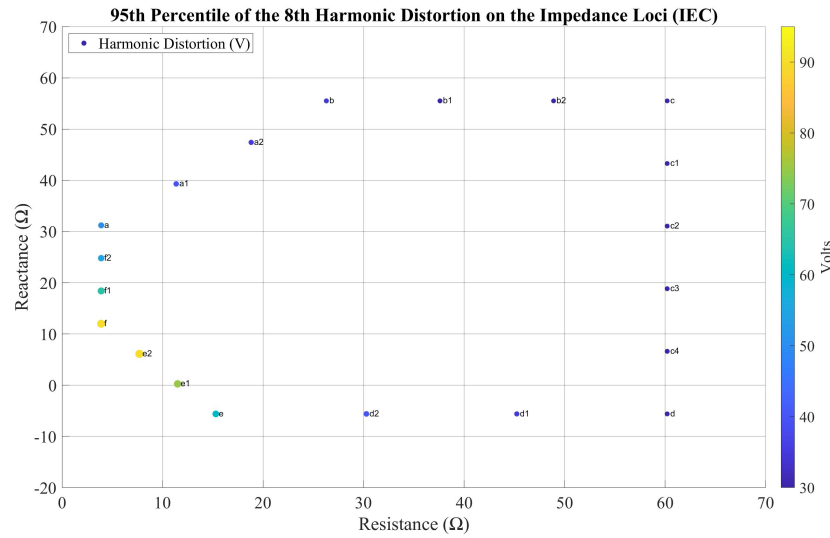


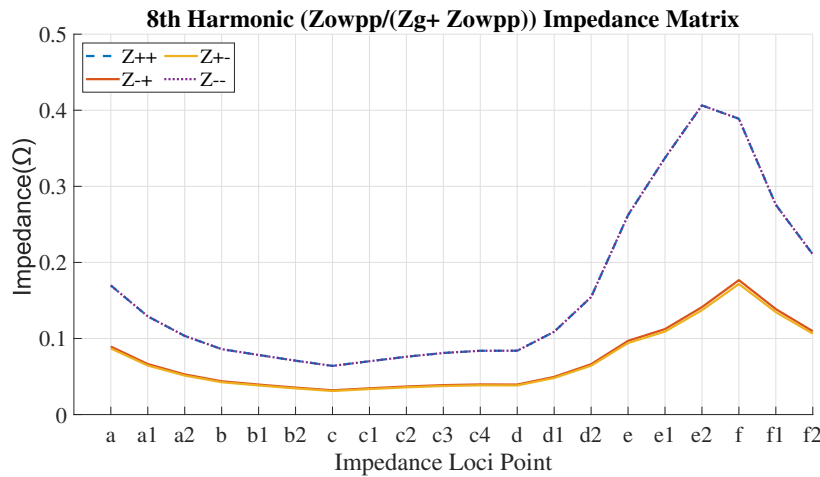
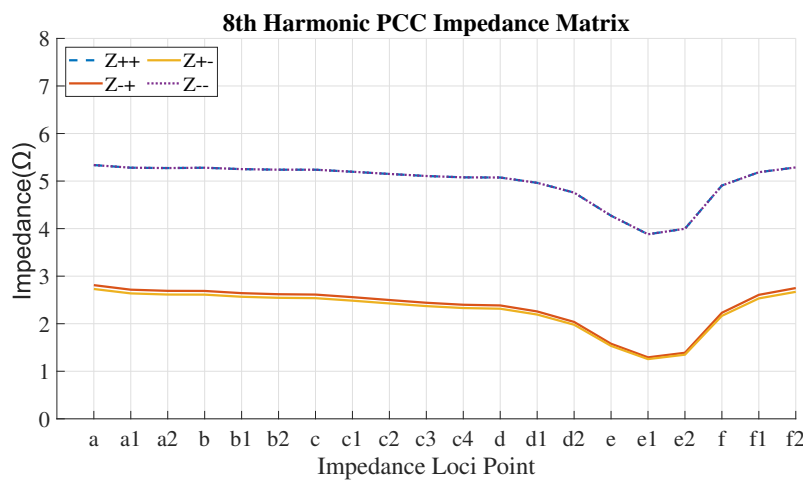
Figure 4.35: 95th Harmonic Distortion of the 8th Harmonic Order on Impedance Loci- IEC Method

Figure 4.37 shows that a PCC impedance of a combination of a relatively inductive and relatively high resistance as in points "a, f, f1 and f2" could lead to IEC underestimating the harmonic distortion, which is a deviation from the general behavior of this harmonic order. Although, none of the impedance loci points' harmonic distortion exceeds the IEC limit of 0.4% planning level, but the variation of the grid impedance would result in a complete range of harmonic distortion at the PCC, and mitigation should be made on the worst-case point that is point "f" for this harmonic order with a 95th percentile of 0.09%.

4.3.3. Case B Conclusion

Unlike the analysis performed for case A where the PDFs shapes play a major role in determining the final harmonic distortion at the PCC, case B is concentrated in the variation of the grid's impedance and how it changes the harmonic distortion compared to case A. The main conclusions and findings of this case are:

1. The results obtained in case B are consistent with the overall results from case A with few deviations caused by the variation of the background grid impedance where IEC underestimated the 5th and 7th harmonics while it overestimates the 8th harmonic.

Figure 4.36: The Harmonic Gain Impedance Matrix for the 8th Harmonic OrderFigure 4.37: The PCC Impedance Matrix for the 8th Harmonic Order

2. The harmonic distortions seen in case A are lower than the highest points in case B since the former's grid impedance is a point within the impedance loci and the highest harmonic distortion is expected at the boundary.
3. The highest harmonic distortion is seen at the same point, point "f", for all the different harmonic orders (the same impedance loci is used). The background impedance at this point has a relatively high reactance with a relatively low resistance, however it has the highest, or one of the highest, harmonic gain impedance.
4. The lowest harmonic distortion is seen at the same point for all the harmonic orders, i.e. point "d". The background impedance of this point is a combination of high resistance and low reactance (capacitive). While the harmonic gain impedance is one of the lowest impedances for this point.
5. The 5th harmonic order resulted in a higher harmonic distortion than the 7th harmonic order in case A, despite the differences in the amplification factors. However, this is not always true for case B where the 7th harmonic has a higher harmonic distortion at 13 out of 20 impedance loci points compared to the 5th harmonic order. Points "b2, c, c1, c2, c3, c4 and d" are where the 5th harmonic has a higher distortion than the 7th harmonic. This could be attributed to the fact that both the harmonic gain and the PCC impedance at these points are relatively low for both harmonic orders, and thus the distortion from the grid is relatively similar, while the PDFs parameters and shape have higher contribution to the final harmonic distortion knowing that the 5th harmonic has a higher magnitude and lower phase angle standard deviation.

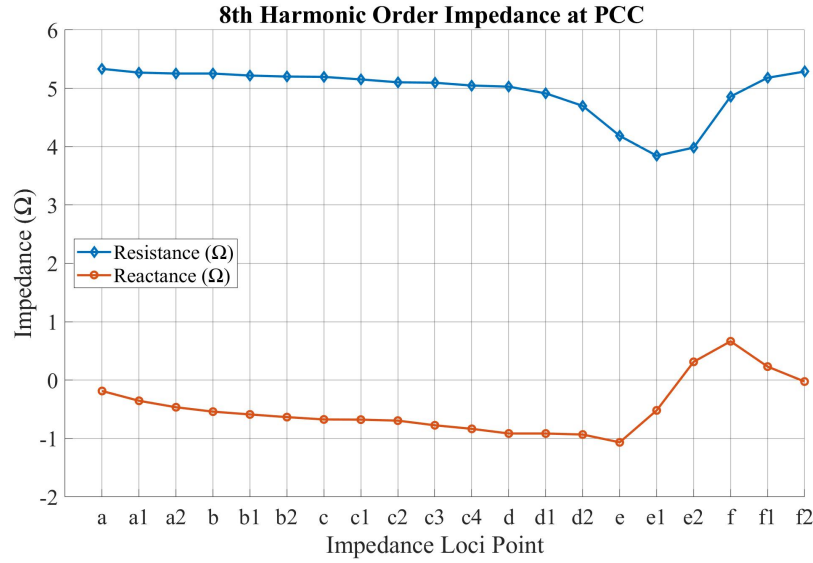


Figure 4.38: The PCC Resistance and Reactance for the 8th Harmonic Order

4.4. Case C (non-linear and fixed grid impedance)

4.4.1. Background

Case C is implemented to answer the third research question, which inquires on how does the presence of frequency coupling between harmonics impact the distortion level at the PCC compared to the frequency decoupled harmonic cases. The frequency-coupling was defined in section 2.1.6 and it is further explain here.

Frequency coupling phenomenon between different frequencies shows that WT's converter will generate harmonic distortion at other frequencies than the harmonic source's frequency as a reaction to the voltage distortion at its terminal or at the PCC. In the previous two cases, the converter was modelled with the assumption of a linear behavior where the converter is injecting harmonic distortion at one particular frequency and the output harmonic distortion has the same frequency. Nonetheless, power-electronic converters are not linear and for one voltage harmonic, the converter would react by generating several harmonic currents, and hence the name "frequency-coupling". Latest findings in the literature show that the converter's PLL can create two relevant couplings that might impact the stability of the converter [60], however their impact on the harmonic distortion of an OWPP has not yet been verified [13]. The nonlinear behavior of the converter depends on both the positive and negative sequence voltages at the fundamental frequency, however since the negative-sequence voltage is very low then it has been decided to neglect it in the model. The model shown in figure 4.39 is the model used in the thesis to analyze the frequency coupling. The linear behavior of the converter is the model used in the previous cases (the Norton equivalent where the impedance is Z_{WT} and I_{WT} is the harmonic current of the converter), and now the non-linear behavior is added. Y_{c1} is the coupling admittance and the $(2\omega_1 - \omega)$ is the formula used to define the coupling frequency. For example, the coupling frequency of the 5th harmonic in the negative-sequence is computed as:

$$f_{c1} = 2 * 50 - (-250) = +350 \text{ Hz}$$

Therefore, it is coupled with the positive-sequence of the 7th harmonic order, and the opposite is also true where the positive-sequence of the 7th harmonic is coupled with the negative-sequence 5th harmonic order. Since these two harmonic orders have been studied in the previous cases, then case C will study these two harmonic orders.

The coupling currents for the negative-sequence 5th harmonic order and the positive-sequence 7th harmonic order can be computed using the following equations [60]:

$$I_c(\omega = -2\pi 250) = - \underbrace{Y_{c1}(\omega = -2\pi 250) e^{-j2\varphi_{v1}}}_{Y_{c1}} V_{POC}(\omega = +2\pi 350) \quad (4.14)$$

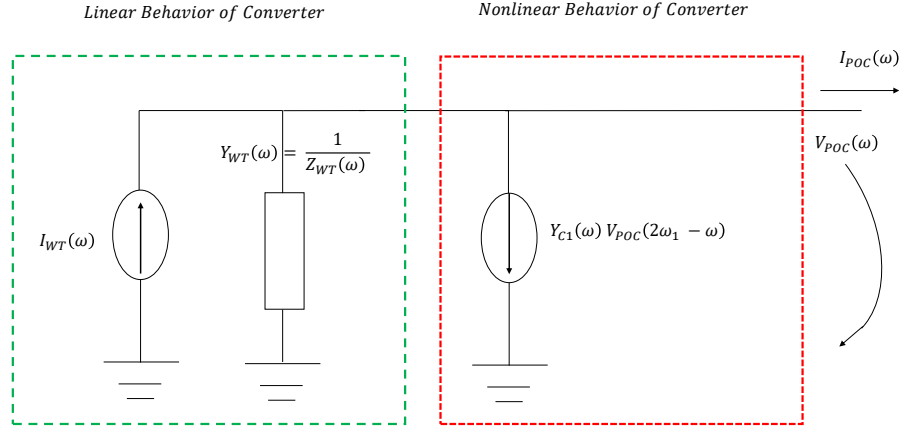


Figure 4.39: The Non-Linear Model of the Converter

[60]

$$I_c(\omega = +2\pi 350) = - \underbrace{Y_{c1}(\omega = +2\pi 350) e^{+j2\varphi_{v1}}}_{Y_{c1}} V_{POC}(\omega = -2\pi 250) \quad (4.15)$$

where Y_{c1} is the negative-sequence admittance coupling for the 5th harmonic and the positive-sequence admittance coupling for the 7th harmonic, which are dependent on the fundamental voltage phase angle at the wind turbine terminal φ_{v1} , and $V_{POC}(\omega = +2\pi 350)$ is the positive-sequence voltage at the WT's terminal used for the negative-sequence 5th harmonic coupling current, and $V_{POC}(\omega = -2\pi 250)$ is the negative-sequence voltage at the WT's terminal used for the positive-sequence 7th harmonic coupling current.

Therefore, the negative-sequence 5th harmonic current $I_{POC}(\omega = -2\pi 250)$ and the positive-sequence 7th harmonic current $I_{POC}(\omega = +2\pi 350)$ that are injected into the OWPP are computed from the model as follow [60]:

$$I_{POC}(\omega = -2\pi 250) = I_{WT}(\omega = -2\pi 250) - Y_{WT}(\omega = -2\pi 250) V_{POC}(\omega = -2\pi 250) - Y_{c1}(\omega = -2\pi 250) V_{POC}(\omega = +2\pi 350) \quad (4.16)$$

$$I_{POC}(\omega = +2\pi 350) = I_{WT}(\omega = +2\pi 350) - Y_{WT}(\omega = +2\pi 350) V_{POC}(\omega = +2\pi 350) - Y_{c1}(\omega = +2\pi 350) V_{POC}(\omega = -2\pi 250) \quad (4.17)$$

The above equations demonstrate that even if I_{WT} is zero at a specific frequency, then the harmonic voltage distortion at the terminal will create a coupling current at another frequency that could impact the final harmonic distortion at the PCC.

4.4.2. Modelling in PowerFactory and Coding in Python

The model and python code for the first two cases have to be modified to include the nonlinear behavior of the converter to determine the harmonic distortion at the PCC and answer the research question. As explained in the previous section, coupling currents have to be computed and included in the model to account for the frequency coupling and ensure that I_{POC} injected into the OWPP are computed using equations 4.16 and 4.17. The coupling current is modelled using a current source *Elmlac* in PowerFactory, thus each WT is connected in parallel to a unique current source. The python code is required to be modified to perform the following steps and as shown in the flow chart in figure 4.42:

1. Perform a power flow in the OWPP to get the phase-angle of the fundamental voltage at all the wind turbines' terminals. Each wind turbine will have a different φ_{v1} Since they are located at different locations in the OWPP.
2. Specify the minimum number of iterations, i.e. 1,000 iterations.

3. Generate and assign a unique random magnitude and phase angle to each WT in the OWPP for the 5th harmonic order from the PDFs in figures 3.2 and 3.3.
4. Perform negative-sequence 5th harmonic load flow and measure the harmonic voltage distortion at each WT's terminal V_{i-1}^{5th} .
5. Generate and assign a unique random magnitude and phase angle to each WT in the OWPP for the 7th harmonic order from the PDFs in figures 3.2 and 3.3.
6. Perform positive-sequence 7th harmonic load flow and measure the harmonic voltage distortion at each WT's terminal V_{i-1}^{7th} .
7. Compute and assign the coupling currents for the negative-sequence 5th harmonic using equation 4.14 and the positive-sequence 7th harmonic using equation 4.15 for each WTs using the fundamental voltage phase angles obtained in step 1 and the negative and positive coupling admittance shown in figures 4.40 and 4.41, respectively.
8. Perform negative-sequence 5th harmonic load flow and measure the harmonic voltage distortion at each WT's terminal V_i^{5th} (using the same random magnitude and phase angle values for the 5th harmonic).
9. Perform positive-sequence 7th harmonic load flow and measure the harmonic voltage distortion at each WT's terminal V_i^{7th} (using the same random magnitude and phase angle values for the 7th harmonic).
10. A tolerance of 0.001 is defined and checked for each wind turbine for both the 5th and 7th harmonic orders using the following equations:

$$\left| \frac{V_i^{5th} - V_{i-1}^{5th}}{V_{i-1}^{5th}} \right| \leq \text{tolerance} \quad (4.18)$$

$$\left| \frac{V_i^{7th} - V_{i-1}^{7th}}{V_{i-1}^{7th}} \right| \leq \text{tolerance} \quad (4.19)$$

11. If the tolerance limit is not met for any wind turbine for either harmonic orders, then V_i^{5th} and V_i^{7th} are used to compute new values of the coupling currents to repeat the steps from step 7 till the tolerance limit is met.
12. When the tolerance limit is met, the harmonic distortion at the PCC for the 5th and the 7th harmonic orders are stored and the process is repeated from step 3 for the minimum number of iterations.
13. Harmonic Distortion histograms are constructed for the both harmonic orders and the 95th percentile is computed.

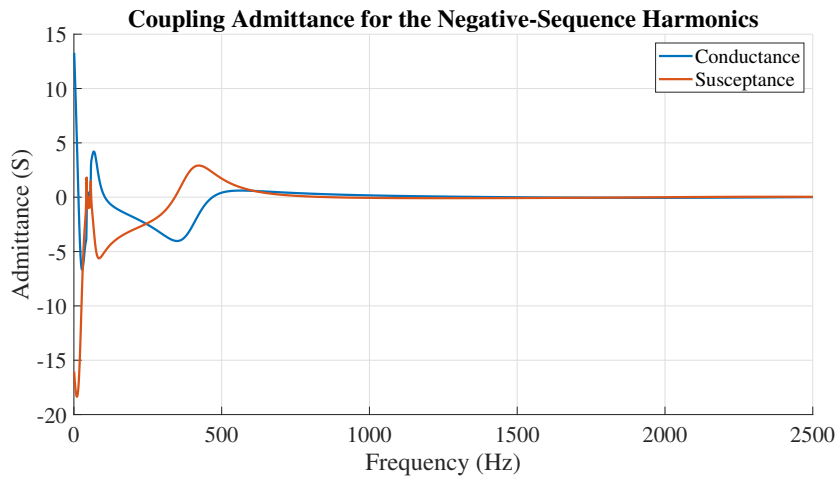


Figure 4.40: Coupling Admittance $Y_{c1}(\omega)$ for the Negative-Sequence Harmonics [13]

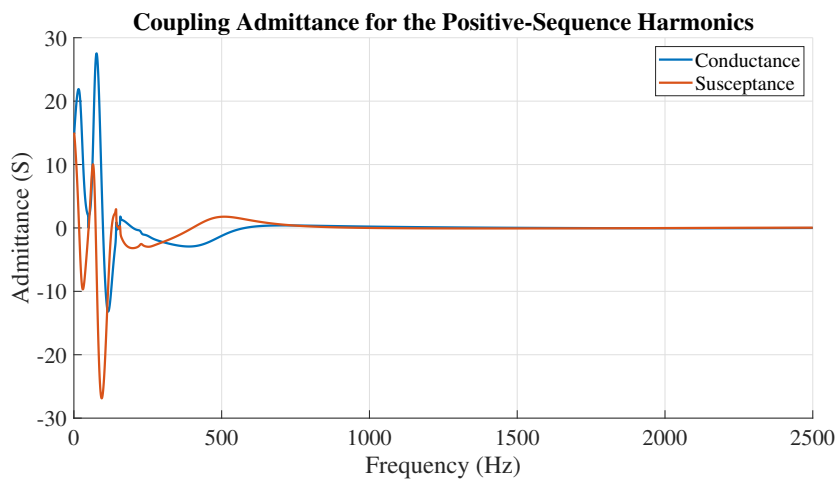


Figure 4.41: Coupling Admittance $Y_{c1}(\omega)$ for the Positive-Sequence Harmonics [13]

4.4.3. Simulation Results

The simulation was performed for the minimum number of iterations, i.e. 1,000 iterations, and the harmonic distortion is plotted in histograms for both the 5th and 7th harmonic orders as presented in figures 4.43 and 4.44.

The 95th percentile of harmonic distortion is then computed and compared to the 95th percentile obtained from case A where the frequency coupling was not considered and the converter was assumed to have linear behavior only. Figure 4.45 shows that the 5th harmonic order has a harmonic distortion that is now 0.2% lower than case A while the harmonic distortion for the 7th order increased by approximately 3.7%. Despite the low error percentage, the frequency coupling has an impact on the final harmonic distortion level when compared to the Monte Carlo method proposed in this thesis. However, it is also important to compare the harmonic distortions of this case with IEC results since the latter is the currently used method. Figure 4.46 and table 4.14 show that IEC would underestimate the harmonic distortion for both harmonic orders and that the inclusion of the frequency couplings increase the harmonic distortion at the PCC. The percentage error is higher than the error obtained when the results are compared to Monte Carlo case A and this could be attributed to the statistical variation of the harmonic current that is emitted in the IEC method.

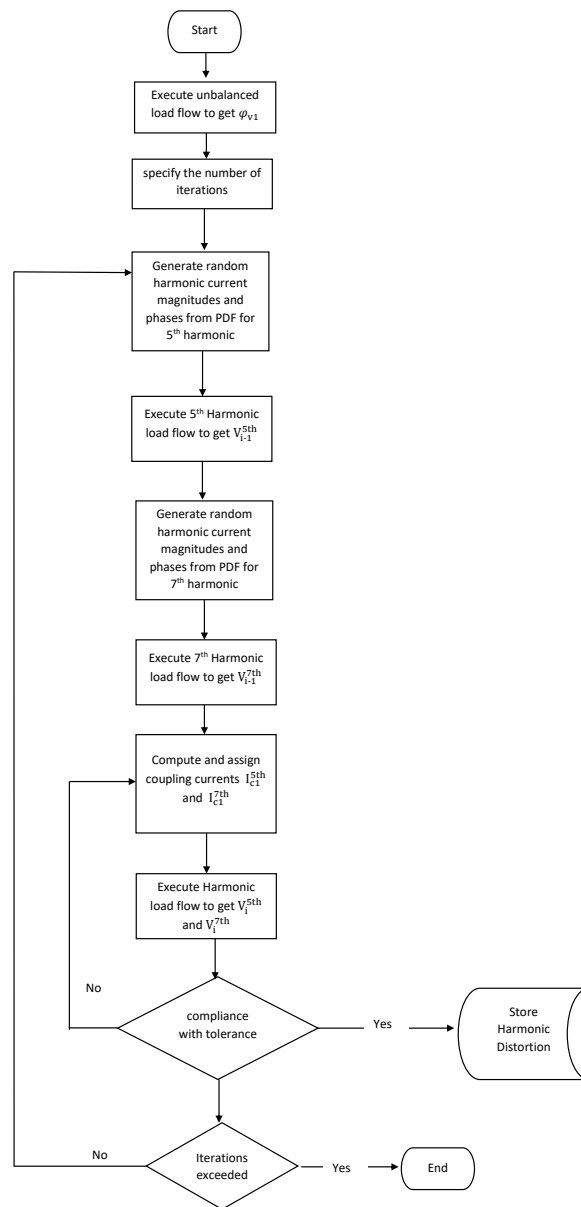
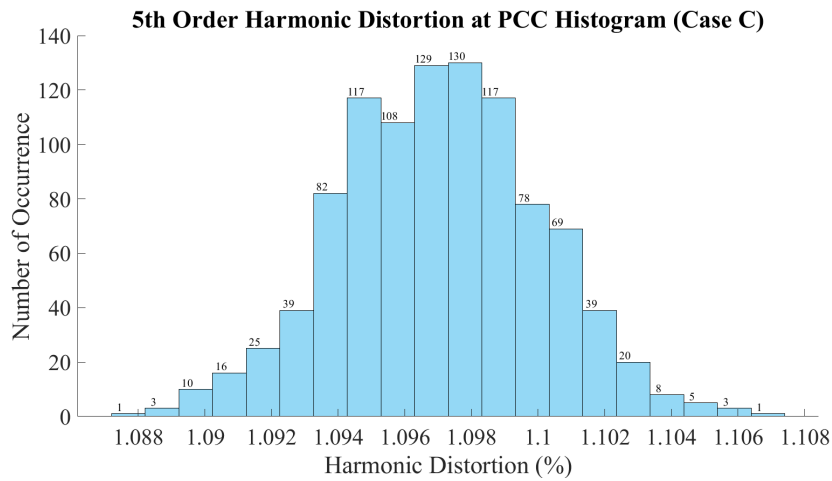
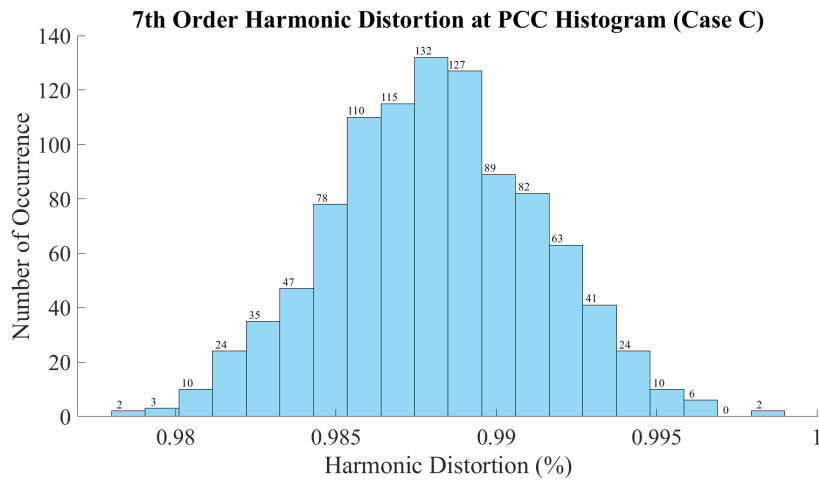
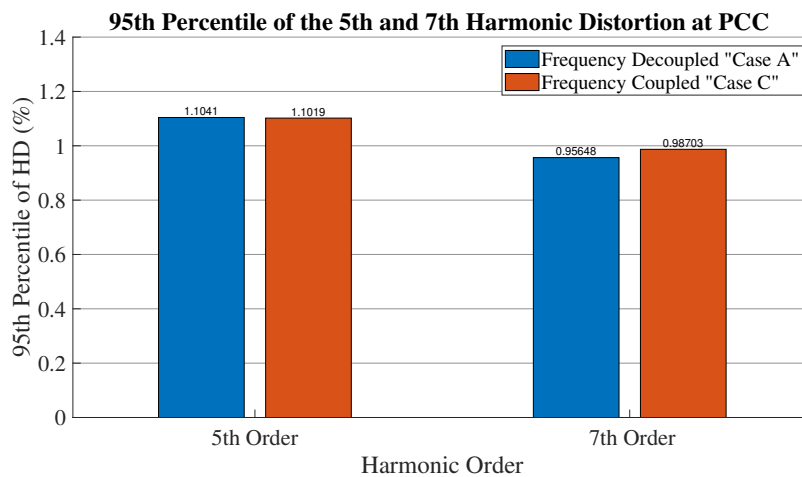


Figure 4.42: Flow Chart of Case C Python Code

Harmonic Order	IEC- 95 th Percentile Harmonic Distortion (%)	Monte Carlo- 95 th Percentile Harmonic Distortion (%)	Percentage Error (%)
5 th	0.98132	1.1019	10.94
7 th	0.87184	0.98703	12.25

Table 4.14: 95th Percentile of the 5th and 7th Harmonic Distortion at PCC-IEC VS. Monte Carlo

Figure 4.43: 5th Order Harmonic Distortion HistogramFigure 4.44: 7th Order Harmonic Distortion HistogramFigure 4.45: 95th Percentile of Harmonic Distortion for Case A versus Case C

4.4.4. Case C Conclusion

The main conclusions from this case are summarized:

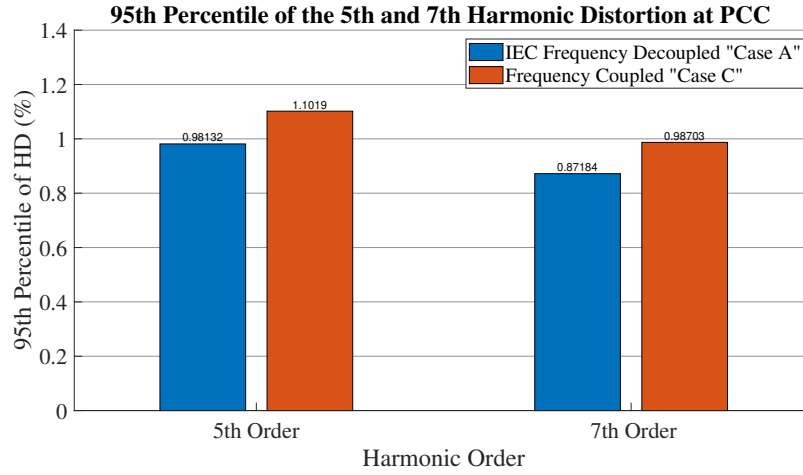


Figure 4.46: 95th Percentile of Harmonic Distortion for IEC versus Case C

- The harmonic distortion of the 5th harmonic is lower when frequency coupling is considered.
- The harmonic distortion of the 7th harmonic is higher when frequency coupling is considered.
- The percentage error between the frequency coupled and frequency decoupled Monte Carlo is not very high. However, the frequency coupled results increase the accuracy of the harmonic distortion and harmonic emission analysis due the higher accuracy in representing the WT's converter nonlinear behavior.
- The percentage error between the frequency coupled and IEC methods is quite high, which supports the recommendation to include the non-linear behavior of the converter into the harmonic emission analysis.

It is noteworthy to mention that executing harmonic emission analysis with varying grid's impedance or different OWPP configurations could yield different, and perhaps higher, percentage error that could further support the recommendation to include the frequency coupling phenomenon in the analysis.

4.5. Case D (non-linear and variable grid impedance)

4.5.1. Background

This case is intended to provide more insights on the impact of the frequency coupling phenomenon on the harmonic distortion at the PCC by considering a variable grid impedance. This case is a combination of the work done on cases B and C where the former investigated how the grid impedance loci resulted in different harmonic distortion, and the latter investigated the frequency coupling phenomenon. Therefore, the background grid impedance seen earlier in case B and in figure 4.20 is utilized here with the modified OWPP and python code explained in case C and figure 4.42.

4.5.2. Simulation Results

5th Harmonic Order

The results of the harmonic studies for all the impedance loci points for the 5th harmonic order are presented in table 4.15 for the Monte Carlo method and the 95th percentile of the harmonic distortion for the all impedance loci points are presented in figure 4.47. The required iterations to achieve the accuracy level of 0.1% error in the mean with a confidence level of 99.75% is accomplished with the minimum number of iterations. Similar to the conclusions made in case B, the variation of the grid impedance impacts the distortion at the PCC.

Impedance Loci Point	Monte Carlo Method					
	Mean of HD (%)	Standard Deviation of HD (%)	95 th Percentile of HD (%)	Mean of HD (V)	95 th Percentile of HD (V)	Required Iterations
a	0.92227	0.00408	0.92926	1014.50	1022.19	175.96
a1	0.76271	0.00432	0.77016	838.98	847.18	288.58
a2	0.66116	0.00443	0.66848	727.28	735.33	403.99
b	0.59103	0.00443	0.59840	650.13	658.23	504.63
b1	0.54399	0.00443	0.55117	598.39	606.29	596.58
b2	0.50208	0.00434	0.50963	552.28	560.59	673.21
c	0.46556	0.00429	0.47247	512.12	519.72	765.54
c1	0.47080	0.00426	0.47815	517.88	525.96	737.69
c2	0.46974	0.00394	0.47634	516.71	523.97	632.96
c3	0.46030	0.00401	0.46678	506.33	513.46	682.11
c4	0.44025	0.00376	0.44647	484.27	491.12	654.88
d	0.40966	0.00377	0.41608	450.62	457.69	760.34
d1	0.48023	0.00347	0.48594	528.25	534.53	470.37
d2	0.60279	0.00310	0.60812	663.07	668.93	237.89
e	0.84945	0.00237	0.85331	934.39	938.65	69.85
e1	1.01822	0.00190	1.02123	1120.05	1123.35	31.31
e2	1.18854	0.00189	1.19177	1307.40	1310.94	22.86
f	1.29882	0.00264	1.30332	1428.70	1433.65	37.28
f1	1.15583	0.00322	1.16099	1271.41	1277.09	69.75
f2	1.02664	0.00390	1.03324	1129.30	1136.56	129.73

Table 4.15: 5th Harmonic Order Monte Carlo Results- Case D

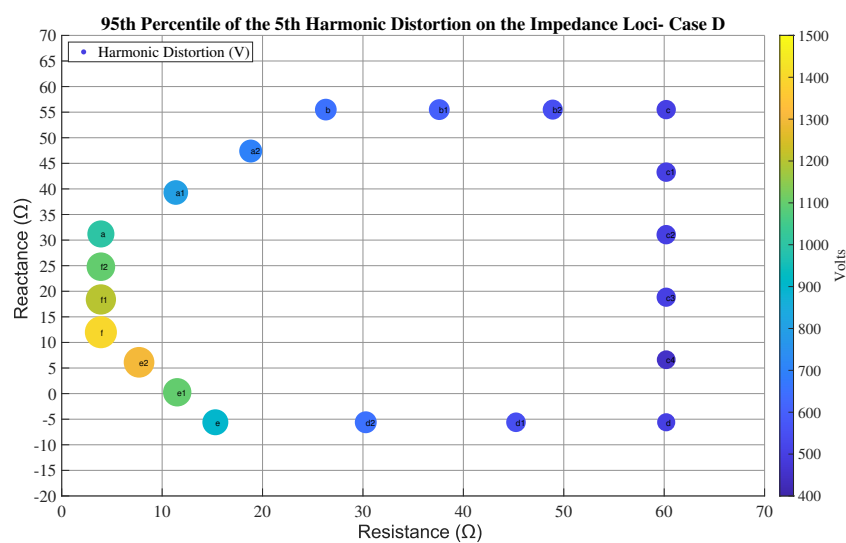


Figure 4.47: 95th Harmonic Distortion of the 5th Harmonic Order on Impedance Loci-Monte Carlo Case D

The focus in this case is to determine the error difference between the frequency coupled and frequency decoupled cases. The results obtained from the Monte Carlo method are compared to the results of the Monte Carlo and IEC methods from case B and presented in table 4.16 and figures 4.48 and 4.49. Case C showed that the frequency coupling phenomenon resulted in a lower harmonic distortion at the PCC. The error was approximately 0.2%, which could have raised a question on whether the inclusion of the nonlinear behavior of the converter in the harmonic study is beneficial. However, the results of this case show that this error could be as high as 5% when considering the variation of the grid impedance. Therefore, recommending the inclusion of the nonlinear behavior of the converter has a stronger support with the results of this case. Moreover, the frequency coupled results are also compared to the IEC summation rule method from case B, as the IEC summation rule is the currently used method in the industry. The frequency coupling leads to higher harmonic distortion at the majority of the impedance loci points. The error ranges between -7.75% to 37.30% for the different impedance loci points, which supports including the frequency coupling in the harmonic studies. The range of error could be explained by analyzing the simple model shown in figure 3.23 where the variation of the grid impedance leads to different harmonic distortion at the WT's terminals, and thus different coupling currents that impact the negative-sequence 5th harmonic current $I_{POC}(\omega=-2\pi 250)$ and the positive-sequence 7th harmonic current $I_{POC}(\omega=+2\pi 350)$ that are injected into the OWPP as computed using equations 4.16 and 4.17.

Impedance Loci Point	95 th Percentile of HD (V) - Case B		95 th Percentile of HD (V) - Case D		Error between Case B and Case D (%)	
	IEC Summation Rule	Monte Carlo	Monte Carlo		Monte Carlo VS. Monte Carlo	IEC VS. Monte Carlo
a	864.25	1055.79	1022.19		-3.18	18.28
a1	685.83	877.03	847.18		-3.40	23.53
a2	571.17	760.59	735.33		-3.32	28.74
b	491.52	681.36	658.23		-3.39	33.92
b1	449.63	627.19	606.29		-3.33	34.84
b2	411.74	578.92	560.59		-3.17	36.15
c	378.53	537.08	519.72		-3.23	37.30
c1	402.23	543.79	525.96		-3.28	30.76
c2	424.43	543.89	523.97		-3.66	23.45
c3	442.59	534.38	513.46		-3.91	16.01
c4	453.90	513.81	491.12		-4.42	8.20
d	456.24	480.19	457.69		-4.69	0.32
d1	553.46	563.07	534.53		-5.07	-3.42
d2	712.53	704.78	668.93		-5.09	-6.12
e	1017.49	986.39	938.65		-4.84	-7.75
e1	1147.49	1159.76	1123.35		-3.14	-2.10
e2	1257.11	1321.56	1310.94		-0.80	4.28
f	1303.81	1423.22	1433.65		0.73	9.96
f1	1136.13	1291.14	1277.09		-1.09	12.41
f2	987.27	1164.70	1136.56		-2.42	15.12

Table 4.16: 5th Harmonic Order Results Comparison - Case D

It is interesting to see that the trend of the errors between case B Monte Carlo and case D Monte Carlo as presented in figure 4.50 has a somehow similar trend to the harmonic gain impedance seen in case B in figure 4.24. It was shown in case B that the harmonic gain impedance plays a major role in the harmonic distortion at the PCC, and that the highest harmonic distortion was seen at point "f" that has the highest impedance. The error at point "f" is the smallest and it is the only impedance loci point where the frequency coupling leads to a higher harmonic distortion than the frequency decoupled case B. On other hand, it seems that as the harmonic gain impedance decreases, the error increases, which could be explained by a lower contribution on the harmonic distortion from the background grid and more from the OWPP. On the other hand, the trend of the errors between case B IEC and case D Monte Carlo as presented in figure 4.51 has a somehow similar trend to the PCC impedance as seen in case B in figure 4.25. This could be attributed to the statistical variation of the harmonic magnitude and phase angle that is not considered in the IEC summation rule. Moreover, this could be explained by the impact of the PCC impedance on the harmonic voltage distortion at the terminals of the WTs that consequently impact the coupling currents and the currents emitted into the OWPP by the WTs, and thus increasing the harmonic distortion at the PCC in the frequency coupled case. In other words, when the PCC impedance is high, the distortion at the PCC is high, and therefore the distortion at the WTs terminals is high, and therefore the coupling effect is high leading to a higher error between the IEC summation and Monte Carlo methods.

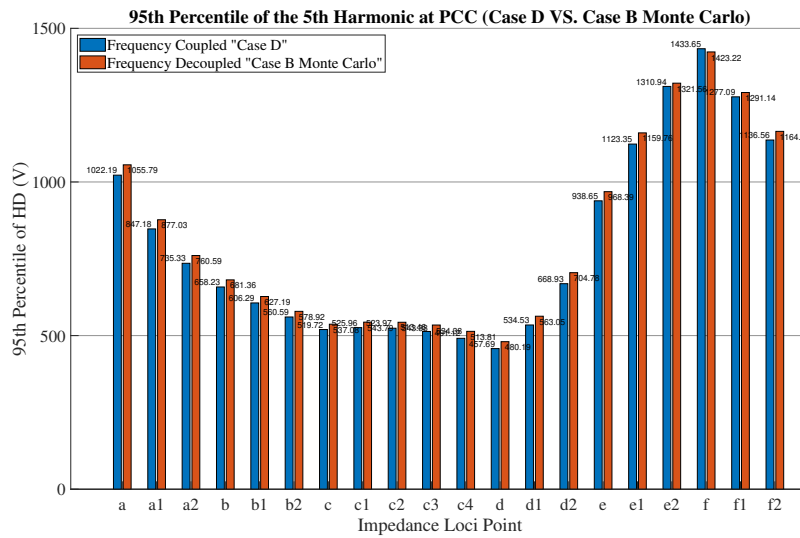


Figure 4.48: Comparison of the 95th Harmonic Distortion of the 5th Harmonic Order between Cases D and B (Monte Carlo VS. Monte Carlo)

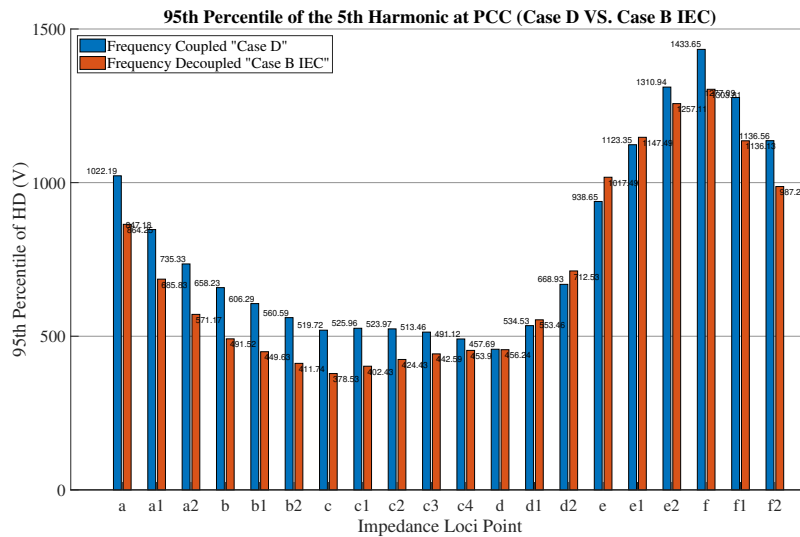


Figure 4.49: Comparison of the 95th Harmonic Distortion of the 5th Harmonic Order between Cases D and B (Monte Carlo VS. IEC)

7th Harmonic Order

The results of the harmonic studies for all the impedance loci points for the 7th harmonic order are presented in table 4.17 for the Monte Carlo method and the 95th percentile of the harmonic distortion for all the impedance loci points are presented in figure 4.52. The required iterations to achieve the accuracy level of 0.1% in the mean with a confidence level of 99.75% is accomplished with the minimum number of iterations. The variation of the background impedance impacts the harmonic distortion at the PCC as seen previously in case B.

Similar to the 5th harmonic, the results obtained from the Monte Carlo method are compared to the results of the Monte Carlo and IEC methods from case B and presented in table 4.18 and figures 4.53 and 4.54. The frequency coupling in case C resulted in higher harmonic distortion at the PCC when compared to case B, the error was approximately 3.7%. The results in this case yield the same behavior where including the nonlinear behavior of the converter leads to higher harmonic distortions for all the impedance loci points. The error ranges between 1.33% to 4.32%. Therefore, including the frequency coupling phenomenon in the harmonic studies demonstrates a higher accuracy in estimating the harmonic distortion of the OWPP. More-

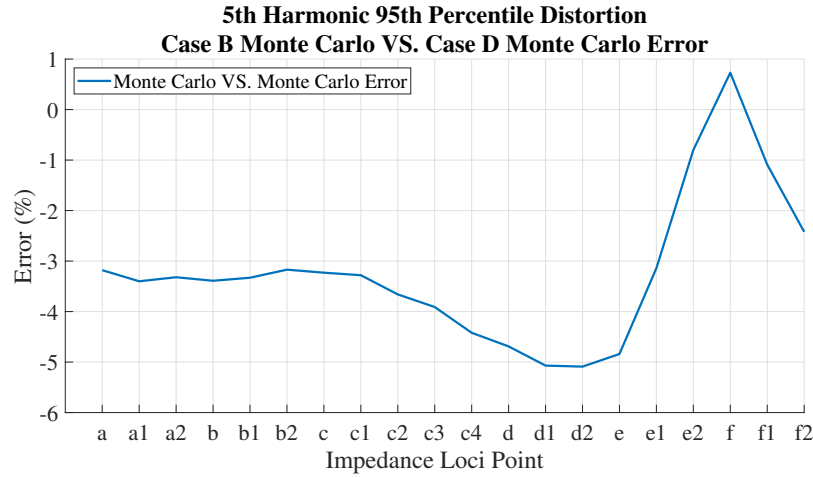


Figure 4.50: The Error in the 95th Harmonic Distortion of the 5th Harmonic Order between Cases B and D (Monte Carlo VS. Monte Carlo)

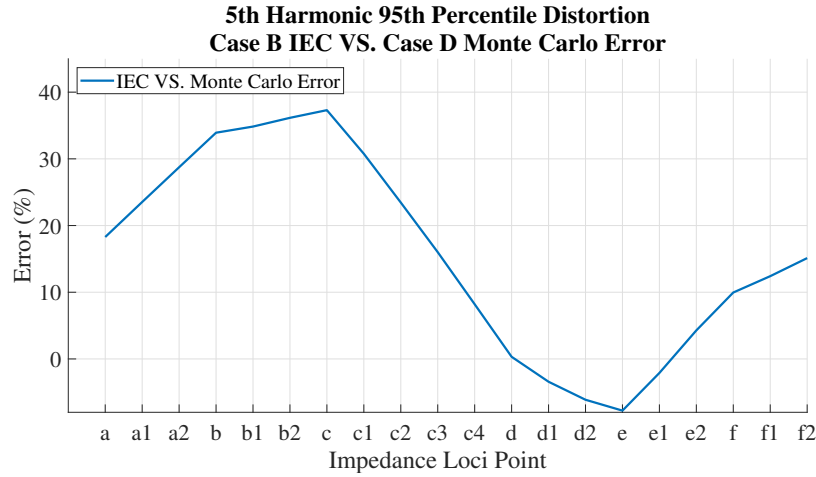
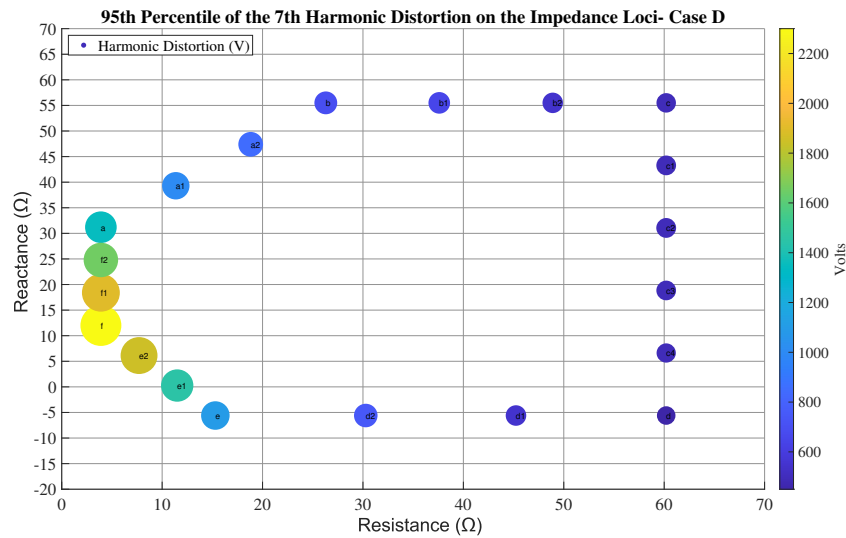


Figure 4.51: The Error in the 95th Harmonic Distortion of the 5th Harmonic Order between Cases B and D (IEC VS. Monte Carlo)

Impedance Loci Point	Monte Carlo Method					
	Mean of HD (%)	Standard Deviation of HD (%)	95th Percentile of HD (%)	Mean of HD (V)	95th Percentile of HD (V)	Required Iterations
a	1.26000	0.00376	1.26626	1386.00	1392.88	80.11
a1	0.94688	0.00344	0.95238	1041.57	1047.62	118.54
a2	0.76896	0.00349	0.77461	845.86	852.08	185.48
b	0.65442	0.00343	0.66028	719.87	726.30	247.63
b1	0.58607	0.00342	0.59198	644.68	651.18	305.70
b2	0.52603	0.00334	0.53136	578.64	584.50	363.01
c	0.47483	0.00336	0.48031	522.31	528.34	451.43
c1	0.48731	0.00355	0.49323	536.04	542.56	477.06
c2	0.49195	0.00359	0.49788	541.15	547.66	478.60
c3	0.48484	0.00343	0.49007	533.33	539.07	449.46
c4	0.46424	0.00333	0.46973	510.66	516.70	462.20
d	0.42989	0.00341	0.43547	472.88	479.02	567.38
d1	0.52893	0.00317	0.53416	581.82	587.57	323.93
d2	0.69708	0.00293	0.70189	766.79	772.08	159.05
e	1.02605	0.00234	1.02996	1128.66	1132.96	46.79
e1	1.32069	0.00199	1.32398	1452.76	1456.38	20.48
e2	1.72015	0.00203	1.72344	1892.17	1895.78	12.54
f	2.11774	0.00279	2.12236	2329.52	2334.59	15.63
f1	1.81123	0.00351	1.81678	1992.35	1998.46	33.84
f2	1.50034	0.00360	1.50643	1650.37	1657.07	51.87

Table 4.17: 7th Harmonic Order Monte Carlo Results- Case D

over, the results of the Monte Carlo in this case are compared to the IEC summation rule results obtained in case B, and this comparison provides a different range of error between -2.5% and 30.50% for the different impedance loci points. The range of errors for both case B Monte Carlo and case D Monte Carlo and case

Figure 4.52: 95th Harmonic Distortion of the 7th Harmonic Order on Impedance Loci-Monte Carlo Case D

B IEC summation and case D Monte Carlo are smaller for the 7th harmonic when compared to the range of errors for the 5th harmonic. This could indicate that the frequency coupling has a bigger impact on the harmonic distortion of the 5th harmonic than it does for the 7th harmonic. This could be as a result of a higher harmonic distortion at the WT terminals for the 7th harmonic when compared to the 5th harmonic, and thus leading to higher coupling currents for the 5th harmonic. It is noteworthy to reiterate that despite the higher harmonic current for the 5th harmonic as seen in figure 3.2, the variation of the grid impedance in case B yielded higher harmonic distortion for the 7th harmonic than for the 5th harmonic for 13 out of 20 points of the impedance loci, while the harmonic distortion for all impedance loci points yielded higher distortion for the 7th harmonic than they did for the 5th harmonic in this case as seen in tables 4.15 and 4.17.

Impedance Loci Point	95th Percentile of HD (V) - Case B		95th Percentile of HD (V) - Case D		Error between Case B and Case D (%)	
	IEC Summation Rule	Monte Carlo	Monte Carlo		Monte Carlo VS. Monte Carlo	IEC VS. Monte Carlo
a	1166.16	1347.07	1392.88		3.40	19.44
a1	852.53	1014.60	1047.62		3.25	22.88
a2	673.36	824.16	852.08		3.39	26.54
b	557.91	702.10	726.30		3.45	30.18
b1	500.41	628.61	651.18		3.59	30.13
b2	449.01	564.22	584.50		3.59	30.18
c	404.86	508.20	528.34		3.96	30.50
c1	433.97	521.18	542.56		4.10	25.02
c2	459.55	526.22	547.66		4.08	19.18
c3	477.40	518.49	539.07		3.97	12.92
c4	483.70	495.82	516.70		4.21	6.82
d	476.85	459.18	479.02		4.32	0.45
d1	592.54	567.86	587.57		3.47	-0.84
d2	785.98	752.48	772.08		2.60	-1.77
e	1162.07	1118.05	1132.96		1.33	-2.50
e1	1442.92	1436.35	1456.38		1.39	0.93
e2	1810.66	1861.51	1895.78		1.84	4.70
f	2144.68	2274.29	2334.59		2.65	8.85
f1	1772.62	1937.25	1998.46		3.16	12.74
f2	1425.84	1603.23	1657.07		3.36	16.22

Table 4.18: 7th Harmonic Order Results Comparison - Case D

The trend of the errors between case B Monte Carlo and case D Monte Carlo is presented in figure 4.55. However, unlike the 5th harmonic order, the trend does not follow the trend of the harmonic gain impedance seen in case B in figure 4.30. The trend of errors between case B IEC summation rule and case D Monte Carlo is presented in figure 4.56, and similarly it does not follow the trend of the PCC impedance see in figure 4.31. The trend of errors for both scenarios could be impacted by a combination of the harmonic gain and PCC impedances, which impact the harmonic voltage distortion at the WTs' terminals. Nonetheless, it is clear that the frequency coupling has an impact on the final harmonic distortion at the PCC and the error could be as

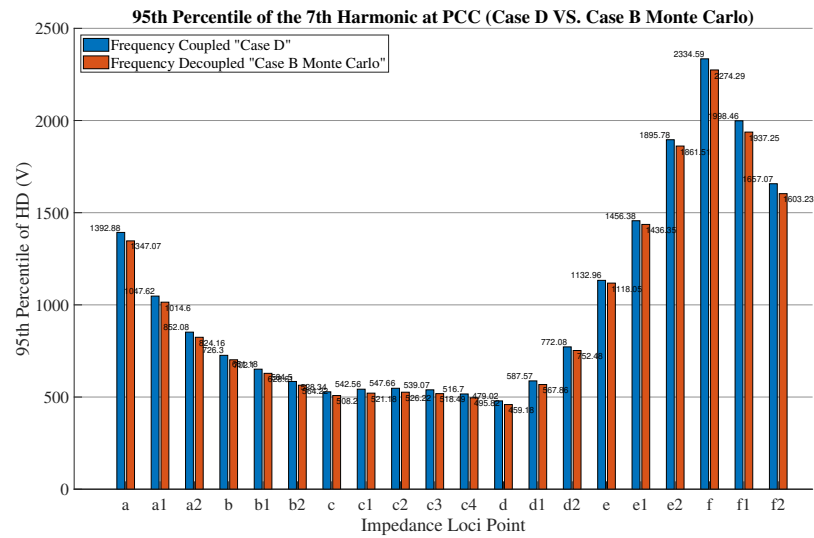


Figure 4.53: Comparison of the 95th Harmonic Distortion of the 7th Harmonic Order between Cases D and B (Monte Carlo VS. Monte Carlo)

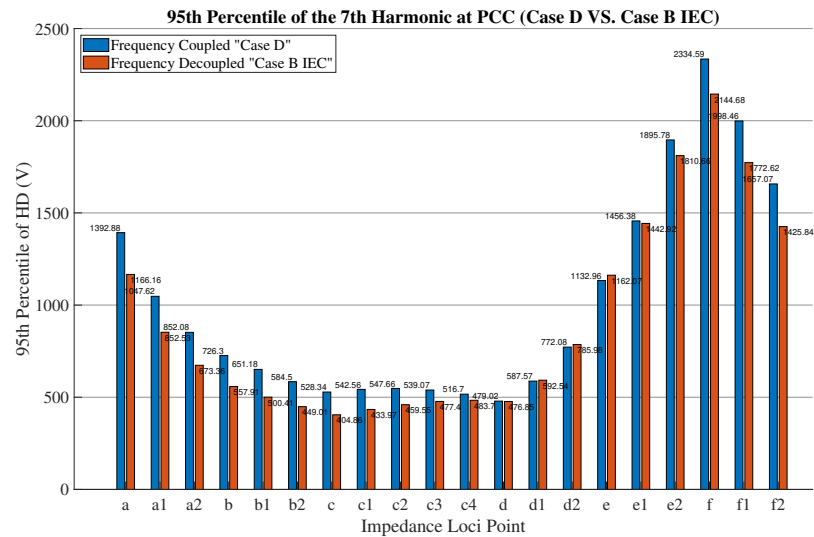


Figure 4.54: Comparison of the 95th Harmonic Distortion of the 7th Harmonic Order between Cases D and B (Monte Carlo VS. IEC)

high as 30%, which necessities including it in harmonic studies.

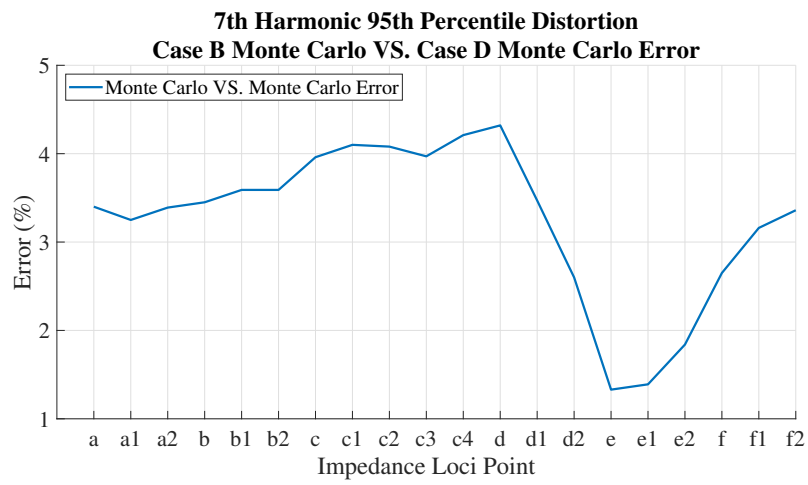


Figure 4.55: The Error in the 95th Harmonic Distortion of the 7th Harmonic Order between Cases B and D (Monte Carlo VS. Monte Carlo)

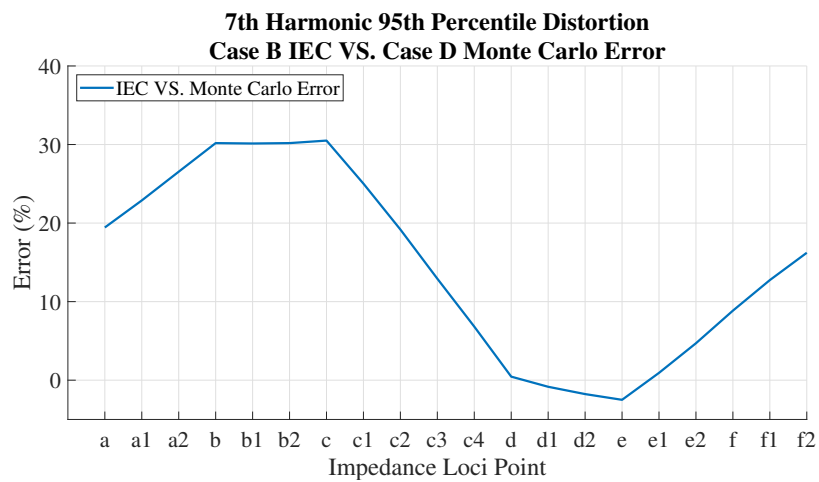


Figure 4.56: The Error in the 95th Harmonic Distortion of the 7th Harmonic Order between Cases B and D (IEC VS. Monte Carlo)

5

Conclusion and Future Work

5.1. Conclusion

The main research objective of this thesis was to determine if a new method based on probability theory would provide more accurate results in determining the harmonic emission of Offshore Wind Power Plant compared to the traditional and highly-criticized IEC summation rule. The IEC summation is currently used to perform harmonic studies and it has been shown in the literature the IEC method does not provide accurate results when compared to actual measurements of OWPP. The IEC relies on the 95th percentile of the harmonic current magnitude and represents the phase angle of the harmonic current by an α exponent. Nonetheless, the harmonic currents were found to have a statistical variation due to the nonlinear operation of the Power Electronic Converter used in the Wind Turbines. A literature review was performed to obtain probability distribution functions for the magnitude and phase angle of different harmonic orders to be used in the study, and also to acquire the know-how to model an OWPP for harmonic studies, for which DIGSilent PowerFactory was used. The OWPP model was interfaced with Python codes to perform Monte Carlo (probabilistic) harmonic analysis utilizing the probability distribution functions from the literature to determine the harmonic distortion at the Point of Common Coupling. Three main research questions were articulated at the beginning of the thesis to achieve the main objective. The questions and their answers are:

1. How does the harmonic grid compliance results compare when studies are performed based on probability distribution function of magnitude and phase angles versus studies performed with the summation rule.

Case A was implemented to answer this research question that compares between the proposed Monte Carlo method and IEC in determining harmonic distortion at the PCC. The two main assumptions of this case are: the converter is operating under its linear behavior and thus frequencies are independent and the external grid has a fixed impedance. The main findings of this case are:

- The shape and parameters of the probability distribution functions of the harmonic current play a major role in the final harmonic distortion at the PCC. It was shown, for example, that the 5th harmonic that has a higher current magnitude and lower phase angle standard deviation had a higher harmonic distortion compared to the other two harmonic orders.
- The amplification of harmonic depends on the PDFs parameters and the PCC impedance.
- The random behavior of the current would exploit the cancellation and summation effect compared to the deterministic approach of the IEC summation rule.
- IEC summation rule underestimates the 5th and 7th harmonics and overestimates the 8th harmonic. The percentage error could be as low as 12% (underestimating) or as high as 25% (overestimating).
- The probabilistic (Monte Carlo) method provides closer results to the expected results than IEC does, hence uncertainty in grid-compliance studies is lower.

2. How does the variation of the grid impedance impact the harmonic distortion level at the PCC.

Case B was implemented to answer this research question by performing harmonic studies with different background impedance. The impedance of the external grid was represented by an impedance Loci and twenty different impedance points were defined and used separately in the harmonic studies. The main findings of this case:

- The variation of the grid impedance could lead to grid non-compliance as seen at point "f" of the impedance loci for the 7th harmonic where this non-compliance was not foreseen with a fixed grid case A nor with a variable grid's impedance IEC method.
 - The variation of the grid impedance results in a big difference in the harmonic distortion between the different impedance loci points. The difference between the biggest and lowest harmonic distortion could be as high as 5 times for the 7th and 8th harmonic and as high as 3 times for the 5th harmonic. This demonstrates the necessity of including the variation of the background impedance in all harmonic emission studies.
 - Similar to case A, IEC underestimates the harmonic distortion for the 5th and 7th harmonic and overestimates the harmonic distortion for the 8th harmonic for the majority of the impedance loci points.
 - The percentage error between IEC and Monte Carlo has a bigger range than case A results, the percentage error could be as twice as high in some cases. This shows that the Monte Carlo would decrease the uncertainty in determining the harmonic distortion with the statistical variation of the magnitude and phase angle of the harmonic current.
3. How does the presence of frequency coupling between harmonics impact the distortion level at the PCC compared to the frequency decoupled harmonic cases.

Case C was implemented to answer the last research question by including the non-linear behavior of the converter into the model and performing harmonic studies with the complex model of the converter. This case was intended to determine the harmonic distortion of the OWPP when the frequency coupling phenomenon is considered. The main findings are:

- The harmonic distortion at the PCC is different for both the 5th and 7th harmonic orders when the frequency coupling is considered.
- The percentage error was found to be very low for the 5th harmonic and low for the 7th harmonic when compared to the results obtained in the Monte Carlo of case A.
- The percentage error was found to be quite high when the results are compared to the IEC summation rule, which is the currently utilized method to determine harmonic emission, and thus the phenomenon could have a big impact on the harmonic distortion of an OWPP. The harmonic distortion is higher for both the 5th and 7th harmonic orders when frequency coupling is considered. Therefore, frequency-coupling should be included in harmonic emission studies.
- Case D demonstrated that the harmonic distortion results could be different when a variation of the grid impedance is considered. The error between cases B and D (i.e. when including or not the influence of the frequency coupling) can be as high as 5% as seen for the 5th harmonic. Moreover, the error range is between -7.75% to 37.30% for the 5th harmonic and between -2.5% to 30.50% when the results are compared to IEC summation rule. This further support the argument made in this thesis to include the frequency coupling phenomenon in harmonic emission studies.

5.2. Future Work

Harmonic emission studies of OWPP are becoming very important due to the increasing number of OWPP grid-connected. The studies are required to ensure grid compliance and the high-quality of power output as seen in the different parts of the thesis. There are many opportunities for further research based on the findings of this thesis:

1. One of the main assumptions made in the thesis was that the magnitude and phase angle of the background distortion are deterministic. However, similar to the statistical variation of the harmonic current injected by the WT's converter, the background's distortion is also a random variable and should be represented by its probability distribution function in the model [18]. Also, it was assumed that the

background's impedance is not linked to the variation of grid's distortion. However, this is a simplification and the background distortion and its statistical variation might also be impacted by the change of the grid's impedance. Thus, the model and the method can be modified to include the statistical variation of the background distortion to increase the accuracy of the final results.

2. The scope of work of this thesis did not have harmonic distortion measurements of actual OWPP to verify the proposed method and it relies solely in simulation in PowerFactory. Therefore, it is recommended that the method is compared to actual measurements to verify how close the results of the Monte Carlo are to the actual measurements and in comparison with IEC.
3. The probability distribution functions of the magnitude and phase angle of the different harmonic orders are assumed to be independent of each other without any correlations. However, this might not be completely true as the magnitude of the harmonic current could be related to its phase angle. In short, there could still be statistical variation of both variables, however some sort of dependencies may exist and should be investigated and included in the model. This could require measurements of harmonic currents at the converter's level and/or analytical analysis.
4. The probability distribution functions of the magnitude and phase angle of the different harmonic orders are used for all the wind turbines in the OWPP. This simplification is based on the fact that the WTs could be operating at the same operating point and therefore their time-varying harmonic currents are the same. Nonetheless, this assumption is required to be further checked and verified from actual measurements of different WTs, and modify the model and Monte Carlo method accordingly based on the findings.
5. The OWPP was modelled with HVAC export cables. However, there is also a trend to use HVDC export cables with Voltage Source Converters in the OWPP, which have different statistical variation and could result in different findings. The proposed method in this thesis could be extended to HVDC-connected OWPP.

A

Appendix

A.1. Amplification Factor and Network Impedance Verification

The amplification factor was verified in a simple model of 7 wind turbines connected in radial connection to an external grid as shown in figure A.1 for the 8th harmonic order. The following simplification was done:

- The array cables have zero impedance.
- The external grid has the background impedance used in cases A and C.
- The parallel PWM filters are disconnected.
- The network impedance shown in figure 4.11 is the WT step-up transformer's impedance.
- The current source of the converters of the WTs are assigned 1% k_h ratio and zero phase angle φ_h that are used to calculate the harmonic current as per equation 3.4.
- The verification is performed using figures 4.11 and 4.12.

The impedance of the OWPP is calculated with the WT and transformer impedances as follows:

$$Z_{WT} = Z_{WT} (8^{\text{th}} \text{ harmonic}) = 0.0288 \angle 78.38 \Omega$$

$$Z_{\text{Network}} = Z_{\text{transformer}} (8^{\text{th}} \text{ harmonic}) = 3.598 E - 3 \angle 85.84 \Omega$$

$$Z_{\text{OWPP}} = \frac{Z_{WT} + Z_{\text{Network}}}{7} = 4.28 E - 3 \angle 71.75 \Omega$$

The equivalent impedance at the PCC is calculated with the grid impedance as follows:

$$Z_{\text{grid}} = 0.01401 \angle 20.82 \Omega$$

$$Z_{\text{PCC}} = Z_{\text{OWPP}} // Z_{\text{grid}} = 8.02 E - 3 \angle 45.37 \Omega$$

The PCC impedance referred to the primary side of the network is:

$$Z_{\text{PCC-high}} = Z_{\text{OWPP}} // Z_{\text{grid}} = 8.03 \angle 60.50 \Omega$$

First, a power flow is performed to measure the fundamental current that is used to calculate the harmonic current of the current source of the Norton equivalent using equation 3.4 as follows:

$$I_{\text{fundamental}} = 3486.3 \angle 33.03 A$$

$$I_{WT} = 34.86 \angle -95.76 A$$

The aggregated model will then have to inject the following harmonic current into the network (using current divider):

$$I_{8\text{-total}} = \frac{Z_{WT}}{Z_{OWPP} + Z_{grid}} \times I_{WT} = 58.93 \angle -49.45 \text{ A}$$

This is the sum of the harmonic currents by the 7 wind turbines, thus each wind turbine is injecting into the network:

$$I_8 = 8.42 \angle -49.45 \text{ A}$$

The above computed harmonic current matches the results obtained from PowerFactory harmonic simulation.

The aggregated harmonic current of the OWPP at the secondary and primary sides, respectively, are computed using the aggregated model in figure 4.12 :

$$I_{OWPP} = \frac{7 \times Z_{WT}}{Z_{WT} + Z_{Network}} \times I_{WT} = 234.49 \angle -89.13 \text{ A}$$

$$I_{OWPP\text{-primary}} = \frac{234.49 \angle -89.13}{47.89} = 4.896 \angle -89.13 \text{ A}$$

The aggregated harmonic current indicates that the network impedance function $f(Z_i)$ is approximately equal to the number of wind turbines in this simple network ¹:

$$f(Z_i) = \frac{7 \times Z_{WT}}{Z_{WT} + Z_{Network}} = 6.73 \angle 6.63 \Omega$$

The computed harmonic voltage distortion at the PCC using the aggregated harmonic current I_{OWPP} and the PCC impedance Z_{PCC} is confirmed to match the value obtained from PowerFactory simulation:

$$V_{PCC} = Z_{PCC\text{-high}} \times I_{OWPP} = Z_{PCC\text{-high}} \times I_{WT} \times f(Z_i) = 39.46 \angle -28.63 \text{ V}$$

The amplification factor is calculated using equation 4.1 from the harmonic voltage distortion and the harmonic current of the current source (referred to the primary):

$$\text{Amplification Factor} = \frac{HD (V)}{I_{WT}(A)} = \frac{39.46}{0.7285} = 54.26$$

This computation confirms that equation 4.13 is correct since:

$$\text{Amplification Factor} = Z_{PCC\text{-high}} \times f(Z_i) = 54.04$$

Therefore, it is confirmed that the amplification factor is a product of the impedance at the PCC Z_{PCC} and the network impedance function $f(Z_i)$, and that analyzing the amplification at the PCC using the PCC impedance matrices might lead to incorrect results as seen for the 8th harmonic order amplification factor in the deterministic magnitude scenario.

¹This is true in this simple model but it is not correct for the 89 WTs model since the network impedance would be different when the impedances of all the OWPP components are considered, which was also checked and verified

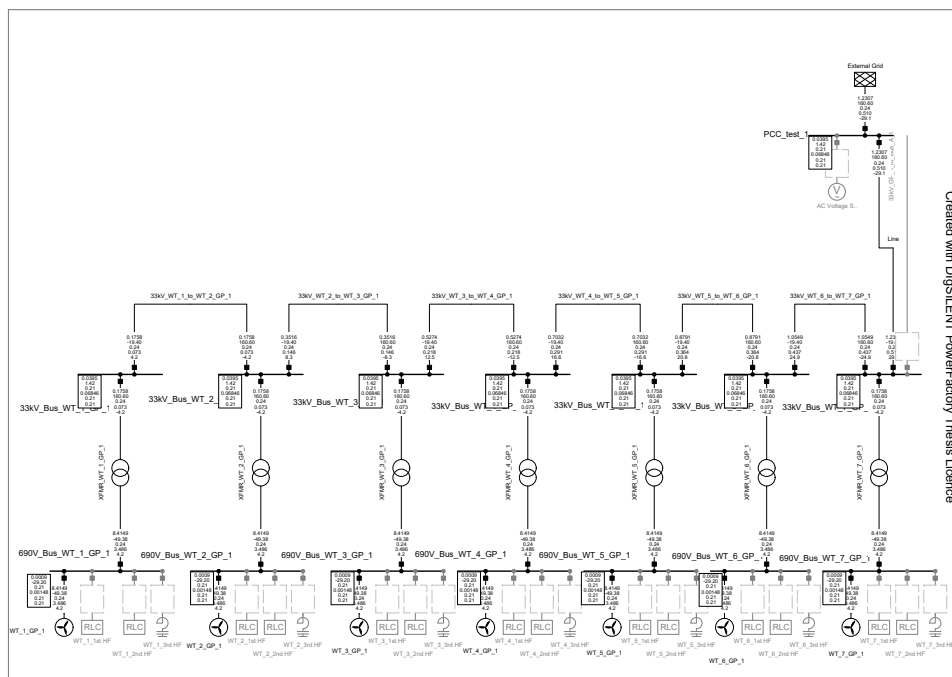


Figure A.1: Simple 7 WTs Network

Bibliography

- [1] *2050 long-term strategy report made by the European commission*, Feb. 2017. [Online]. Available: <https://ec.europa.eu/clima/policies/strategies/2050>.
- [2] *Wind energy today*. [Online]. Available: <https://windeurope.org/about-wind/wind-energy-today/>.
- [3] I. Komusanac, G. Brindley, D. Fraile, and L. Ramirez, *Wind energy in Europe 2020 statistics and the outlook for 2021-2025*, R. O'Sullivan, Ed., Feb. 2021. [Online]. Available: <https://windeurope.org/>.
- [4] E. P. Soares-Ramos, L. de Oliveira-Assis, R. Sarrias-Mena, and L. M. Fernández-Ramírez, "Current status and future trends of offshore wind power in Europe," *Energy*, vol. 202, p. 117 787, 2020. DOI: [10.1016/j.energy.2020.117787](https://doi.org/10.1016/j.energy.2020.117787).
- [5] L. Ramírez, D. Fraile, and G. Brindley, *Offshore wind in Europe key trends and statistics 2020*, R. O'Sullivan, Ed., Feb. 2021. [Online]. Available: <https://windeurope.org/intelligence-platform/product/offshore-wind-in-europe-key-trends-and-statistics-2020/>.
- [6] P. Bresesti, W. L. Kling, R. L. Hendriks, and R. Vailati, "HVDC connection of offshore wind farms to the transmission system," *IEEE Transactions on Energy Conversion*, vol. 22, no. 1, pp. 37–43, 2007. DOI: [10.1109/TEC.2006.889624](https://doi.org/10.1109/TEC.2006.889624).
- [7] T. May, Y. M. Yeap, and A. Ukil, "Comparative evaluation of power loss in HVAC and HVDC transmission systems," Nov. 2016, pp. 637–641. DOI: [10.1109/TENCON.2016.7848080](https://doi.org/10.1109/TENCON.2016.7848080).
- [8] *Hornsea two offshore wind farm in the UK*. [Online]. Available: <https://hornseaprojects.co.uk/hornsea-project-two>.
- [9] *The land high voltage station*. [Online]. Available: <https://www.geminiwindpark.nl/>.
- [10] L. H. Kocewiak, "Harmonics in large offshore wind farms," Ph.D. dissertation, Department of Energy Technology, Aalborg University, 2012, pp. 1–333.
- [11] L. H. Kocewiak, R. Blasco, C. Buchhagen, J. Bum Jwn, Y. Sun, A. Trevisan, M. Larsson, and X. Wang, "Overview, status and outline of stability analysis in converter-based power systems," *19th Inte'l Wind Integration Workshop*, pp. 1–10, Nov. 2020.
- [12] W. Wiechowski and P. Borre Eriksen, "Selected studies on offshore wind farm cable connections - challenges and experience of the danish tso," *2008 IEEE Power and Energy Society General Meeting - Conversion and Delivery of Electrical Energy in the 21st Century*, 2008. DOI: [10.1109/pes.2008.4596124](https://doi.org/10.1109/pes.2008.4596124).
- [13] L. Beloqui Larumbe, Z. Qin, and P. Bauer, "Introduction to the analysis of harmonics and resonances in large offshore wind power plants," in *2018 IEEE 18th International Power Electronics and Motion Control Conference (PEPMC)*, 2018, pp. 393–400. DOI: [10.1109/EPEPMC.2018.8521974](https://doi.org/10.1109/EPEPMC.2018.8521974).
- [14] Z. Emin, F. Fernandez, G. Williamson, and M. Poeller, "Harmonic distortion specification and compliance of an offshore wind generation," *10th IET International Conference on AC and DC Power Transmission (ACDC 2012)*, 2012. DOI: [10.1049/cp.2012.1958](https://doi.org/10.1049/cp.2012.1958).
- [15] L. H. Kocewiak, S. Chaudhary, and B. Hesselbaek, "Harmonic mitigation methods in large offshore wind power plants," in *Proceedings of the 12th Wind Integration Workshop Conference date: 22-10-2013 Through 24-10-2013*, GmbH, 2013, pp. 443–448, ISBN: 978-3-9813870-7-0.
- [16] M. Eltouki, T. W. Rasmussen, E. Guest, L. Shuai, and L. Kocewiak, "Analysis of harmonic summation in wind power plants based on harmonic phase modelling and measurements," *17th Int'l Wind Integration Workshop*, pp. 1–7, Oct. 2018.
- [17] K. Van Reusel and S. Bronckers, "Summation rule for wind turbines' harmonics challenged by measurements," *2016 17th International Conference on Harmonics and Quality of Power (ICHQP)*, 2016. DOI: [10.1109/ichqp.2016.7783356](https://doi.org/10.1109/ichqp.2016.7783356).

- [18] C. Jensen, C. Bak, L. H. Kocewiak, J. Hjerrild, and K. Berthelsen, "Probabilistic aspects of harmonic emission of large offshore wind farms," 10th International Workshop on Large-Scale Integration of Wind Power into Power Systems as well as on Transmission Networks for Offshore Wind Power Plants ; Conference date: 25-10-2011 Through 26-10-2011, Energynautics GmbH, 2011.
- [19] L. Sainz, J. J. Mesas, R. Teodorescu, and P. Rodriguez, "Deterministic and stochastic study of wind farm harmonic currents," *IEEE Transactions on Energy Conversion*, vol. 25, no. 4, pp. 1071–1080, 2010. DOI: [10.1109/tec.2010.2045379](https://doi.org/10.1109/tec.2010.2045379).
- [20] A. Romero, G. Suvire, H. Zini, and G. Rattá, "Time-varying harmonic analysis in electric power systems with wind farms, through the possibility theory," *DYNA*, vol. 82, pp. 185–194, Aug. 2015. DOI: [10.15446/dyna.v82n192.48617](https://doi.org/10.15446/dyna.v82n192.48617).
- [21] Y. Cho, C. Lee, K. Hur, Y. Kang, E. Muljadi, S.-H. Park, Y.-D. Choy, and G.-G. Yoon, "A framework to analyze the stochastic harmonics and resonance of wind energy grid interconnection," *Energies*, vol. 9, no. 9, p. 700, 2016. DOI: [10.3390/en9090700](https://doi.org/10.3390/en9090700).
- [22] S. T. Tentzerakis and S. A. Papathanassiou, "An investigation of the harmonic emissions of wind turbines," *IEEE Transactions on Energy Conversion*, vol. 22, no. 1, pp. 150–158, 2007. DOI: [10.1109/tec.2006.889607](https://doi.org/10.1109/tec.2006.889607).
- [23] M. Kazem Bakhshizadeh, X. Wang, F. Blaabjerg, J. Hjerrild, L. Kocewiak, C. L. Bak, and B. Hesselbæk, "Couplings in phase domain impedance modeling of grid-connected converters," *IEEE Transactions on Power Electronics*, vol. 31, no. 10, pp. 6792–6796, 2016. DOI: [10.1109/TPEL.2016.2542244](https://doi.org/10.1109/TPEL.2016.2542244).
- [24] V. Preciado, M. Madrigal, E. Muljadi, and V. Gevorgian, "Harmonics in a wind power plant," in *2015 IEEE Power Energy Society General Meeting*, 2015, pp. 1–5. DOI: [10.1109/PESGM.2015.7285774](https://doi.org/10.1109/PESGM.2015.7285774).
- [25] L. Depla, E. T. S. d'Enginyeria Industrial de Barcelona, and U. P. de Catalunya. Departament d'Enginyeria Elèctrica, *Harmonic Interactions in HVAC-connected Offshore Windfarms*. Universitat Politècnica de Catalunya. Escola Tècnica Superior d'Enginyeria Industrial de Barcelona, 2019. [Online]. Available: <https://books.google.nl/books?id=BjgRzgEACAAJ>.
- [26] R. Vazquez, M. Muñoz Diaz, M. Alonso, H. Amaris, and C. Alvarez, "Background harmonic distortion measurement at power networks with wind farms," *Renewable Energy and Power Quality Journal*, pp. 873–878, May 2016. DOI: [10.24084/repqj14.500](https://doi.org/10.24084/repqj14.500).
- [27] PowerFactory, *DIGSILENT PowerFactory User Manual*. Aug. 2020, pp. 1–1253.
- [28] S. M. Halpin and A. Card, "40 - power quality," in *Power Electronics Handbook (Third Edition)*, M. H. Rashid, Ed., Third Edition, Boston: Butterworth-Heinemann, 2011, pp. 1179–1192, ISBN: 978-0-12-382036-5. DOI: <https://doi.org/10.1016/B978-0-12-382036-5.00040-9>. [Online]. Available: <https://www.sciencedirect.com/science/article/pii/B9780123820365000409>.
- [29] M. Val Escudero, G. Lietz, Z. Emin, C. Jensen, and L. H. Kocewiak, *CIGRE TB 766: JWG C4/B4.38 network modelling for harmonic studies*, Apr. 2019.
- [30] J. C. Das, *Power System Analysis: Short-Circuit Load Flow and Harmonics, Second Edition*. CRC Press, 2016.
- [31] L. Shuai, K. Høj Jensen, and L. H. Kocewiak, "Application of type 4 wind turbine harmonic model for wind power plant harmonic study," in *Proc. 15th Int. Workshop Large Scale Integr. Wind Power Power Syst*, pp. 1–7, Nov. 2016.
- [32] K. Yang, M. H. Bollen, H. Amaris, and C. Alvarez, "Decompositions of harmonic propagation in wind power plant," *Electric Power Systems Research*, vol. 141, pp. 84–90, 2016, ISSN: 0378-7796. DOI: <https://doi.org/10.1016/j.epsr.2016.06.029>. [Online]. Available: <https://www.sciencedirect.com/science/article/pii/S0378779616302371>.
- [33] L. H. Kocewiak, C. Álvarez, P. Muszynski, J. Cassoil, and L. Shuai, "Wind turbine harmonic model and its application-overview, status and outline of the new IEC technical report," in *14th Wind Integration Workshop WIW15-163*, Oct. 2015.
- [34] H. Ghanavati, L. H. Kocewiak, and Alireza, "Updated harmonic and interharmonic current summation rule in wind power plants with type III wind turbines," in *Conference: 18th International Workshop on Large-Scale Integration of Wind Power into Power Systems as well as on Transmission Networks for Offshore Wind Power Plants At: Dublin, Ireland*, Oct. 2019.

- [35] K. Yang, M. Bollen, and A. Larsson, "Aggregation and amplification of wind-turbine harmonic emission in a wind park," in *2015 IEEE Power Energy Society General Meeting*, 2015, pp. 1–1. DOI: [10.1109/PESGM.2015.7285778](https://doi.org/10.1109/PESGM.2015.7285778).
- [36] B. Zhang, A. Huang, and B. Chen, "A novel IGBT gate driver to eliminate the dead-time effect," in *Fourtieth IAS Annual Meeting. Conference Record of the 2005 Industry Applications Conference, 2005.*, vol. 2, 2005, 913–917 Vol. 2. DOI: [10.1109/IAS.2005.1518427](https://doi.org/10.1109/IAS.2005.1518427).
- [37] C. D. Townsend, G. Mirzaeva, and G. C. Goodwin, "Deadtime compensation for model predictive control of power inverters," *IEEE Transactions on Power Electronics*, vol. 32, no. 9, pp. 7325–7337, 2017. DOI: [10.1109/TPEL.2016.2630712](https://doi.org/10.1109/TPEL.2016.2630712).
- [38] F. M. Dekking, *A modern introduction to probability and statistics: understanding why and how*. Springer, 2005.
- [39] P. M. Ivry, "Predicting stochastic harmonics of multiple converters in a power system (microgrid)," Ph.D. dissertation, University of Nottingham, 2016, pp. 1–264. [Online]. Available: <http://eprints.nottingham.ac.uk/33041/>.
- [40] E. Bukaçi, T. Korini, E. Periku, S. Allkja, and P. Sheperi, "Number of iterations needed in Monte Carlo simulation using reliability analysis for tunnel supports," *International Journal of Engineering Research and Applications*, vol. 6, pp. 60–64, Jun. 2016.
- [41] K. Jansen, B. van Hulst, C. Engelbrecht, P. Heslen, K. Velitsikakis, and C. Lakenbrink, "Resonances due to long HVAC offshore cable connections: Studies to verify the immunity of dutch transmission network," in *2015 IEEE Eindhoven PowerTech*, 2015, pp. 1–6. DOI: [10.1109/PTC.2015.7232408](https://doi.org/10.1109/PTC.2015.7232408).
- [42] L. H. Kocewiak, J. Hjerrild, and C. Bak, "Harmonic analysis of offshore wind farms with full converter wind turbines," English, in *Proceeding of the 8th International Conference on Large-Scale Integration of Wind Power into Power Systems*, Energynautics GmbH, 2009.
- [43] PowerFactory, *Technical Reference-Static Generator*. Feb. 2020, pp. 1–46.
- [44] D. Vree, L. Beloqui Larumbe, Z. Qin, P. Bauer, and B. Ummels, "Impact of WTG converter impedance model on harmonic amplification factor of the Dutch 110kV transmission network using a 383MW wind farm case study," English, in *CIGRE C4-302*, Cigré, 2020.
- [45] C. Bak, J. Hjerrild, and L. H. Kocewiak, "Wind turbine converter control interaction with complex wind farm systems," *IET Renewable Power Generation*, vol. 7, pp. 380–389, Jul. 2013. DOI: [10.1049/iet-rpg.2012.0209](https://doi.org/10.1049/iet-rpg.2012.0209).
- [46] G. Mendonça, H. Pereira, and S. Silva, "Wind farm and system modelling evaluation in harmonic propagation studies," *Renewable Energy and Power Quality Journal*, pp. 647–652, Apr. 2012. DOI: [10.24084/repqj10.415](https://doi.org/10.24084/repqj10.415).
- [47] W. Wiechowski, "Harmonics in transmission power systems," Ph.D. dissertation, Institut for Energiteknik, Aalborg Universitet, 2006, ISBN: 87-89179-69-2.
- [48] F. F. d. Silva and C. L. Bak, *Electromagnetic transients in power cables*. Springer, 2013.
- [49] C. H. Chien and R. W. G. Bucknall, "Harmonic calculations of proximity effect on impedance characteristics in subsea power transmission cables," *IEEE Transactions on Power Delivery*, vol. 24, no. 4, pp. 2150–2158, 2009. DOI: [10.1109/TPWRD.2009.2016800](https://doi.org/10.1109/TPWRD.2009.2016800).
- [50] Ø. Garvik, "Analysis of harmonic conditions in subsea electrical power systems for oil and gas installations," Ph.D. dissertation, 2015.
- [51] PowerFactory, *Technical Reference-Cable System*. Jun. 2020, pp. 1–29.
- [52] T. Worzyk, *Submarine Power Cables Design, Installation, Repair, Environmental Aspects*. Springer Berlin, 2013.
- [53] ABB, *XLPE Submarine Cable Systems: Attachment to XLPE Land Cable Systems-User's Guide*, pp. 1–12.
- [54] K. Shaarbafi, *Transformer Modelling Guide*, pp. 1–304, 2014.
- [55] C. Liu, "Comparison and selection of three-core cable and single-core cable," *IOP Conference Series: Earth and Environmental Science*, vol. 300, p. 042 047, Aug. 2019. DOI: [10.1088/1755-1315/300/4/042047](https://doi.org/10.1088/1755-1315/300/4/042047).

- [56] F. da Silva, "Analysis and simulation of electromagnetic transients in HVAC cable transmission grids," Ph.D. dissertation, Institut for Energiteknik, Aalborg Universitet, Jul. 2011, ISBN: 978-87-89179-99-5.
- [57] ABB, *XLPE Land Cable Systems: User's Guide*, pp. 1–28.
- [58] PowerFactory, *Technical Reference-Filter/Shunt*. Feb. 2020, pp. 1–46.
- [59] F. D. Freijedo, S. K. Chaudhary, R. Teodorescu, J. M. Guerrero, C. L. Bak, Ł. H. Kocewiak, and C. F. Jensen, "Harmonic resonances in wind power plants: Modeling, analysis and active mitigation methods," in *2015 IEEE Eindhoven PowerTech*, 2015, pp. 1–6. DOI: [10.1109/PTC.2015.7232382](https://doi.org/10.1109/PTC.2015.7232382).
- [60] L. Beloqui Larumbe, Z. Qin, L. Wang, and P. Bauer, "Impedance modelling for three-phase inverters with double synchronous reference frame current controller in the presence of imbalance," *submitted to IEEE Transactions on Power Electronics*, 2021.